New Jersey Institute of Technology

Digital Commons @ NJIT

Fall 1-31-1999

Characterization of tantalum coatings on steel substrates

Prabha Shivaramkrishnan
New Jersey Institute of Technology

ABSTRACT

CHARACTERIZATION OF TANTALUM COATINGS ON STEEL SUBSTRATES

by
Prabha Shivaramkrishnan

Sputtered tantalum can be used as an effective corrosion resistant barrier if the coating is continuous, free from defects and is adherent to the substrate it is intended to protect. For corrosion-applications 100% bcc phase tantalum is preferred. X-ray diffraction results indicate that sputtered tantalum deposits typically contain a mixture of bcc and beta phases. Depending on the deposition conditions the morphology of tantalum coatings as studied using scanning electron microscopes can vary from irregular, dendritic structure to a defined step type structure. A "cauliflower type" structure has also been observed. Extended x-ray absorption fine structure measurement was used to investigate the local structure of tantalum coatings. The results show that tantalum coatings with 100% bcc phase possess a long-range crystalline order. For coatings with pure beta phase and a mixture of both phases XAFS measurements indicate that the near number coordinations around tantalum atom are not simply well ordered bcc or fcc and that the sample arehigly disordered on a local scale – a result not previously observed. The adhesion and delamination behaviour of tantlaum coatings indicated that coatings with pure bcc phase exhibited excellent adhesion characteristics while pure beta phase coatings and coatings with a mixture of both phases showed poor adhesion. The beta phase tantalum coatings has an as deposited resistivity of 175 $\mu\Omega$ cm while for alpha phase the values are between 20-80 $\mu\Omega$ cm.

CHARACTERIZATION OF TANTALUM COATINGS ON STEEL SUBSTRATES

by
Prabha Shivaramkrishnan

A Thesis
Submitted to the Faculty of
New Jersey Institute of Technology
in Partial Fulfillment of the Requirements for the Degree of
Master of Science in Materials Science and Engineering

Department of Materials Science and Engineering

January 1999

APPROVAL PAGE

CHARACTERIZATION OF TANTALUM COATINGS ON STEEL SUBSTRATES

Prabha Shivaramkrishnan

Dr. Trevor A. Tyson, Thesis Advisor   Date
Professor of Physics, New Jersey Institute of Technology

Dr. Roland A. Levy, Committee Member   Date
Distinguished Professor of Physics, New Jersey Institute of Technology

Dr. N.M. Ravindra, Committee Member   Date
Professor of Physics, New Jersey Institute of Technology

Dr. Mark C. Croft , Committee Member   Date
Professor of Physics, Rutgers The State University of New Jersey

BIOGRAPHICAL SKETCH

Author: Prabha Shivaramkrishnan

Degree: Master of Science in Materials Science and Engineering

Date: January 1999

Undergraduate and Graduate Education:

- Master of Science in Materials Science and Engineering
  New Jersey Institute of Technology, Newark, NJ, 1999

- Bachelor of Science in Metallurgical Engineering,
  Maharaja Sayajirao University, Baroda, India, 1991

Major: Materials Science and Engineering

Publications and Presentations:

Refereed Journals:

"*Improved powder metallurgical Ag-ZnO electrical contacts*" P.B. Joshi, Prabha S. Krishnan, R.H.Patel, V.L. Gadgeel, V.K. Kaushik and P. Ramakrishnan, *International Journal of Powder Metallurgy*, vol. 34,no.4, May 1998

"*Powder metallurgical silver-metal oxide electrical contacts by an electroless coating process*", P.B. Joshi, R.H.Patel, Prabha S. Krishnan, V.L. Gadgeel, V.K. Kaushik and P. Ramakrishnan, *Journal of Advanced Powder Technology, Japan*, vol. 7, no. 2, 1996.

"*Opto-electrical and Adhesion characteristics of electroless silver coatings*", P.B. Joshi, N.C. Chourasia, H.M. Pandit, Prabha S. Krishnan and S.B. Kalkundri, *Journal of Metal Finishers association of India*, vol. 5, no.2, 1996.

"*Processing of electrical contact grade Ag-ZnO powder by alternative routes*" P.B. Joshi, Prabha S. Krishnan, V.L. Gadgeel and P. Ramakrishnan, *Powder Metallurgy Science & Technology Quarterly International Journal*, vol. 6, no. 2, Jan 1995.

Conference Presentations:

"New silver zinc oxide DC contacts for automatic applications ", " P.B Joshi, <u>Prabha S. Krishnan,</u> V.L. Gadgeel and P. Ramakrishnan, in *Proceedings of International conference of Powder Metallurgy '97 on powder metallurgy for automatice components,* Feb, 1997.

"Highly dispersed Ag-ZnO electrical contacts grade composite powders by in-situ reduction technique", P.B. Joshi, <u>Prabha S. Krishnan,</u> R.H.Patel, S.C. Khurana and V.L. Gadgeel, at the 34th *National Metallurgist Day,* New Delhi, Nov. 1996.

"Opto-electrical and Adhesion characteristics of electroless silver coatings", H.M. Pandit, <u>Prabha S. Krishnan</u> and S.B. Kalkundri, P.B. Joshi and N.C. Chourasia, at *Materials Research Society of India, 6th Annual general meeting,* Feb 1995.

This work is dedicated to
my parents

ACKNOWLEDGEMENT

TABLE OF CONTENTS

Chapter   **Page**

TABLE OF CONTENTS
(Continued)

TABLE OF CONTENTS
(Continued)

TABLE OF CONTENTS
(Continued)

LIST OF TABLES

LIST OF FIGURES

LIST OF FIGURES
(Continued)

CHAPTER 1

INTRODUCTION

1.1 Objective

Tantalum metal, is one of the most versatile corrosion resistant metals known. It combines the inertness of glass with the strength and ductility of low carbon steel and has a much higher heat transfer capability than glass [1,3]. Tantalum metal, because of its refractory nature and high ductility, is being investigated as a protective material for applications at elevated temperatures, pressures, and high force [1]. Due to its inherent corrosion resistance, tantalum is used to handle highly corrosive chemicals in industrial chemical processing. Most often, this material is used as a liner, allowing a less expensive material, such as steel, to serve as the back up to supply the required strength [2-3]. As compared to tantalum, nonmetallics, such as graphite and glass, are susceptible to mechanical damage, often caused by temperature and pressure surges, which may result in leakage and catastrophic failures. In addition, the high coefficient of linear expansion of fluorocarbons (for graphite and glass) can become a problem at elevated temperatures while tantalum is essentially free of such problems.

The objective of the present study is to find a possible replacement material for chromium coatings in gun barrels and more generally on steel substrates. Tantalum can be considered as an excellent replacement material for chromium coatings because of its excellent corrosion resistance in practically any media and also at elevated temperatures. However, the most important advantage that tantalum offers is its low toxicity when compared with chromium.

The goal in the present study is to investigate and characterize the properties of tantalum coatings deposited on gun steel using different characterization methods and to determine its structural properties, mechanical properties and electrical properties.

1.2 Background Information

The superlative corrosion resistance of tantalum and also its high costs are well known. The combination has long made the tantalum coating on steel substrates a firm favorite of physical vapor deposition (PVD) studies. Most of the investigations of tantalum thin films have been carried out using films deposited by sputtering [4]. This is partly due to the relative ease and speed with which films can be sputtered. However, the main reason for the use of sputtering has been that sputtered films have been of practical use in the microelectronics and process industry. Two other common processes used to produce coatings of this material are chemical vapor deposition and electro-deposition from fused salt baths, which involves heating of the substrate to temperatures 800°C or higher [1]. Consequently these methods have a potential disadvantage of exceeding the tempering temperature of steel substrates which can cause a change in the properties of steel substrates. Sputtering does not require substrate heating to form the coating, and heat produced by the process itself (e.g., from exposure to the plasma discharge and kinetic energy of the sputtered neutrals) can be removed from thermally conductive metal substrates by external cooling.

Tantalum coatings produced by sputtering are typically observed in one of the two crystallographic forms. In the bulk, tantalum has a bcc crystalline structure (a=3.304Å) which is the thermodynamically stable, with physical properties that make it attractive as

a material for protective coatings. The meta-stable beta phase has a tetragonal structure

(a=5.313 Å, c=10.194 Å) and has distinctly different physical and electrical properties

from those of bulk tantalum. The increase in the lattice constant of bcc tantalum in thin

films over that of the bulk material is most likely due to the inclusion of impurities in the

film during the deposition process. The maximum concentration of hydrogen (30%) in

solid solution in bulk tantalum increases the lattice constant to 3.4 Å, nitrogen (maximum

about 4%) increases in to 3.32 Å, and there is an increase to 3.34 Å for oxygen at a

maximum concentration of about 5%[5]. Thin films are often capable of dissolving more

impurities that the bulk material.

Beta tantalum spontaneously reverts back to the bcc phase at temperatures between 750

and 800°C. Properties of the two phases of tantalum is listed in the TABLE 1.1 below

[6]:

Table 1.1 Properties of Tantalum

TANTALUM PHASE	DENSITY (theoretical) gm/cc	RESISTIVITY μΩcm	TEMPERATURE COEFFICIENT OF RESISTANCE Ppm/°C	SUPER CONDUCTIVITY °K9	STRUCTURE
Bulk tantalum	16.555	13	+3800	4.4 °K	bcc a=3.303 Å
Sputtered Bcc tantalum	16.55-16.27	24-50	+500 +1800	3.25°K9	bcc a=3.31-3.33 Å
Sputtered Beta tantalum	16.9	180-220	-100 +100	0.5°K9	tetragonal a=5.313 Å c=10.194 Å

If sputtered tantalum is to be used effectively as a corrosion resistant barrier, the deposited material must be continuous, have relatively few defects, and be adherent to the substrate it is intended to protect. Furthermore, protective coatings subjected to stresses in the presence of high temperature, high-pressure gases must be capable of withstanding repeated operating cycles without detaching.

Sputtered tantalum deposits typically contain a mixture of the two phases (bcc and beta phase). Tantalum coatings containing a large percentage of beta phases will be harder than bcc-only coatings, but are less ductile resulting in cracks due to intrinsic stresses. Therefore, the beta phase is limited in corrosion protection applications. Coatings consisting of continuous bcc tantalum with an interfacial layer of the beta phase should provide an adequate protective barrier in the absence of mechanical or thermal stresses; otherwise this beta layer is a potential site for crack generation and de-bonding of the coating [1].

1.3 Factors Affecting the Nature of the Deposit

A number of process parameters have been identified that appear to influence the structure of sputtered tantalum. These parameters include sputtering gas purity, the nature of the substrate surface, substrate bias during deposition, length of pre-sputtering time and the substrate temperature [1,4,7]. There remains, however, considerable controversy regarding the specific effects of each of these variables, primarily because of the difficulty in fully isolating each variable from the effects of others [1]. In addition to above effects vacuum system impurities have also been found to have a large effect on the nucleation and growth of Ta films. In one of the laboratory runs leakage of the oil

from the vacuum pump resulted in carbon deposition along with the tantalum resulting in poor adhesion of the tantalum coating to the substrate.

1.3.1 Literature Review

Matson, Merz and McClanahan [1] identified two parameters that affect the formation of the bcc phase: one is the effect of substrate temperature, and the other is modification of the substrate surface by introducing an intermediate layer of material between the substrate and the coating. Independently, the factors were observed to influence the growth characteristics of the bcc and beta sputtered tantalum. The effect of modification of the surface layer with an intermediate layer was more pronounced. Face and Prober [8] demonstrated that under-layers of niobium as thin as 1 nm could be used to promote exclusive nucleation of the bcc phase in thin tantalum films deposited by ion beam sputtering on Si (100) substrates. The lattice mismatch between bcc tantalum and niobium is less than 0.1%. Niobium under-layer of all thickness resulted in a large increase in the amount of bcc tantalum. In addition, the niobium under-layer covered and neutralized oxide and hydroxide species present on the substrate surface, which were thought to promote the preferential nucleation of beta tantalum in sputtered films. The presence of surface oxide and hydroxide formed by the reaction of H_2O with the surface favored the nucleation of beta-tantalum. Also high substrate temperatures (>600 °C) favored the formation of bcc tantalum. Using substrate temperatures in the range of 175 to 250 °C promoted an initial deposition of the beta phase followed by transition to bcc phase (>600°C), which continues to grow. Feinstein and Huttemannin [7] found that chemisorbed hydroxides and physisorbed water covered silica, alumna and metal oxide

surfaces. Physisorbed water was removed by heating the substrates to a few hundred degrees in vacuum. However, temperatures necessary for removing chemisorbed surface hydroxyls ranged from about 500° to 700°C. As, water vapor is always present in the residual atmospheres of the sputtering chambers, substrates will have to be maintained at the above mentioned temperatures, in order to, sputter tantalum on to water free surface. In the present study the substrate temperatures were maintained around 100 °C as, working at higher substrate temperatures (between 450 and 600°C) would eventually change the properties of gun barrel steel. Another reason of working around 100 °C is to avoid complications when the process will used in full-scale [9].

Feinstein and Huttemannin [7] studied RF and DC diode tantalum sputtering on twenty substrate materials of different types, including amorphous, crystalline and single crystal materials. The substrates investigated were classified into different categories with respect to their influence on the structure of sputtered tantalum. The substrates that readily formed surface oxides in air at room temperature (e.g. SiO_2, amorphous glass and metals like Cu and Ni) nucleated beta tantalum. The substrates, that do not readily form surface oxides even in an oxidizing atmosphere, always nucleated bcc tantalum (eg. Au, Pt, Rh and W). The third category consisted of substrates which do not rapidly form surface oxides in air at RT but which may be oxidized at elevated temperatures; nucleated bcc tantalum when deposited directly on the substrate (not tantalum) that were not subjected to elevated temperatures previously. They formed beta tantalum when oxidized, and a mixture of both phases when partially oxidized.

Another parameter, which has been shown to affect the tantalum structure, is the substrate bias. However different results have been reported for different sputtering

apparatus or conditions. Vratny et.al [10] reported a change from beta tantalum to bcc

tantalum at a bias above +10 V or below −100 V with dc diode sputtering in a bell jar

system. On the other hand, Cook [6] reported no phase transformation of beta tantalum

even at a bias of −200V in a two-chamber dc diode system. Matson et. al. [1] reported

that higher substrate biases (-110 to −150 V) appeared to have less beta phase. These

findings are consistent with that reported by others [4,5] that higher substrate biases favor

the formation of bcc phase in sputtered tantalum film. Substrate biases to −150V were not

adequate in themselves to eliminate the beta phase formation, as other factors to be have

also taken into consideration. While all the results indicate that bias sputtering changes

film purity, more work is needed to define the effect of bias on structural changes.

CHAPTER 2

SPUTTERING THEORY AND SYSTEMS

2.1 Interaction of Ions with Surfaces

When an ion approaches the surface of a solid usually called the *target* one or all of following phenomenon [11] may occur. First, the ion may be reflected, probably being neutralized in the process. This reflection is known as *ion scattering*. Second, the impact of the ion may cause the target to eject an electron usually referred to *secondary electron*. Third, the ion may become buried in the target. This is *ion implantation*. The ion impact may be also responsible for some structure rearrangements in the target material, or may set up a series of collisions between atoms of the target, possibly leading to the ejection of one of these atoms. This ejection process is known as *sputtering*. Any suitably energetic atomic particle impinging against a surface can cause sputtering.

2.1.1 Sputtering Systems

A wide variety of sputtering systems [4] have been used in the preparation of tantalum films and they fall in to four basic types:

- Ion beams systems
- dc diode systems
- dc triode systems
- rf sputtering systems

8

The ion beam method is essentially the simplest since it requires only the acceleration of an ion beam to the target in a reasonable vacuum. In the diode systems, the sputtering target is one of the electrodes in glow discharge. Once the glow is established, it is maintained by ionization of gas atoms by secondary electrons emitted by the cathode and there is, therefore, a pressure below which the glow cannot be maintained. This pressure may be reduced by effectively increasing the electrode separation and this can be accomplished by application of a magnetic field. The negative potential on the tantalum target causes acceleration of positive ions to it.

In the triode systems, electrons are supplied from a hot filament so that the glow may be maintained at lower pressure than in the diode system. A magnetic field may also be applied in this case to further reduce the pressure. The tantalum target is maintained at a high negative potential to accelerate ions out of the plasma.

In the rf systems, a high frequency (typically 13.56 MHz) is used to cause ionization of the plasma. Since an electron may be accelerated back and forth in the gas, a discharge may be maintained at a lower pressure than in the dc diode system. A high negative potential may be induced on the target by the rf signal by suitable circuitry or a separate dc potential may be applied. The simplest sputtering system, apart from the ion beam, which is rather limited in its application, is the dc diode system and it has been used in the majority of studies.

2.2 A Conventional DC Sputtering System

Normally in a conventional dc sputtering system Fig. (1.1) [11], the material we wish to sputter is made into the sputtering target which becomes the cathode of an electrical

circuit, and has a high negative voltage V (dc) applied to it [11]. The target is nearly

always solid, although powders and even liquids are sometimes used. The substrate,

which we wish to coat, is placed on an electrically grounded anode a few inches away.

These electrodes are housed in a chamber, which is evacuated. Argon gas is introduced to

the chamber at some specific pressure. The action of the electric field is to accelerate an

electron which in turn collide with the argon atoms, breaking some of them up into argon

ions and more electrons to produce the glow discharge.
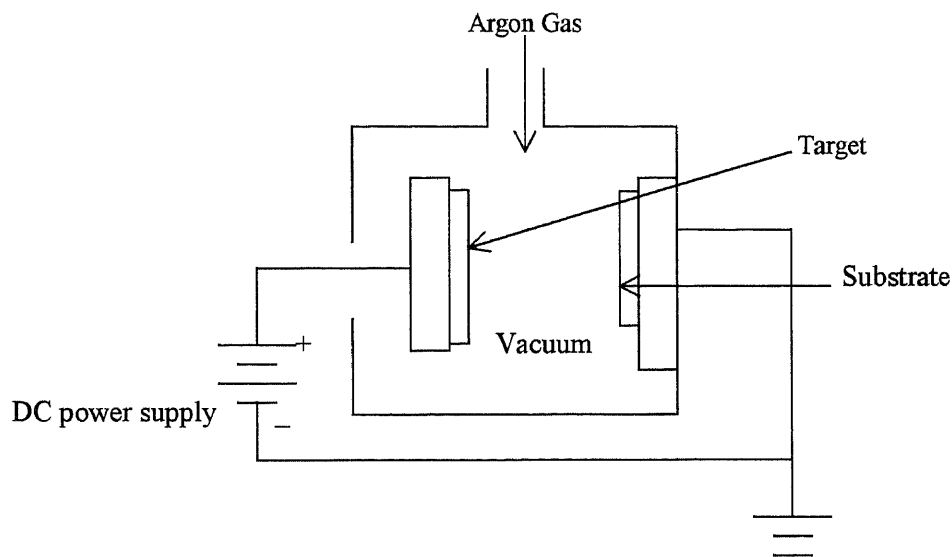
Fig.1.1 Schematic of a dc Sputtering System

The charged particles produced are accelerated by the field, the electron tending towards

the anode, causing more ionization on the way, and the ions towards the cathode, so that

a current I flows. When the ions strike the cathode, they may sputter some of the target

atoms off. They may also liberate secondary electrons from the target. The sputtered

atoms from the target fly off in random directions, and some of them land on the

substrate (on the anode), condense and form a thin film.

2.2.1 Choosing the Sputtering Gas

It is much easier to ionize atoms when they are in gaseous state, and easy to accelerate ions to the energies. Noble gas ions are chosen because they do not react with the target or growing film. Sometimes, gaseous ions are trapped in the deposited atoms however we consider this an innocuous happening. Argon [11] is almost always used in sputtering deposition because it is easily available and cheaper.

2.2.2 Choosing the Gas Pressure

A vacuum gas enables one to control the operating pressure inside the sputtering system. Operating pressure limitations are imposed by the requirements of both the glow discharge and film deposition. The glow discharge sets a lower pressure limit. The discharge is sustained by electron making collisions in the gas. The number of ionizing collisions will decrease with decreasing gas density or pressure. A different problem arises from the high density or pressure because when electrons undergo collision, the sputtered-material from the target collides with gas atoms on its way to the substrate, and will increase the gas pressure. The result of the collision is to deflect the sputtered atom, and hence decrease the deposition rate.

2.3 Practical Aspects of Sputtering System

2.3.1 Ground Shield

The target is surrounded by a dark space shield, known as the ground shield. The purpose of ground shield is to restrict ion bombardment and sputtering to the target only.

2.3.2 Shutter

A shutter can be rotated into place between the electrodes. This has its use during the pre-sputtering period when the first few atomic layers of the target are removed by sputtering for cleaning purposes.

2.3.3 Target Cooling

Sputtering is a very inefficient process, and most of the power input to the system appears finally as target heating. Such heating can become excessive and can lead to damage of the bonding between the target and the backing electrode of the target itself.

2.4 Applications of Sputtering

The sputtering process can apply to knock an atom out of the surface of a target and this is called sputter *etching*. By repeating this process over and over, the target surface will be cleaned or can be made thinner. In addition, it can be used to generate a topographic pattern on the surface. Besides these applications, sputter deposition can also be used. Atoms ejected from the target move through space until they strike and condense on the surface of the substrate. By repeating this process over and over, one can build a coating of several atomic layers of the target material on the substrate.

2.4.1 Sputtering as a Deposition Process

Sputtering is current application for the deposition of tantalum thin films. In sputter deposition, the atoms diffuse around the substrate. This motion determined by the binding energy of the atoms to the substrates and is also influenced by the nature and temperature

of substrate. The atom will either jump over the barrier into an adjacent site or might even re-evaporate. After a certain time, the atom will either evaporate from the surface or will join another diffusing single atom to form a doublet, which is less mobile but more stable than a single atom.

The chance probability of forming the atomic pair will depend on the single atom density and hence on the deposition rate. With time, the doublets will combine with other single atoms, to form triplets and so on. This is *nucleation stage* of thin film growth, leading to the formation of quasi-stable *islands*. The islands grow in size rather than in number. Eventually, they grow large enough to touch, this is the *agglomeration or coalescence stage* that proceeds until the film attains uniformity.

2.5 Implementation

2.5.1 Experimental Specifications

The tantalum coatings were deposited on stainless steel substrates having dimensions $12.5 \times 12.5 mm^2$ and 5mm thickness. The substrate preparation included mechanical and chemical treatment of substrates by surface- active matters and ultrasonic cleaning using acetone. This was generally followed by water jet treatment and by acetone cleaning. Water jetting is a process where water flows into a nozzle and is forced to come out through orifices which are generally of a much smaller size as compared to the feed line. The orifice focuses the water into a coherent stream or jet, and directs the stream towards the required point on the target surface of the work piece. Sometimes in order to polish hard materials (eg. glass and metals) abrasive particles are added to the jet stream. These particles acquire the speed of water, and provide most of the cutting action when the jet

hits the target. The water jet treatment was done on standard industrial equipment with a specially constructed nozzle for 10 to 15 minutes and after the treatment the samples were dried in hot air. The processing parameters maintained during the water jet processing were water pressure of 30 kpsi and travel speed of 400 i/min).

The final cleaning of the substrate was done using high voltage glow discharge in vacuum (Pressure 1-5 mTorr, Voltage 1-10kV, Current 2-5 mA, time of cleaning 30-60 minutes).

Sputter deposition was carried out in the TORUS industrial standard magnetron sputtering assembly [See Appendix A for layout]. In this system stainless steel substrates (12.5×12.5mm^2 and 5mm) were loaded inside the chamber.

The steel substrates were positioned under the target during deposition. The deposition details along with the sample name are listed in Table 2.1 and Appendix B.

Table 2.1 Deposition Details for Tantalum Coatings

SAMPLE NAME	THICKNESS (MICRONS)	DEPOSITION DETAILS
Tantalum powder	-325 mesh	Tantalum powder purchased from Alridge Chemical co. 99.9% purity
Pure Bcc(Alpha)Tantalum	25μ	Watervilet sample, deposition details not known
Pure BetaTantalum	25μ	Watervilet sample, deposition details not known
Argon Sample Tantalum film deposited on a thick steel substrate	150	Temperature 25°C Pressure 10×10^{-3} Torr Time 360 min Voltage 385 V Current 1 A Sample cleaned using alcohol and ultrasonic cleaning and prepared using water jet treatment
Nitrogen Sample Tantalum film deposited on a thick steel substrate	150	Temperature 25°C Pressure 10×10^{-3} Torr Time 360 min Voltage 385V Current 1A Sample cleaned using alcohol and ultrasonic cleaning and prepared using water jet treatment
TS J4 Tantalum film deposited on a thick steel substrate	60	Temperature=25°C Pressure=10 μTorr Time=60 min Voltage=460V Current=1.4 A ultrasonic cleaning water jet treatment
TS J5 Tantalum film deposited on a thick steel substrate	60	Temperature=25°C Pressure=10 μTorr Time=60 min Voltage=460V Current=1.4 A Sample cleaned using alcohol and ultrasonic cleaning water jet treatment

Table 2.1 (cont.)

SAMPLE NAME	THICKNESS (MICRONS)	DEPOSITION DETAILS
TA 1 Tantalum film deposited on thin steel substrate	5	Temperature=25°C Pressure=10×10^{-3} Torr Time=15 min Voltage=480V Current=0.75A Sample cleaned using alcohol and ultrasonic cleaning No water jet treatment
TS S1 Tantalum film deposited on a thick steel substrate	70	Temperature=25°C Pressure=10 ×10 $^{-3}$Torr Time=120 min Voltage=460V Current=1.4 A Sample cleaned using alcohol and ultrasonic cleaning and prepared using water jet treatment

CHAPTER 3

MEHTODS FOR CHARACTERIZATION

3.1 X-ray Diffraction

X ray diffraction [12-14] is used to obtain information about the crystal structure, composition, number of phases, and the percentage of phases that are present for a given material. Some other typical applications are precise measurements of lattice constants and residual strains and refinement of atomic coordinates. The samples may be in the form of powders, solids, pastes, thin films or ribbons.

3.1.1 Crystal Systems

For x-ray diffraction, one has to clearly understand the crystal systems, miller indices, inter-planar spacing and structure factors associated with different systems. The crystal system is classified according to seven types of cells, which are triclinic, monoclinic, orthorhombic, tetragonal, cubic, trigonal and hexagonal. Of all these cells types the simple cubic system is considered a primitive cell. The simple cubic cell can be sub classified as simple cubic (SC), body centered cubic (bcc) and face centered cubic (fcc).

Table 3.1 Characteristics of cubic lattices

Characteristics	Simple	Body-centered	Face-centered
Volume	a^3	a^3	a^3
Number of nearest neighbors	6	8	12
Nearest neighbor distance	a	$2/a^3$	$4/a^3$

Table 3.1(cont.)

Characteristics	Simple	Body-centered	Face-centered
Number of second neighbors	12	6	6
Second neighbor distance	$2^{1/2}a$	a	a

For all crystal systems, the position of a point in the unit cell is specified in terms of

atomic coordinates x, y, z. Each coordinate is a fraction of the axial length a_1, a_2, a_3 in the

direction of the coordinated axis, with the origin taken at one corner of the unit cell. X-

ray diffraction is based on the principle of Bragg's law:

$$n\lambda = 2d \sin\theta \text{ or } \lambda = 2d_{hkl} \sin\theta$$

From x-ray diffraction point of view, it turns out that for structural analysis one must

know the orientation of the plane, which are expressed as miller indices (hkl) of planes or

index of plane. The miller indices of planes are determined by the following rules:

- Find the intercepts on the axes in terms of lattice constants.

- Take the reciprocal of these numbers and then reduce to three integers having

  the same ratio.

Another important point to be considered during x-ray diffraction is the structure factor

for different structures. At any given time, only an insignificant number of known

crystalline substances consist of a single kind of atom at specific points of a simple

lattice. Most of the times real crystals contain more than one kind of atom and/or atom

groups. For defining structure factor, one must also know about atomic scattering factor.

It is defined as the intensity scattered by a single atom. In order to determine the

combined scattering power of all the atoms in a unit cell, it is necessary to relate the differences between the path lengths of x-rays scattered by each atom. When there are many atoms in a unit cell, there can be two possibilities: One being the condition where scattering by different atoms in a unit cell could cause the waves to be completely suppressed, because of interference. In the second case there will be reinforcement of the waves scattered by the corresponding points in the lattice. This factor causing reinforcement or disappearance of diffraction maxima is called Structure Factor (denoted by F). The general equation for Structure factor is:

$$\mid F_{hkl} \mid = \{[\ \Sigma\Sigma f_n \cos 2\pi\ (hx_n + ky_n + lz_n)\ ]^2 + [\Sigma\Sigma\ f_n \sin\pi\ (hx_n + ky_n + lz_n)]^2\ \}^{1/2}$$

f_n = atomic scattering factor for n atom

hkl = miller indices of reflection

xyz = atomic coordinates of nth atom

For simple cubic (SC), the structure factor F2 is independent of hkl and is same for all reflections. For body centered cubic (bcc), SF is not the same for all reflections.

For h+k+l = even F_{hkl} = 2f

For h+k+l = odd F_{hkl} = 0

For mixed hkl reflections, such that hkl is two odd and one even,

F_{hkl} = 2f

For mixed hkl reflections, such that hkl is two even and one odd

F_{hkl} = 0

For face centered cubic (fcc), the structure factor F2 is not the same for all reflections.

For unmixed hkl, all odd or all even, F_{hkl} = 4f

For mixed hkl, two even or one odd or vice versa, F_{hkl} = 0.

3.1.1(a) Determination of Crystallite Size and Lattice Strain

For polycrystalline specimen consisting of sufficiently large and strain free crystallites diffraction theory predicts that the lines of powder diffraction will be exceedingly sharp. However in actual practice, such sharp lines are never observed. If a material is internally stressed then the original sharp lines of the polycrystalline (powder) diffraction pattern become broadened indicating that the original degree of perfection of crystallites has been lost. There have been several suggestions advanced as to the nature of these imperfections:

- The material is broken up into crystallites, or coherently diffracting domains in the case of metallic grains, so small (100 to 1000A) that diffraction broadening occurs.

- The material is broken up into crystallites (10000A) in size, with lattice spacing differing from one to another.

- The crystallites though fairly large are fairly individually elastically distorted or suffer from deformation faults or both.

These peak-broadening effects due to the presence of small crystallites can be studied by calculating the crystallite size and the lattice strain associated with different samples. Broadening resulting from small crystallite size is expressed in terms of Scherrer 's equation,

$$L = K\lambda/B\cos\theta$$

where, K=constant, λ = wavelength of x-rays, θ = angle of diffraction, L = the mean dimension of crystallites and B= breadth of pure diffraction profile.

The lattice strain resulting from above effects is calculated using the equation,

$$e = B/4\tan\theta$$

where e = Lattice strain and all other parameters are defined before.

3.1.2 Description of X- Ray Diffraction

When a beam of monochromatic x-rays is directed at a crystalline material, x- rays are diffracted at various angles with respect to the primary beam. The relationship between the wavelength of the x- ray beam, λ, the angle of diffraction, 2θ, and the distance between each set of atomic planes of the crystal lattice, d, is given by the Bragg equation:

$$n\lambda = 2d \sin\theta \text{ or } \lambda = 2d_{hkl} \sin\theta$$

Here, n represents the order of diffraction. From the above equation the inter-planar distances of the crystalline material can be studied. These distances depend solely on the dimension of the crystal's unit cell, whereas, the intensities of the diffracted rays are a function of the placement of the atoms in the unit cell. The expression of d_{hkl} in the above equation is called interplanar spacing. Crystal systems have formulas for calculating the interplanar spacing.

Table 3.2 Formula for calculating interplanar spacings (d_{hkl})

System	Axial Translation	Axial Angles	d_{hkl}
Cubic	a=b=c	$\alpha=\beta=\gamma=90°$	$a(h^2+k^2+l^2)^{-1/2}$
Tetragonal	a=b≠c	$\alpha=\beta=\gamma=90°$	$[(h^2/a^2) + (k^2/a^2) + (l^2/c^2)]^{-1/2}$
Orthorhombic	a≠b≠c	$\alpha=\beta=\gamma=90°$	$[(h^2/a^2) + (k^2/b^2) + (l^2/c^2)]^{-1/2}$
Hexagonal	a=b≠c	$\alpha=\beta=90°, \gamma=120°$	$[(4/3a^2) + (h^2+k^2+hk) + (l^2/a^2)]^{-1/2}$

The x ray pattern of the crystalline substance can be thought of as a " fingerprint," as each material has, within limits, a unique diffraction pattern. The International Center for Diffraction Data has published the powder diffraction patterns for around 60,000 compounds and these data are available on the CDROM. An unknown compound is identified by comparing the inter-planar spacing and intensities of its powder pattern to the patterns in the powder diffraction file. In addition to identifying the compounds in a powder, analysis of the diffraction patterns is used to determine the crystallite size, the degree of crystallinity, and the phase composition.

3.1.3 Application

X ray diffraction analysis of sputtered tantalum coating using copper $K\alpha$ (λ=1.54Å) radiation yielded reflection corresponding to bcc tantalum for most of the preliminary samples studied in the green manufacturing project, and a mixture of bcc and beta tantalum in case of one of the samples. Also, for corrosion measurements, as the oxide coating is formed the coatings will be assessed by x- ray diffraction.

3.2 Environmental Scanning Electron Microscopy and Energy Dispersive X-ray Spectroscopy (SEM/EDX)

The primary use of ESEM is the study of surface morphology, shape, size, porosity etc. of solid samples. The resolution of these instruments is typically between 1.5 and 3 nm, approximately two orders of magnitude better than optical microscopes and one order of magnitudes less than transmission electron microscopes, thereby bridging the gap between these related techniques. Any solid samples may be studied however sample size is restricted to less than 10 cm in diameter. ESEM can be applied to metals, ceramics,

polymers, composites and biological materials. Energy dispersive x-ray spectroscopy (EDX) is used for the determination of elemental composition and quantitative information of the local composition of the material. This analysis is used in conjunction with ESEM imaging, thereby allowing analysis to be performed directly on areas under electron beam observation.

3.2.1 Description

In ESEM, an electron beam passes through an evacuated column. It is then, focussed by electromagnetic lenses onto the specimen surface. The beam is then rastered over the specimen in synchrony with the beam of a cathode ray display screen. The (in-elastically-scattered) secondary electron emission from the sample (determined to a large extent by surface topography) is then used to modulate the brightness of the cathode ray display screen, thereby forming the image [12-14]. If elastically back-scattered electrons are used to form the image the image contrast is determined largely by the compositional differences of the sample surface rather than topographic features. The most important feature of a scanning electron microscope is the image contrast. In addition to the secondary electron detector, the scanning electron microscope is also equipped with a back-scattered electron detector. The secondary electron (SE) detector is most widely used while the back-scattered electron (BSE) detector compliments the SE detector and provides information that is not available from a secondary electron signal. The contrast mechanisms observed due to SE or BSE emissions can be subdivided as follows:

- Collection contrast
- Emission contrast

The SEM micrographs are often taken with a beam/surface tilt angle of 60 to 80° rather than at normal incidence where the tilt angle is 90°. This causes a dramatic decrease in shadowing effects as all the secondary electrons are trapped in the lens and the collection efficiency is maximum. Emission contrast generally involves edge effects or Z (atomic number) effects. The edge effects are generally based on the SE that the generated by effects near the edge of a feature. This effect is most prominent in protruding fibers, and sudden changes in cross-sections. For a beam voltage of 20 to 30 keV, a large atomic number difference between two points in the same sample, will change the BSE signal more than the SE signal and result in contrast in these two regions.

In EDX, [12-14] the emission of x-rays from the surface of material upon exposure to a primary beam of electrons of suitable energy is characteristic of the atom from which the rays originated. The energy of this emission is measured by EDX detectors positioned at the periphery of the microscope stage such that qualitative and quantitative information can be obtained from the same portion of the sample under direct microscopic observation.

3.2.2 Application

Compositional mapping for tantalum coating on steel using ESEM/EDX revealed trace impurities. For unstressed samples the morphology showed a globular structure which may indicate an amorphous oxide film. The morphology of the tantalum deposited coatings will be evaluated.

3.3 X-ray Fluorescence Spectroscopy

3.3.1 Introduction

X-ray fluorescence (XRF) is a simple and, in general, nondestructive method for

qualitative and quantitative analysis of elemental composition in a wide range of

materials over a wide range of composition. This method is extremely useful because of

the ease in sample preparation and because of its ability to detect and analyze elements

down to aluminum and, under certain circumstances, to boron. For qualitative elemental

analysis, the samples can be run in "as received" condition with virtually no sample

preparation. The sample can be in any shape (powder, pellet, film, fiber, or chunk of

material) and state (liquid, solid, or suspension). The sample can be several centimeters in

diameter or weigh as little as a few milligrams. For quantitative analysis, virtually no

preparation of samples is required in liquid form. For solids, some preparation, such as

pulverizing, mixing with a fluxing agent or a binder may be required to insure sample

homogeneity.

3.3.2 Description

XRF is based on the photoelectric effect [12-15]. When an atom is irradiated with highly

energetic photons, an electron from one of the inner core shells may be ejected. As the,

vacant core level is filled by an electron from an outer shell, a photon with energy

characteristic of the atom energy level spacing is released. This radiation is called

fluorescent radiation, and each element has its own set of characteristic emission or XRF

lines. The intensity and the energy of these lines are measured using a spectrometer.

Typically cryogenically coated semiconductor Ge or Si detectors are used. A photon of

energy $h\mu$ will create pulse of electrons and hole carriers, where the number of carriers is propotional to $h\mu/E_g$, where E_g is the semiconductor gap energy. Thus the pulse strength tells us the energy and the number of pulses tells the number of x-rays. Most recent spectrometers use microprocessors and/or personal computers to automate data collection and data reduction and to present the results of elemental analysis in an easily understandable format.

3.3.3 Application

Qualitative and quantitative analysis of unknown samples can be accomplished using x-ray fluorescence. In qualitative analysis, the untreated sample is excited by radiation and the identification of unknown elements is accomplished by reference to tables of emission lines of the elements. The qualitative information can be converted to semi-quantitative data by careful measurements of the peak heights. To obtain a rough estimated of the concentration, the following relationship is used:

$$P_x = P_s \; W_x$$

where, P_x is the relative line intensity measured in terms of number of counts for a fixed period, and W_x is the weight fraction of the element in the sample. The term P_s is determined with a sample of the pure element or a standard sample of known composition. The above equation is based on the assumption that the emission from the species of interest is unaffected by the presence of other elements in the sample.

In quantitative analysis by calibration against standards, the relationship between the analytical line intensity and the concentration is determined empirically with a set of standards that closely approximate the samples in overall composition. Here it is assumed

that the absorption and enhancement effects are identical for both unknown samples and the standards. The empirical data thus obtained is employed to convert emission data to concentrations. The degree of compensation achieved to a large extent depends upon the closeness of match between the samples and standards.

3.4 X -Ray Absorption Fine Structure Spectroscopy

3.4.1 Introduction

X-ray absorption fine structure spectroscopy, has emerged as a useful probe of the local structure around specific atomic species in solids, liquids and molecular gases [16,17]. XAFS technique has been widely recognized and utilized as a tool for local structure studies, especially in systems lacking long range order, such as systems with defects and local distortions, where traditional diffraction studies can only provide information about the unit cell averaged structure [18-19].

3.4.2 Description

The simplest XAFS experiments are done in transmission mode [17]. Polychromatic x-rays are produced by a synchrotron radiation source or from a conventional laboratory source (rotating anode system) and a desired energy band of approximately 1 eV bandwidth ($\Delta E/E \approx 10^{-4}$ eV) is then selected by diffraction from a silicon double crystal monochromator. Only those x-ray photons that are of the correct wavelength λ ($\lambda = h\,c/E$ where h is the Planck's constant and c is the speed of light) to satisfy the Bragg condition $n\lambda = 2d\,\sin\theta$ at the selected angle θ will be reflected from the first crystal; the others will be absorbed. The parallel second crystal is used as a mirror to restore the beam in original

direction. The monochromatic x-rays are then allowed to pass through the sample t which should absorb approximately 50-90% of the incident x-rays. The incident and transmitted x-ray fluxes are monitored usually with gas ionization chambers.

narrow band of x-rays of energy (E)   fluorescence detector   sample

Synchrotron source   monochromator

transmitted flux monitor

x- rays (white beam with continuous
λ(E) distribution)   incident flux monitor   fluorescence x-rays
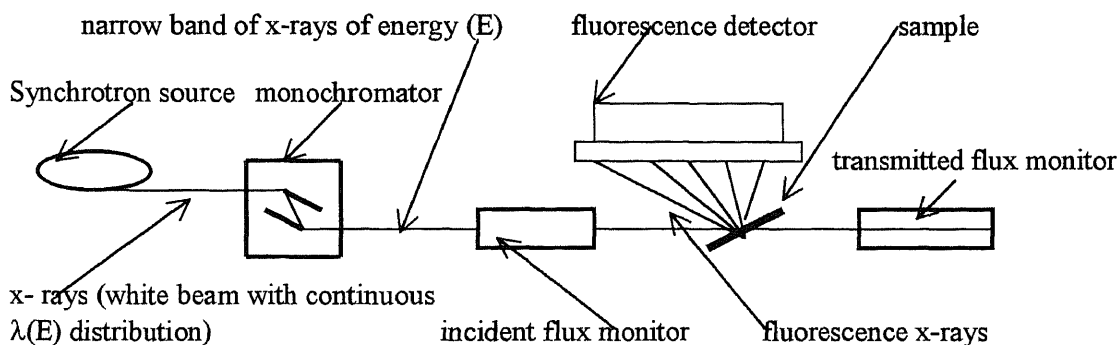
Fig.3.1 Schematic XAFS Experiment

For a homogeneous sample of uniform thickness x the absorption coefficient μ (E) is related to the transmitted (I) and incident (I_o) fluxes by the equation:

$$I/I_o = \exp\left(-\mu\,(E)\,x\right)$$

The absorption coefficient decreases as the energy E increases as approximately as $1/E^3$ except for sudden increases in absorption coefficient called absorption edges that occur at energies characteristic of the element which make up the sample.

The sudden rise in absorption edge occurs when an incident x-ray photon has just sufficient energy to cause transition of an electron out of a core level such as 1s (K-edge), 2s (L_1-edge) state of some element in the sample to an unfilled state of predominantly p character ($2p_{1/2}\,L_{ii}$ edge) or ($2p_{3/2}\,L_{iii}$ edge)[Appendix B]. In the "near edge" region the absorption coefficient (with in about 30 eV of the edge jump) is called "X-ray Absorption

Near Edge Structure" (XANES) and well above the absorption edge (≥ 30 eV) they are called "Extended X-ray Absorption Fine Structure"(EXAFS). EXAFS utilizes the interference effect between the ejected photoelectron wave, produced when an x-ray is absorbed by an atom, and the fraction of the wave that is back-scattered from neighboring atoms. Thus it is possible to obtain information about the distances to and the number of neighboring atoms and thereby the local structure of different elements. For very high atomic number elements the L-edges (2S,2P) are suitable for measuring XAFS as the K-edge energies may be experimentally difficult to reach.

3.4.3 Elementary Data Processing and Data Analysis

The traditional method of data analysis involves a series of steps [16,17]. The first step consists of processing of the data and includes steps that change the raw data into the normalized EXAFS data that can be interpreted according to the usual theoretical formulations. Some of these steps in the processing include pre-edge subtraction, normalization, deglitching, alignment of the energy scale, EXAFS background removal and transformation to k space. The second step consists of data analysis to extract the information of interest and some of these procedures are Fourier transform of the data, including effects of weighting and windows, filtering in r space, single and multiple shell fitting.

3.4.3.1 Data Processing

3.4.3.1(a) Pre-Edge Background Removal: In the EXAFS data one is usually interested only in the region above the absorption edge. The removal of the background

involves a fitting of the data before the edge to some functional form and extrapolation of this function into the data region. Generally, a simple polynomial routine is most convenient where either a linear or a quadratic polynomial in energy is used for absorption data and a linear polynomial for fluorescence data.

3.4.3.1(b) Data Normalization: Energy independent normalization of the EXAFS data basically removes the effects of sample thickness so that different sample may be directly compared. Energy dependent normalization is normally carried out for transmission data. Normalization is one of the steps to obtain $\chi(E)$ curve from the $\mu(E)$ curve and involves creating a step in the absorption coefficient at the edge (μ_o). The normalization point should be chosen far enough above the edge to be away from any near edge structure yet not so far enough above the edge that the cross section has fallen appreciably from its value at threshold. Typically this point is in the range of 20 to 50 eV above the edge. Another important point to be noted while doing normalization is that this point should be chosen as consistently as possible among the unknown and standard sets used in a particular experiment.

3.4.3.1(c)Deglitching: Absorption and fluorescence data taken at synchrotron sources often include sharp structures due to spurious reflections from the crystal monochromator, taking away incident photons. These "glitches" may be many times larger than the EXAFS signal. The common technique is to fit the data on both sides of the glitch with a polynomial that is then used to interpolate through the glitch region. Fortunately this procedure is rarely needed and clearly evident when required.

3.4.3.1(d) Isolation of the Fine-Structure Oscillations: This step consists of subtracting out the smooth background from the absorption data. There are many methods used for this procedure all of which are dependent on the background being slowly varying compared with the EXAFS oscillations. These methods include subtractions of:

1. A cubic least square spline-approximant to the data.

2. A simple polynomial background, followed by digital high pass filtering.

3. A cubic smoothing spline-approximant to the data.

The first technique is probably the most foolproof and is recommended for most applications. A cubic spline is a curve constructed out of linked cubic polynomials; the function value and first derivative are matched at the "knots" where the polynomials meet. Typical values for the number of "knots" range from 2 to 6.

3.4.3.2 Data Analysis

3.4.3.2(a) Fourier Transform: is merely an intermediate step used to isolate the data from different shells. One of the practical problems associated with Fourier transforming data is due to the finite data range. The FT is calculated according to the formula:

$$FT(r) = (2/\pi)^{1/2} \int_{kmin}^{kmax} \chi(k) \exp(-2ikR) dk$$

Where k_{max}, k_{min}, and R denote the ranges of Fourier Transform and W(k) is the window function and $\chi(k)$ is the expression for the oscillatory fine structure as a function of the photoelectron wave number and is a sum of contributions from back scattering from the different atomic coordination shells. Five window functions are available: Rectangular,

Kaiser-Besssel, Gaussian and Hanning. In the present XAFS analysis the Kaiser-Bessel function was used.

$$W(k) = J_o (\pi A \{1 - (1 - k/k^{*2})\}^{1/2})/ J_o(\pi A)$$

These window functions have the following purpose:

- To truncate the data smoothly at the ends of the transform range so as to minimize truncation ripple at the expense of some peak broadening.

Another type of windowing, which is applied to the data before Fourier transform, is weighting the spectrum by a factor k^n, where n is typically chosen between 1 and 3.

3.4.3.2(b) Interpretation of Transforms: Although Fourier transform is usually an intermediate step in the analysis, a great deal of structural information may be learned form direct inspection. For systems with small disorder (eg. $2k^2\sigma^2 <<<1$) with a single atomic species in a shell, the radial distances may be determined with relatively high precision. Inspection of the transform gives information about various shell radii amplitudes, disorder, noise level etc. Examination of the imaginary (or real) part of the transform as well as the magnitude as by suitable comparison with reference compounds or theoretically modeled data it is often possible to tell the types of atoms contributing to a given shell.

3.4.3.3 Curve Fitting: In the single scattering curved wave approximation an EXAFS signal $\chi(k)$ can be parameterized in the following form:

$$\chi(k) = \Sigma S_o^2 (N_i/kR_i^2) f_i(\Pi, k, Ri) \exp(-2\sigma_i^2 k^2 + 2/3 C_{4i} k^4) \times \exp(-2r_i/\lambda(k)) \sin$$
$$(2kri - 4/3 C_{3i} k^3 + \varphi_I(\pi, k, Ri))$$

Where $k=\{k^2 + (2m_e/h^2)\,\Delta E_{oi}\}^{1/2}$ is the photoelectron wave vector corrected for the difference in energy origin between experiment and theory; S_o^2 is the scale factor taking into account amplitude damping die to the multielectron effects, N_i is the coordination number of the i-shell, R_I is the radius of the i-shell; σ^2 is the mean square radial displacement or Debye Waller factor; C_{3i}, C_{4i} are the cumulants of a distrubution taking into account anharmonic effects and/or non Gaussian disorder; fi (π, k, Ri) is the backscattering amplitude of the photoelectron due to the atoms of i coordination shell. The fitting parameters are S_o^2, Ni, Ri, σ^2, ΔE_{oi}, C_{3i} and C_{4i}.

The curve fitting technique attempts to best fit the $k^n \chi$ (k) spectra in k or R space with EXAFS models. Typically, up to four parameters can be varied in each shell (N, σ, R and E_o).

3.5 Adhesion Measurement

3.5.1 Introduction

The durability of coatings is of prime importance in many fields, and one of the main factors that govern this durability is adhesion. This is particularly noticeable if the coating, or the substrate is subject to external forces or a corrosive environment, as under these conditions the coating may peel. One of the simplest ways to measure adhesion is to apply an adhesive tape to the surface of the coating or the film, and to subsequently examine the result of stripping. Those, which were weakly bonded to the substrate, will come off easily while those, which are strongly bonded, will remain on the substrate. However, the above method is highly qualitative and gives no indication of the relative magnitudes of adhesive forces. Hence, it is necessary to assign a finite value as a measure

of adhesion. The first detailed work for measuring adhesion quantitatively was undertaken by Heavens [12] who used a chrome steel ballpoint, which was drawn across the film surface. A vertical load was applied to the point and was gradually increased until a critical value of the load was reached at which the film was completely stripped from the substrate, leaving a clear channel behind. The critical load was determined by examining the resultant scratches made in the film under an optical microscope. This critical load is taken as a measure of adhesion. Benjamin and Weaver implemented this method on a quantitative basis [12].

In the field of protective and wear resistant coatings, the scratch test is used to evaluate and to control the mechanical resistance of the coating-substrate interface. Essentially the test consists in deforming the coating-substrate interface by straining the substrate. The mechanical resistance of the interface and/or of the coating is characterized by a critical load that, is the minimum load, at which damage by lack of adhesion can be observed. The critical load depends not only depends on coating adhesion but also on several other parameters. They are intrinsic parameters, which are related to the test itself and extrinsic parameters, which are related to the coating/substrate combination. The intrinsic parameters include loading rate and scratching speed, indenter tip radius and wear of the diamond. The extrinsic parameters include substrate hardness and coating thickness, coating roughness, substrate roughness prior to coating and friction force and friction coefficient. Steinmann *et al.* [19] made following recommendations while conducting scratch test:

- The loading rate should be around 10Nmm^{-1} and the Rockwell diamond tip should be around 200 μm.

- The sample roughness should not be higher than 0.3 μm.

- The initial roughness of the substrate prior to coating should be kept as low as possible.

There are different means for determining the critical load at which lack of adhesion is observed. They are:

- Microscopic observation: This is the most reliable method to detect coating damage. This technique is able to differentiate between cohesive failure within the coating and adhesive failure at the interface of the coating-substrate system.

- Acoustic emission detection: This method is basically detection of elastic waves generated as a result of the formation and propagation of micro-cracks. The AE sensor is insensitive to mechanical vibration frequencies of the instrument.

- Tangential force recording: This method records the force fluctuations along the scratch and thus enables us to follow the force fluctuations along the scratch.

3.6 Resistivity Measurement

3.6.1 Introduction

Resistivity is an important property because it can be related directly to the impurity content of a sample [21-24]. The measurement of resistivity however can be difficult for several reasons, including problems of making good contact with the material.

Probes have been designed for making resistivity measurements, and these probes

typically use a hard metal such as tungsten, ground to a sharp point. Because contact

resistance is so great, a four- point probe is used. The outer two contacts supply a

constant current, and the inner contacts measure the voltage drop across a portion of the

sample. With the geometry of the probe and wafer known, resistivity can then be

calculated. The precaution to be observed while making resistivity measurements using a

four-point probe is to provide adequate shielding of the contacts and electrical leads.

3.6.2 Description

The four- point probe is one of the most common methods for measuring resistivity for

thin films and wafers [1]. A current source, I_S, forces current through the wafer using the

two outer probes, while a voltmeter measures the voltage, V across the inner probes (fig.

3.2).
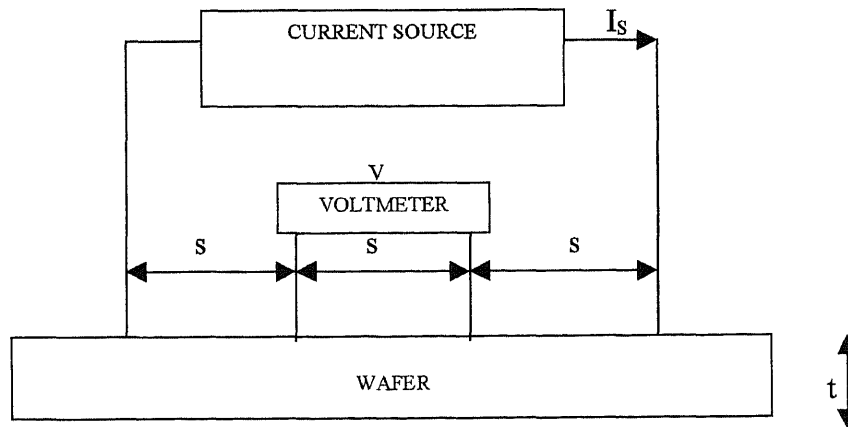
Fig. 3.2 Four point Probe Resistivity Measurement Set-up

The resistivity is then calculated from the voltage, current, probe spacing, and sample thickness. For bulk materials (t>>S) where t is the sample thickness and S is the probe spacing; resistivity is calculated by the following equation:

$$\rho = 2\Pi S \; V / I_S$$

[where ρ is the, volume- resistivity (Ω-cm)]

For thin layers (t<<S) resistivity is computed in the following manner:

$$\rho = [\Pi t/\ln 2] \; [V_M / I_S]$$

The sheet resistance, R_S (ohms) can be computed from the resistivity as follows:

$$R_S = \rho/t$$

The resistivity of tantalum as reported in literature can be listed as follows:

- Bulk tantalum = 12.5 μohm-cm at RT

- Bcc tantalum = 24 to 50 μohm-cm at RT

- Beta tantalum = 180-200μohm-cm at RT

CHAPTER 4

RESULTS AND DISCUSSION

Structural Properties

4.1 X- Ray Diffraction

The x-ray diffraction measurements for the tantalum coatings were conducted using

Phillips x- ray diffractometer type PW304D-MP Sr. No.D4715. The diffraction patterns

obtained from tantalum coatings are somewhat complicated by variations in type and the

degree of preferred orientation, and by variations in the cell parameters. Depending on

sputtering and substrate conditions, the composition of the films varied in the relative

amounts of the beta-tantalum and bcc tantalum present. It also varied in the values of the

cell parameters of each phase, and in the type and degree of preferred orientation. Each of

these effects caused profound changes in the X-ray diffraction patterns, and hence care

must be exercised in determining the structures of the tantalum phases based on the

analysis of these patterns. One of the most accurate methods of obtaining x-ray

diffraction patterns is by using the Debye-Scherrer wide film technique [25]. However, in

the present study the diffraction patterns were obtained using routine diffractometer

measurements. The x ray diffraction measurements for sputtered films of beta-tantalum

and bcc tantalum on glass surfaces were studied by M. H Read and co-workers [25].

They determined that in case of films containing mixtures of bcc and beta-tantalum

phase, parallel expansion of the bcc and beta-tantalum cell maintained a near coincidence

of the (110) bcc and (202) beta-tantalum x-ray reflections. This means that the near

coincidence of the (110) bcc tantalum and (202) beta tantalum x-ray reflections in the

range of d=2.35-2.37 Å will always occur for all the relative mixtures of bcc and beta

tantalum. By performing x-ray diffraction studies of tantalum film on silicon substrates

D.W. Face et al [26] has reported that bcc tantalum films have a compressive stress of

$\approx 1.2 \times 10^{10}$ dyn/cm^2 in the plane of the film. Many workers have reported variations in

the value of the cell constant and this is the result of preparation technique and dissolved

impurities. Previous reports [5] indicate that routine film preparations include 2-16 at. %

hydrogen, 0.5-3.0 at. % argon, and lesser amounts of other impurities in each phase. In

the case of bulk tantalum addition of 16 at. % hydrogen changes the cell constant by

1.2%. Since deposited material is frequently able to dissolve a larger portion of impurities

than bulk material [5], it is likely that the observed 2% variations in the lattice constants

are due to the presence of dissolved impurities. In some sputtering techniques (dc

sputtering) a deliberated inclusion of additional reactive impurities such as nitrogen or

oxygen [5] is done to inhibit the formation of beta-tantalum, and the bcc phase is formed.

The indexing of the x-ray diffraction patterns in the present study were done by

comparing the data obtained from the spectra to the standard powder diffraction data for

bcc tantalum (JCPDS ref. card no. 04-788) and beta tantalum (JCPDS ref. card no. 25-

1280). For proper understanding of the structure of beta tantalum, the work reported by

M.H Read et al [25] and P. T Moseley et al [27] was also considered. On the basis of x-

ray diffraction studies M. H Read [25] has suggested that the beta tantalum has a fiber

texture and that the orientation is same whether the film is sputtered on an amorphous, a

polycrystalline, or a mono-crystalline substrate, including metallic or nonmetallic

materials. The indexing bcc tantalum was done in terms of a body centered cubic unit cell

with a= 3.304 Å and for beta tantalum it was done in terms of a tetragonal unit cell with

a= 10.194 ± 0.003Å and c= 5.313 ± 0.002 Å. The cell constant or cell parameter was

calculated for each of the reflections and is reported in Table 4.1. In the present study

most of the reflections showed variations of up to 2% or more in the lattice constants and

this is consistent with the work reported by other workers. These variations probably

result from the effects that different sputtering conditions have on the film density and the

impurity content of the films. Since tantalum coatings were prepared by sputtering

technique the diffraction data in most of the cases has suffered from the effects of

preferred orientation.

The crystallite size has been calculated on the basis of the Scherrer equation

L=Kλ/Bcosθ). For lattice strain the formula e= B/4 tanθ has been used.

Each of the diffraction patterns has been discussed in detail along with the diffraction

patterns in subsequent pages. For deposition details refer to Appendix B.
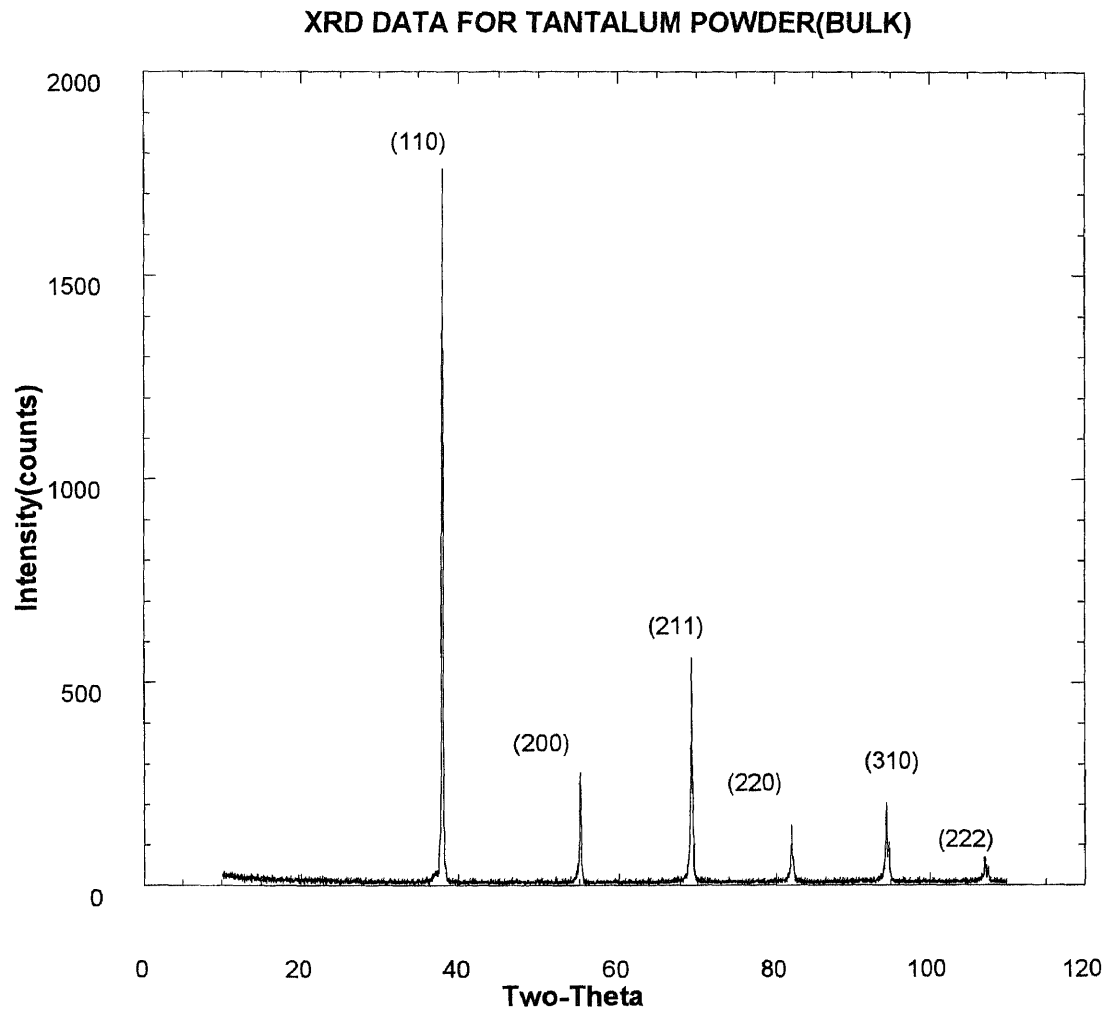
Fig. 4.1 X-ray Cu K_α diffractometer scan for Ta-powder

The diffraction peaks observed in the spectra correspond to the bcc phase of tantalum. From the standard powder diffraction pattern for tantalum (JCPDS ref. card 04-788) the (110) diffraction peak is expected to be twice as intense as the (211) peak. In the above spectra, the relative intensities of the tantalum peaks are in accordance with the predicted ratios of the standard bcc phase.

XRD DATA FOR TANTALUM ALPHA SAMPLE
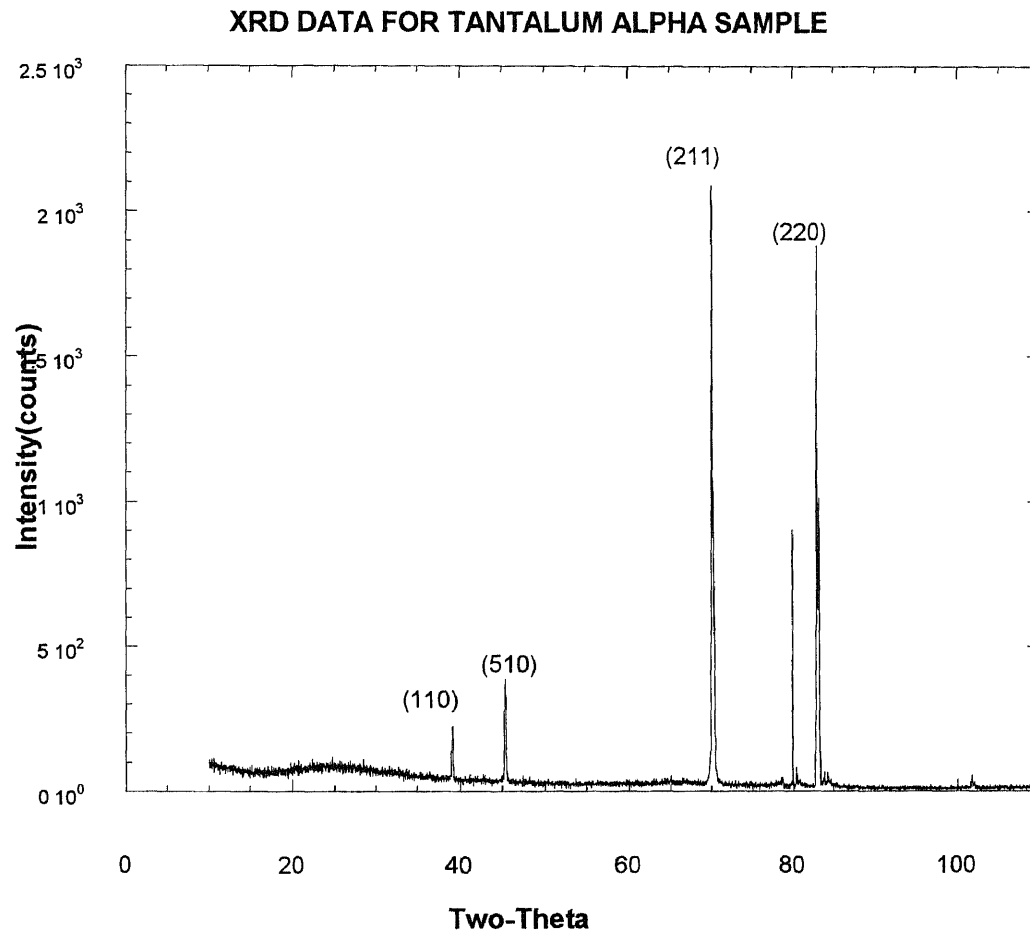
Fig. 4.2 X-ray Cu K_α diffractometer scan for Ta- film deposited on steel substrate

For the alpha sample the observed spectra showed that the (110) peaks are very much lower in intensity as compared to the (211) and (220) peaks, thus indicating a high degree of preferred orientation in these films away from the close packed (110) planes. The unindexed reflection in the diffraction profile corresponds to steel (major iron phase) and the corresponding miller indices in (211) for iron.

XRD DATA FOR TANTALUM BETA SAMPLE
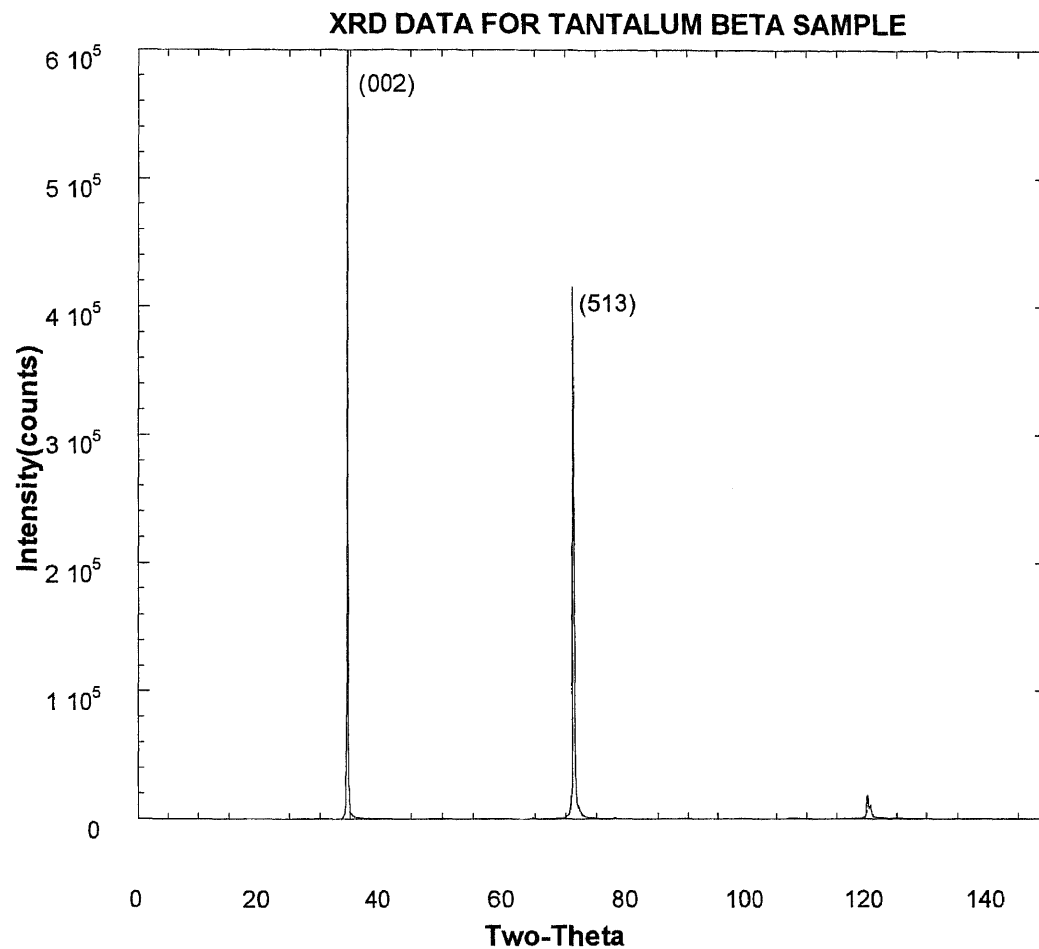
Fig. 4.3 X-ray Cu K_α diffractometer scan for Ta- film deposited on steel substrate

The diffraction peaks correspond to the beta phase of tantalum. They have been indexed using the powder diffraction pattern of beta tantalum (Cu k_α radiation) by P T. Moseley, C J. Seabrook in terms of a tetragonal unit cell with a= 10.195 Å and c= 5.313 Å.

XRD DATA FOR TS K, TS S1, FOIL 0.5mm, FOIL 1MM
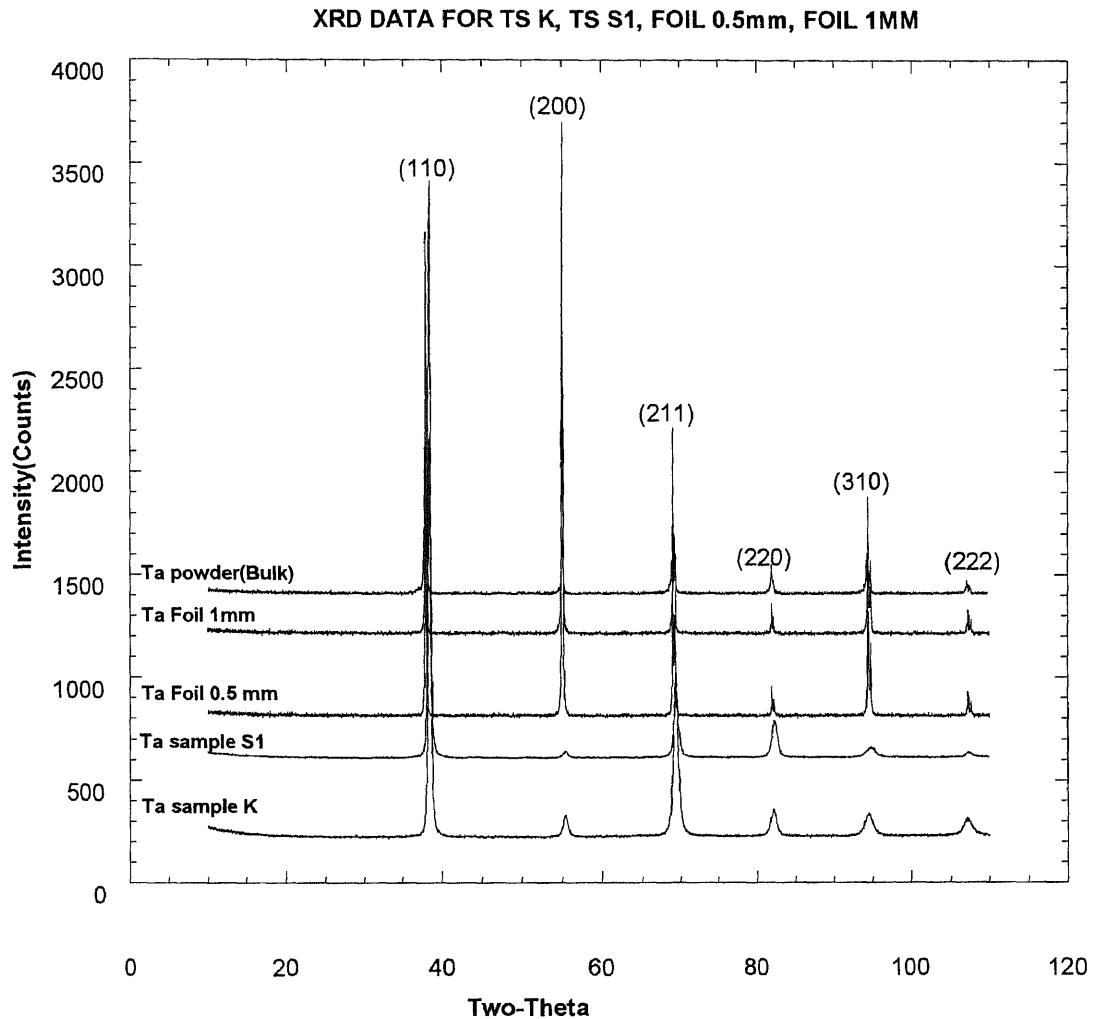
Fig. 4.4 X-ray Cu K_α diffractometer scan for Ta-coatings deposited on steel substrate and Ta-foil

The observed x-ray diffraction spectra for sample TS K and TS S1 are similar to the bulk tantalum. For tantalum foil 0.5mm and 1.0 mm thick the (200) diffraction peak is as strong as the (110) peak thus showing the difference between foil which is deformed and samples TS K and TS S1 made by sputtering technique. This explains that specimens subjected to deformations can develop inhomogeneous fiber texture that can introduce some degree of preferred orientation in to the crystallite structure and cause variations in the diffracted intensities.
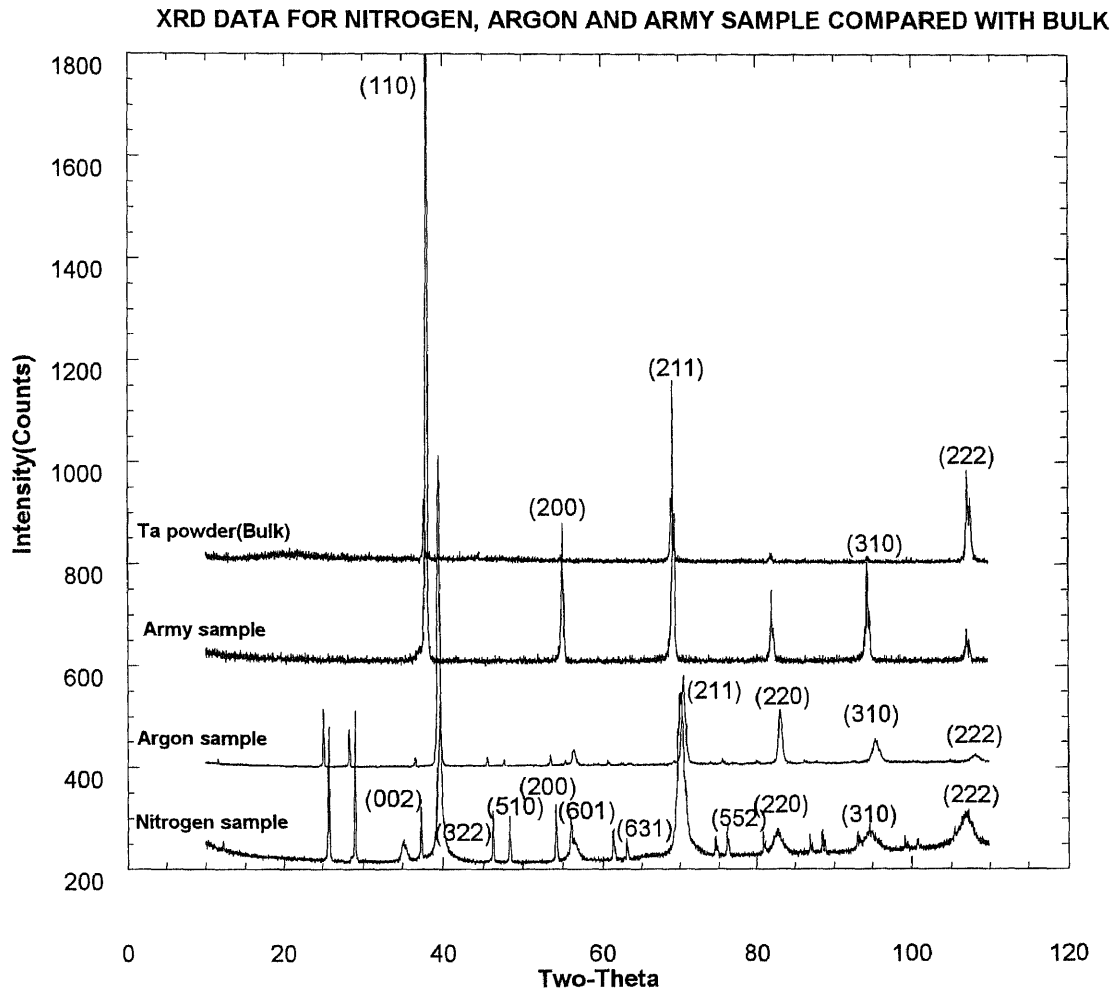
Fig. 4.5 X-ray Cu K_α diffractometer scan for Ta-coatings on steel substrate

For the "army sample" (Fig. 4.5) the x-ray diffraction spectra show similar trends as bulk tantalum. Slight traces of beta-tantalum (002,322,510,01) are visible in argon sample while for the nitrogen sample, the x-ray spectra shows strong bcc (110) peak with weak beta-tantalum peaks (002,322,510,601,631,552). This indicates that the (110) peak show a high degree of preferred orientation. In argon sample the beta tantalum peaks have much lower intensity when compared to nitrogen sample.

XRD DATA FOR TS 11, TS J4, TS J5, TS C1
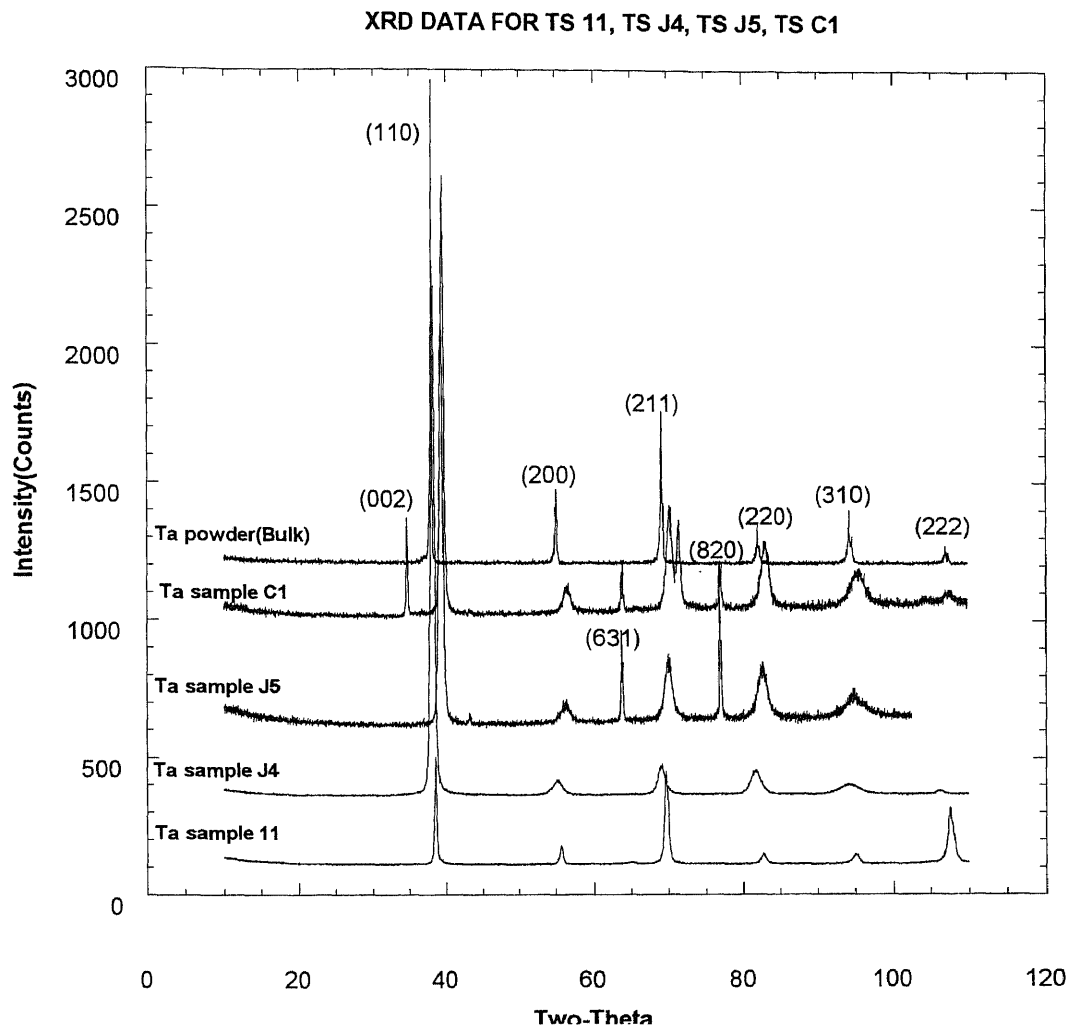
Fig. 4.6 X-ray Cu K_α diffractometer scan for Ta-coatings on steel substrate

In samples TS J4 and TS 11 the observed spectra showed diffraction peaks corresponding to bcc tantalum. The trends observed were similar to the bulk tantalum. In samples TS J5 and TS C1 beta-tantalum peaks (002,631,820) were also observed in addition to bcc tantalum(110,200,211,220,310,222). The samples showed a very strong pattern of (110) oriented bcc- tantalum and a weak beta tantalum.
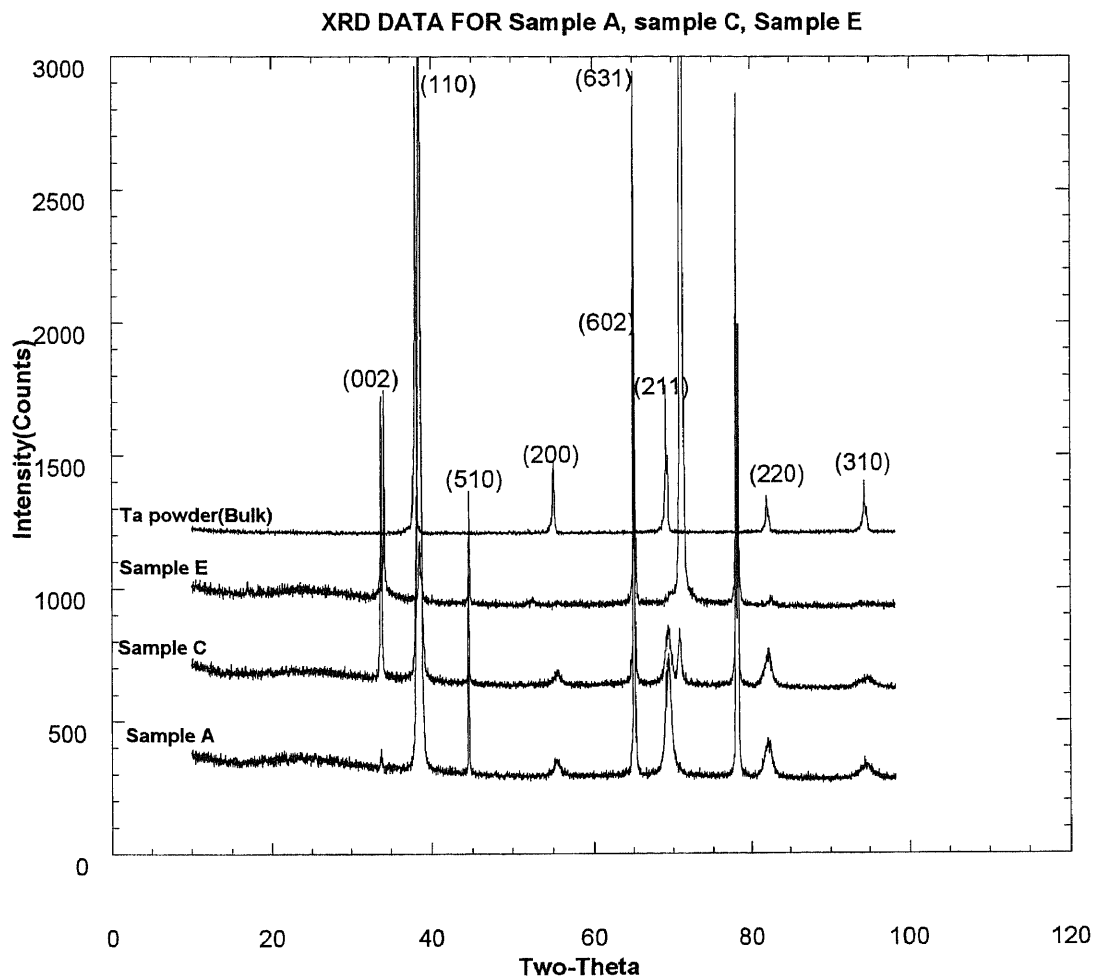
Fig. 4.7 X-ray Cu K_α diffractometer scan for Ta-coatings on steel substrate

For samples A, C and E x-ray diffraction pattern shows equal amounts of (110) oriented bcc peak and (631) oriented beta-peak. All the three samples showed very strong bcc (211) peaks thus making it very difficult to predict the degree of preferred orientation. The unindexed reflection in the diffraction profile corresponds to steel(major iron phase) with miller indices of reflection as (211) for iron.
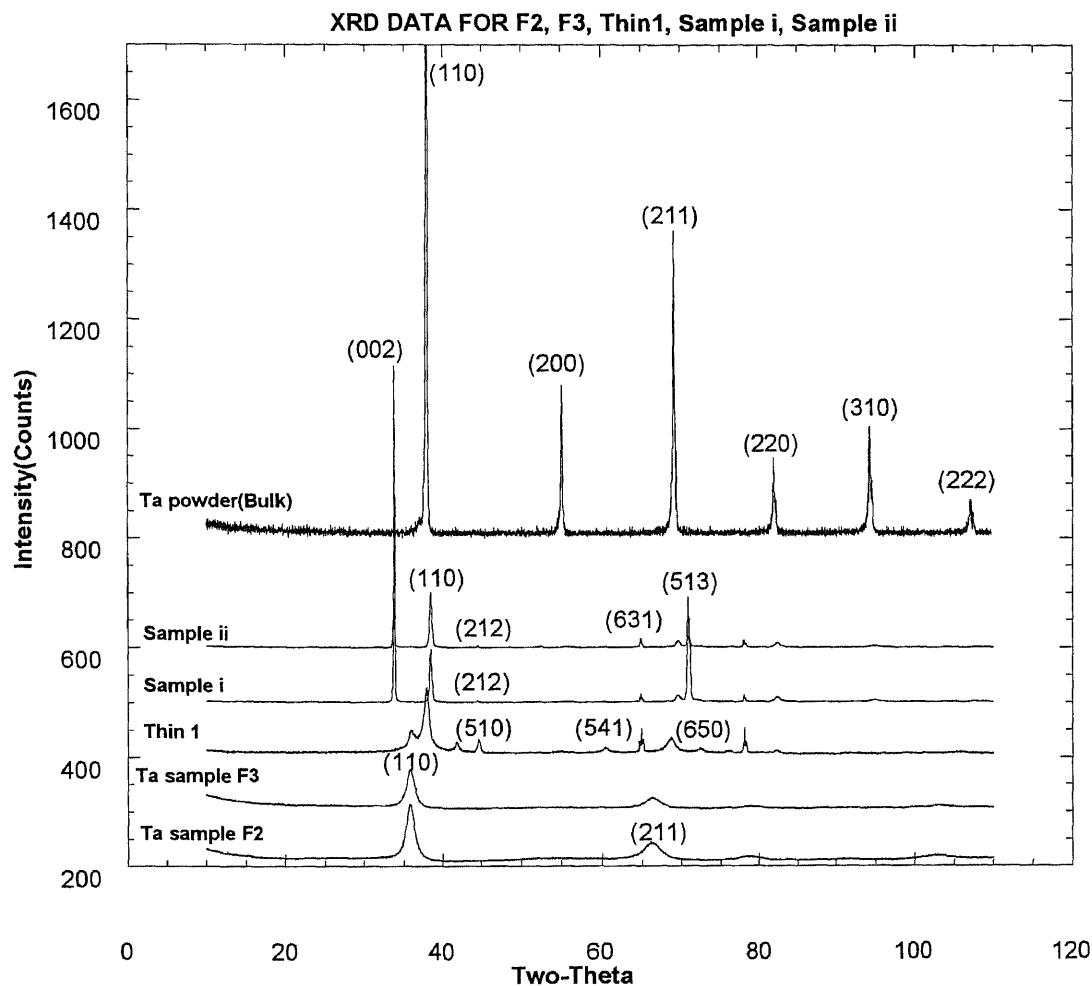
Fig. 4.8 X-ray Cu K_α diffractometer scan for Ta-coatings on steel substrate

For Samples i and ii the x-ray diffraction spectra showed a very strong beta (002) peak as compared to beta(212) relflection thus indicating a strong degree of preferred orientation in the (001) direction. For samples TS F2 and TS F3 observed spectra showed similar trends as observed in bulk tantalum. Sample thin 1 showed very weak reflections of the beta phase (510,541,650) and very strong (110) peak. The intensity of beta tantalum peak (002, 513) in sample i and sample ii was stronger as compared to thin 1.
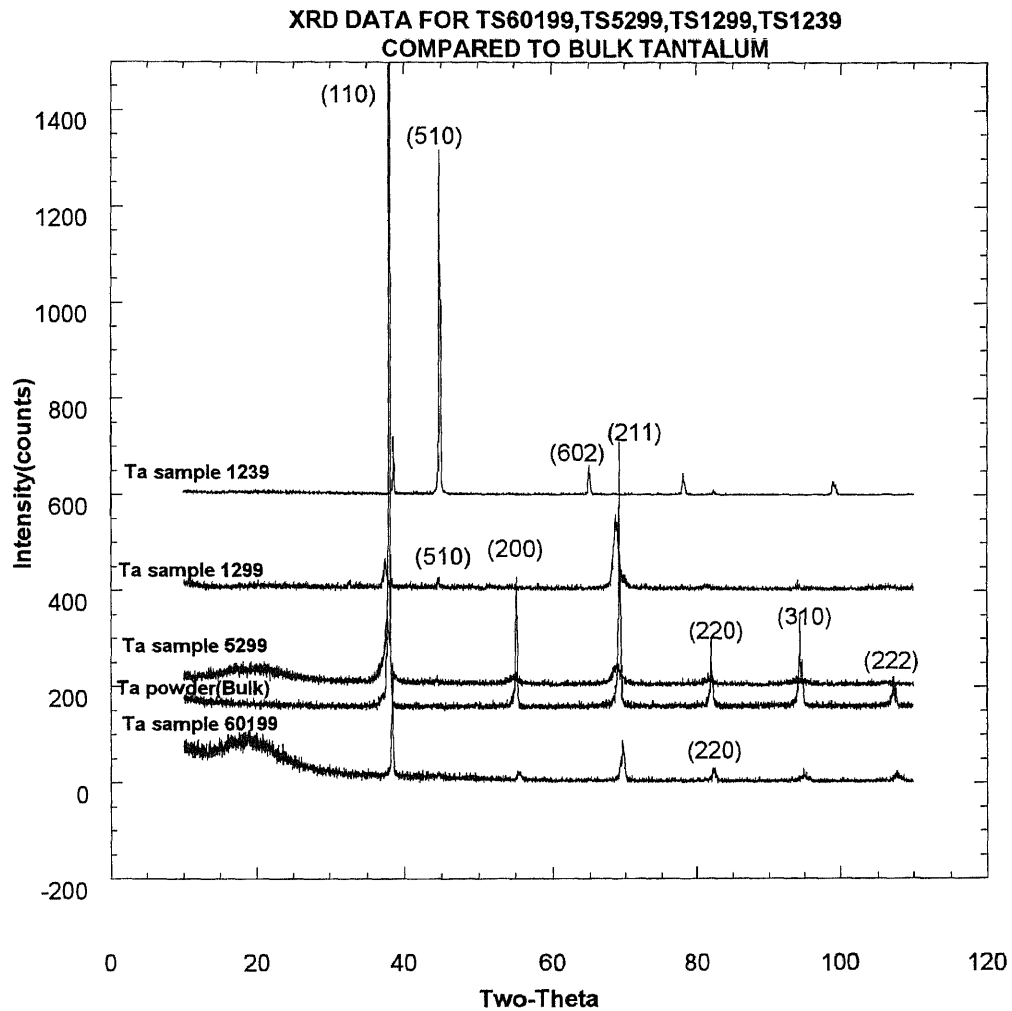
Fig. 4.9 X-ray Cu K_α diffractometer scan for Ta-films deposited on steel foils

Samples TS 60199, TS 5299, TS 1299 showed similar trends as observed in bulk tantalum (110, 200,211,310,222). Sample TS 1239 showed diffraction peaks corresponding to both bcc tantalum (110,211) and beta-tantalum (510,602). In TS 1239 the intensity of the beta tantalum peak is much higher than the bcc tantalum thus indicating that the mixture is predominantly beta tantalum.

Table 4.1 Cell Constants, Crystallite Size and Lattice Strain for Tantalum Coatings

SAMPLE NAME	(hkl)	RI (%)	a(A)[a]	% α:β	CRYSTALLITE SIZE[b]	LATTICE STRAIN[c]
TA POWDER	(110) α	100	3.344	100:0	-	-
	(200) α	15.1	3.33		-	-
	(211) α	29.7	3.316		-	-
	(220) α	7.8	3.319		-	-
	(310) α	10.8	3.316		-	-
	(222) α	1.6	3.314		-	-
TA FOIL 0.5 mm	(110) α	9.6	3.359	100:0	4199	0.076
	(200) α	100	3.3378		2239	0.089
	(211) α	35.7	3.329		2410	0.062
	(220) α	0.4	3.3228		351	0.195
	(310) α	0.6	3.3253		194	0.288
	(222) α	5.9	3.3055		1117	0.067
TA FOIL 1 mm	(110) α	51.3	3.35	100:0	-	-
	(200) α	100	3.333		-	-
	(211) α	40.3	3.326		-	-
	(220) α	5.6	3.3206		-	-
	(310) α	26.3	3.317		-	-
	(222) α	4.533.	3.3058		-	-
ALPHA SAMPLE	(110) α	5.8	3.257	98:2	1054	0.170
	(200) α	-	-		-	-
	(211) α	100	3.307		4845	0.041
	(220) α	76.1	3.305		-	-
	(310) α	-	-		-	-
	(222) α	-	-		-	-
	(510) β	16.6	10.183			
TS S1	(110) α	100	3.309	100:0	300	0.439
	(200) α	1	3.317		561	0.210
	(211) α	11.4	3.312		1208	0.094
	(220) α	6	3.313		479	0.152
	(310) α	1.4	3.31		195	0.285
	(222) α	0.8	3.314		372	0.149

Table 4.1 (cont.)

SAMPLE NAME	(*hkl*)	RI (%)	*a(A)*	% α:β	CRYSTALLITE SIZE	LATTICE STRAIN
ARGON SAMPLE	(110) α	100	3.26621	90:10	351	0.382
	(200) α	1.6	3.3183		-	-
	(211) α	0.8	3.3242		689	0.138
	(220) α	16.1	3.2844		2634	0.049
	(310) α	0.6	3.2918		-	-
	(222) α	2	3.2937		670	0.095
	(212) β	5	9.9490			
	(510) β	2.8	10.145			
	(431) β	1.7	10.214			
	(541) β	1.6	10.194			
NITROGEN SAMPLE	(110) α	100	3.3041	85:15	2111	0.108
	(200) α	30.7	3.2814		-	-
	(211) α	99	3.2985		970	0.108
	(220) α	12.6	3.2993		353	0.192
	(310) α	10.5	3.3095		976	0.084
	(222) α	18.3	3.3085		1118	0.067
	(322) β	33.7	10.494			
	(511) β	30.7	10.219			
	(601) β	30.7	10.240			
TS J4	(110) α	99.8	3.33	100:0	1401	0.145
	(200) α	-	-		-	-
	(211) α	5.4	3.33		-	-
	(220) α	-	-		-	-
	(310) α	-	-		-	-
	(222) α	0.7	3.34		827	0.083
BETA SAMPLE	(002)	100	5.174	0:100	-	-
	(513)	51	7.027		-	-

a. $a = d_{hkl} / (h^2 + k^2 + l^2)^{1/2}$; **b.** $L = K\lambda/B \cos\theta$; **c.** $e = B/4 \tan\theta$

4.2 Environmental Scanning Electron Microscopy/Energy Dispersive X Ray Spectroscopy (ESEM/EDX)

4.2.1 Scanning Electron Micrographs

The microstructure of the tantalum coating is very sensitive to deposition conditions.

Tantalum coatings frequently show a transition in microstructure, even with minor

variations in the deposition parameters. In the present study the deposition parameters

were nearly kept constant for most of the samples with some minor variations. Jerreat

et.al [28] has reported that the microstructure of tantalum coatings, vary from large,

irregular columnar grains with voids and etch pits to very small columnar grains with

many growth steps and spirals. To the unaided eye the former structure has a dull

appearance while the latter has a smooth and shiny finish. Some of the dendrite filaments

had flat tops and were thicker at the top than at the base.

In some cases the surface morphology became highly irregular. Here large and small

crystals grow alongside each other with many voids very much in evidence.

A J. Perry and colleagues [29] confirmed the presence of a "cauliflower" type structure

that has been observed in the present study also. Perry also defined the concept of

structure zones to classify the microstructure of thick evaporated films and sputtered

films. The zone classification is most conveniently discussed in terms of the predominant

process involved [30]:

- Zone I consist of an open structure with either columnar[30] or "cauliflower" growth [Fig. 4.10]depending upon whether substrate or gas stream process predominates.

- Zone II consists of a dense columnar structure with a smooth matte surface.

- Zone III consists of equi-axed grains of increasing size with a smooth shiny surface.

Between Zone I and II there is a transition zone T consisting of a dense array of poorly defined grains.

The "cauliflower" like structure is a substrate induced structure (zone I) is observed at high partial pressures while at higher speeds of the gas stream the gas stream induced open columnar structure is seen.

In the present course of study we encountered a variety of microstructures ranging from coatings showing a globular morphology with small crystallites protruding from the surface to a highly defined 'cauliflower' type structure. In some cases, dendritic and irregular growth is seen in some areas. Also present, are non-metallic inclusions, voids and etch pits. Most of the ESEM micrograph was taken at 50μ with the exception of some. The scanning electron micrographs were taken on Electroscan ESEM model 2020. More scanning electron micrographs of different tantalum coatings can be seen in Appendix E.
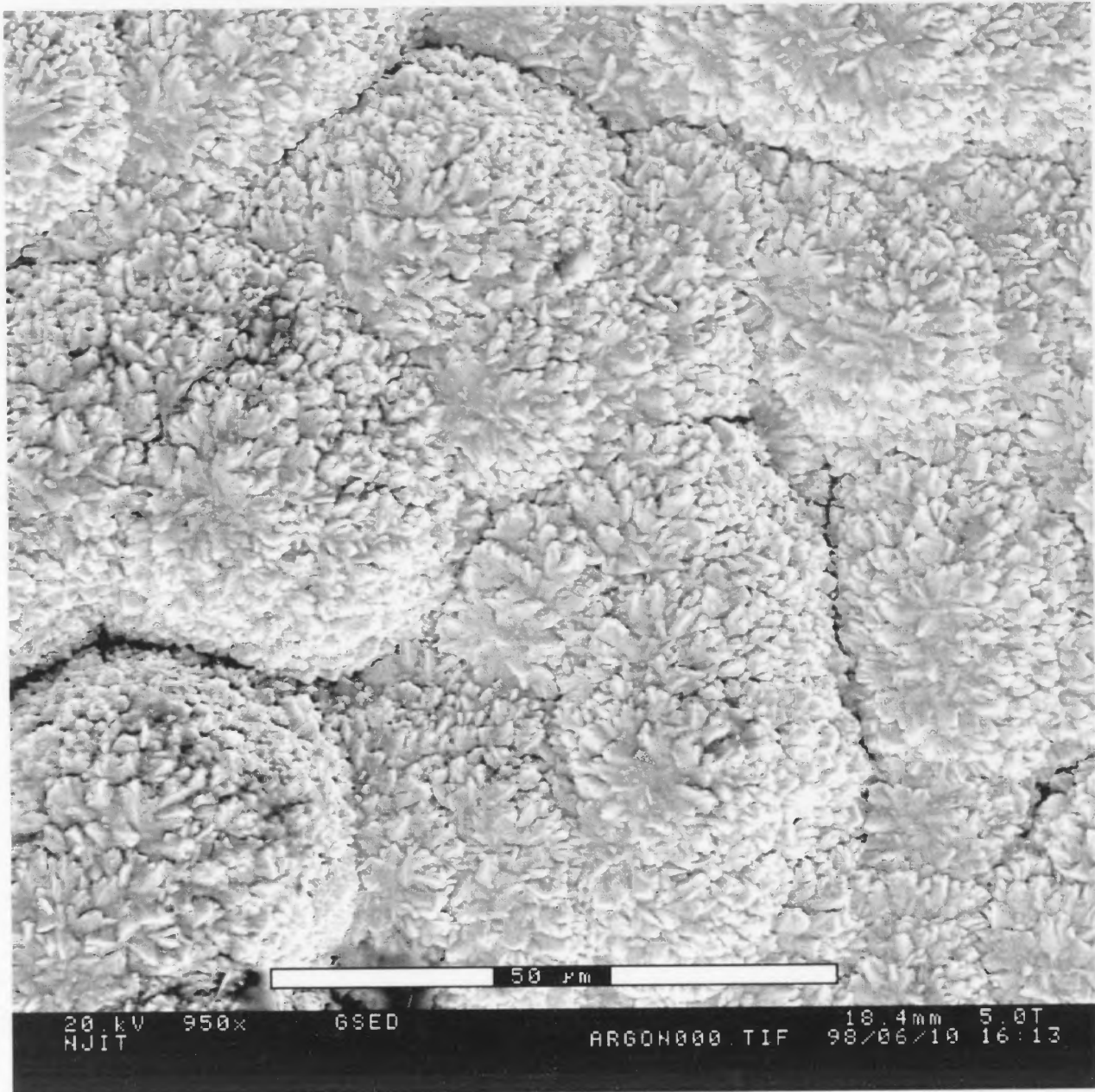
Fig. 4.10 ARGON SAMPLE
Scanning electron micrograph showing a 'cauliflower' type structure observed at high partial pressures
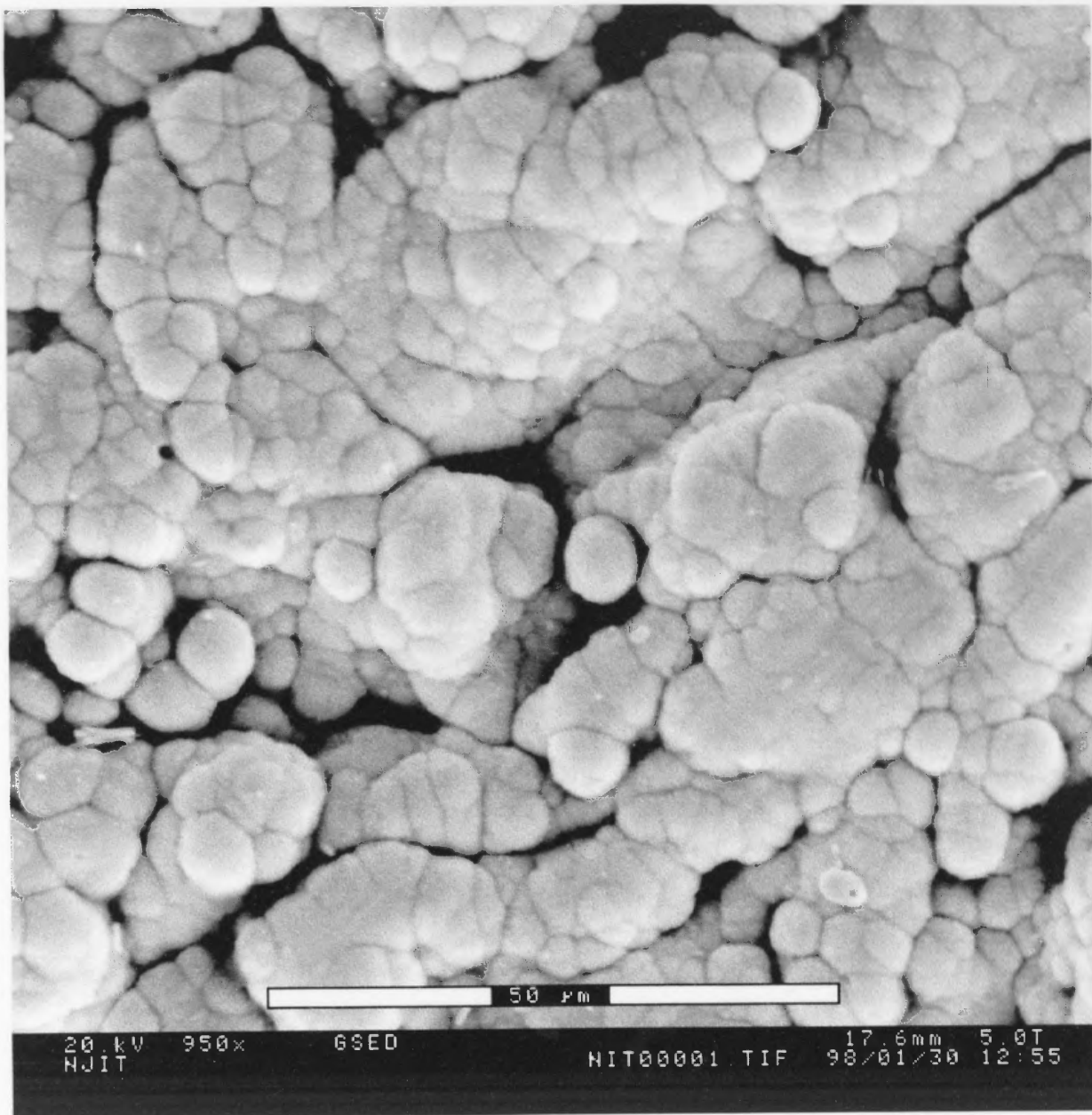
Fig. 4.11 NITROGEN SAMPLE
Scanning electron micrograph showing a globular morphology (small globules) protruding from the surface
which could be a result of the post treatment involving nitrogen gas
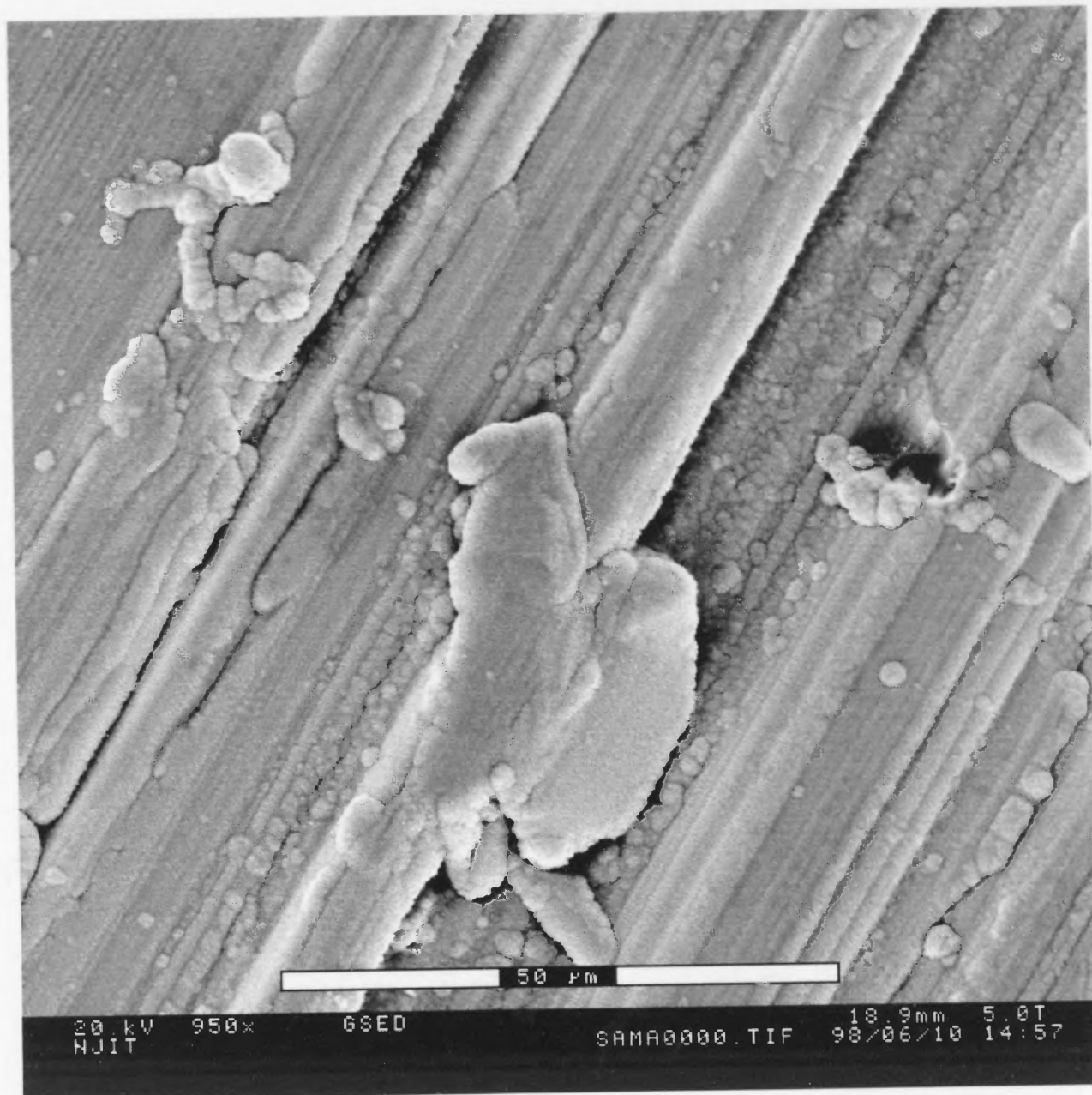
Fig. 4.12 SAMPLE A

Scanning electron micrograph showing filamentary growth and dendritic growth in some areas
Filamentary growth in this sample could be influenced by very short deposition times during the course of
deposition and is along the direction of machining and polishing of the steel substrate
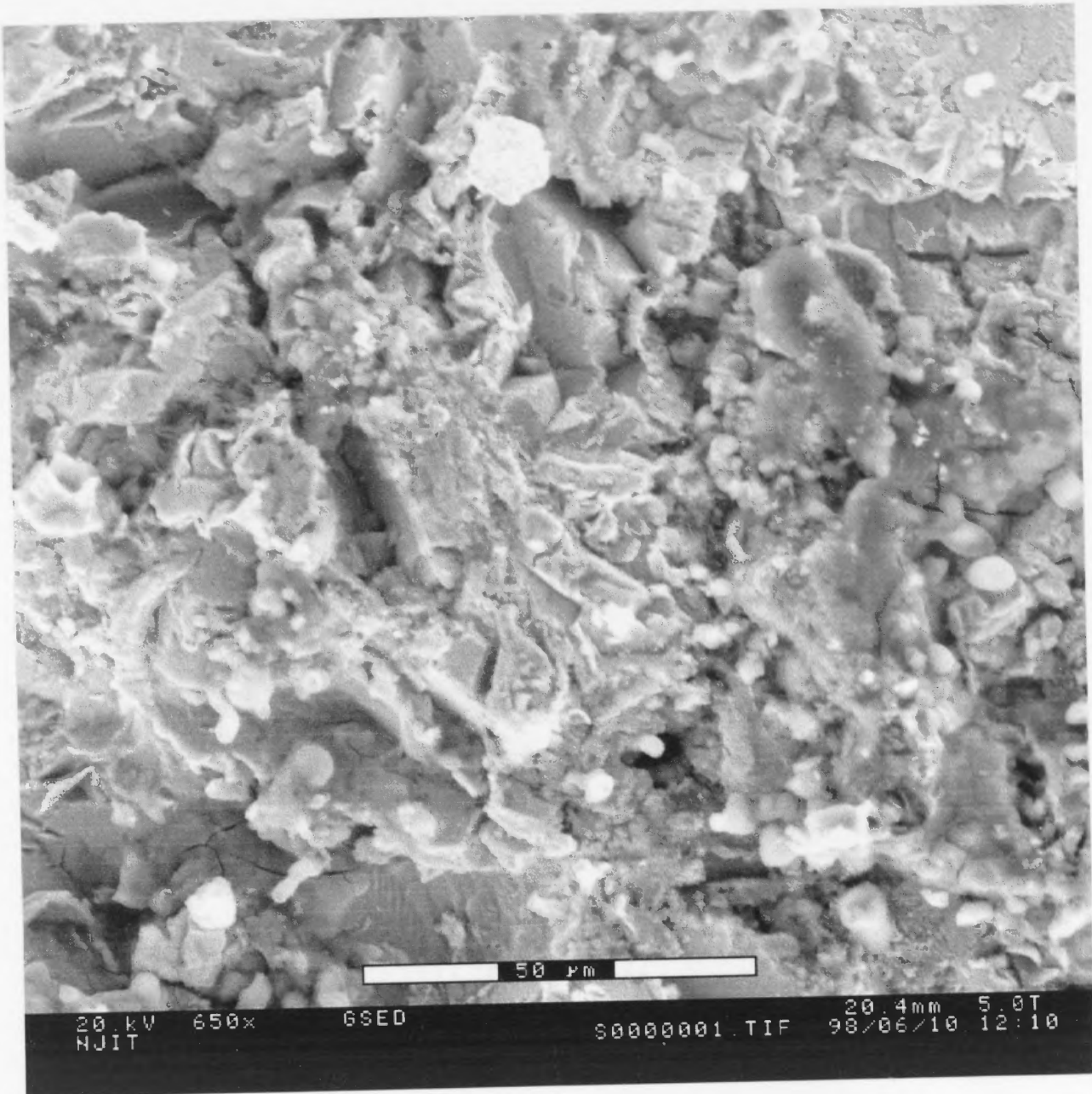
Fig. 4.13 TANTALUM SAMPLE S1

Scanning electron micrograph showing highly irregular grains, here the surface morphology has become highly irregular with large and small sized crystals growing alongside each other with voids very much in evidence. These structures could be due to high speed at which the argon gas is purged in the chamber.
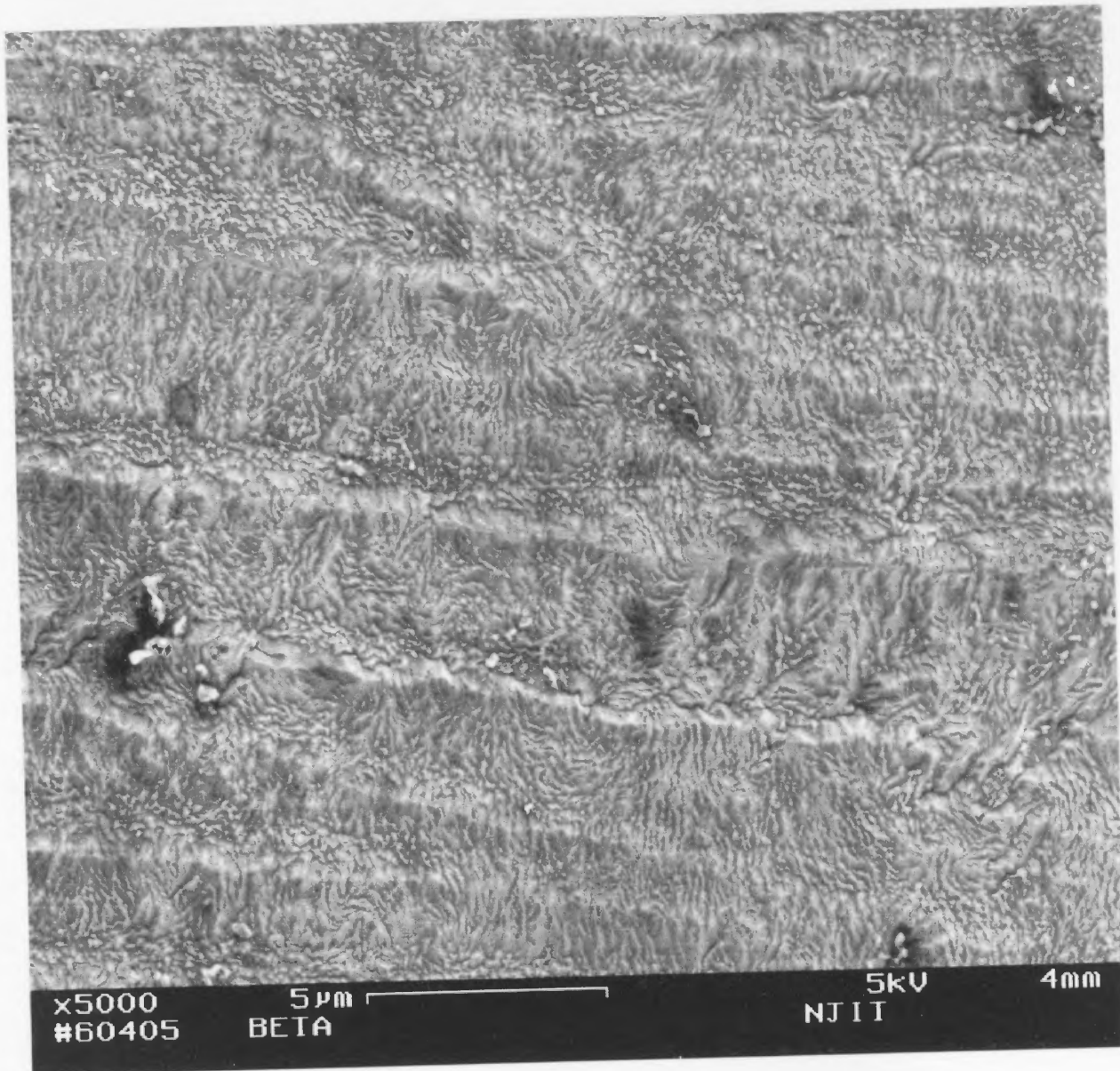
Fig. 4.14 BETA SAMPLE
Scanning electron micrograph of a tantalum coating with 100% beta phase showing a high degree of
preferred orientation and showing high degree of texture. Deposition conditions not known.
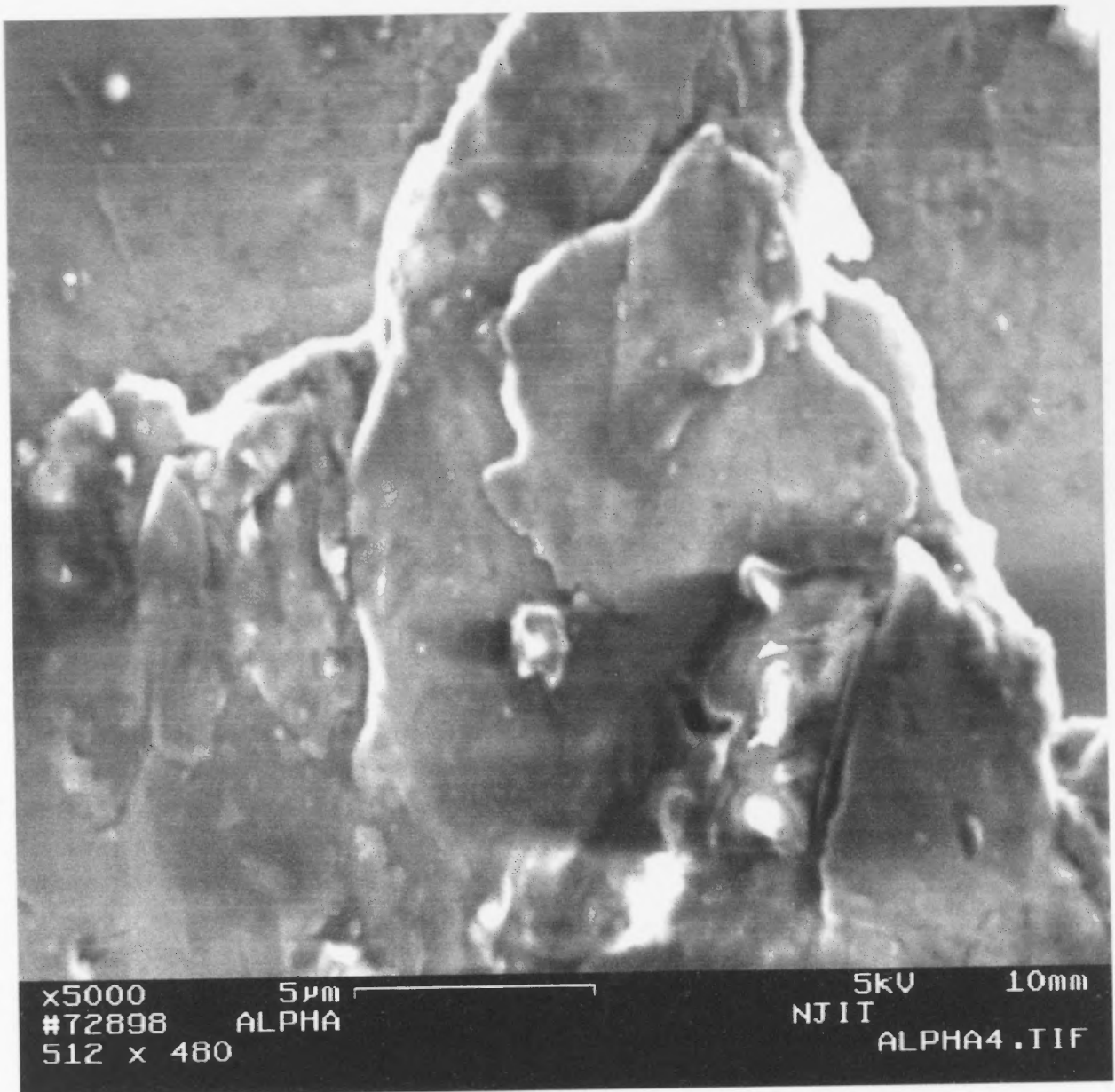
Fig. 4.15 ALPHA (PURE BCC) SAMPLE
Scanning electron micrograph showing step growth surface morphology and the deposits have a smooth and a shiny finish. Deposition conditions not known.

4.2.2 Study of Interface Between Tantalum Coating and Steel Substrate

A polished cross section of the tantalum coating was used to study the interface between tantalum and steel. For this purpose a 0.5" square tantalum coating was cross- sectioned using the least aggressive cutting method. A Buehler Isomet (fig.4.16) with a diamond impregnated brass cutting wheel was used for this purpose. The sample was secured in the cutting fixture with the Ta coating facing the diamond cutting wheel.

Fig. 4.18 Schematic of a Cutting Wheel

This was done so as to prevent any separation of the coating, at the interface of the coating and the substrate or within the coating itself, due to the force of the cutting operation. The diamond wheel was lubricated with ethylene glycol to prevent any heat die during cutting from altering the steel/Ta morphology. After cutting the metallographic sample was cleaned using acetone and compressed air. The freshly cut surface was then mounted in a thermal setting epoxy for subsequent metallographic preparation and examination. The remaining section was examined under a conventional stage microscope. This examination was specifically aimed at the coating surface and along the edge of the freshly cut surface.
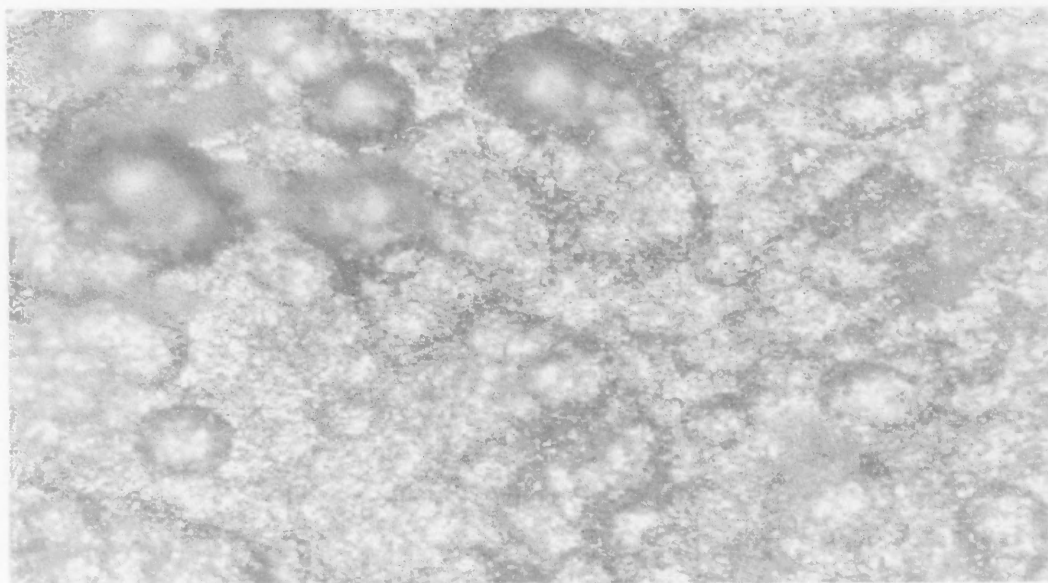
Fig. 4.17 Optical image of the Surface of the Coating (the grains appear dimpled because of non uniform deposition throughout the surface 200X)
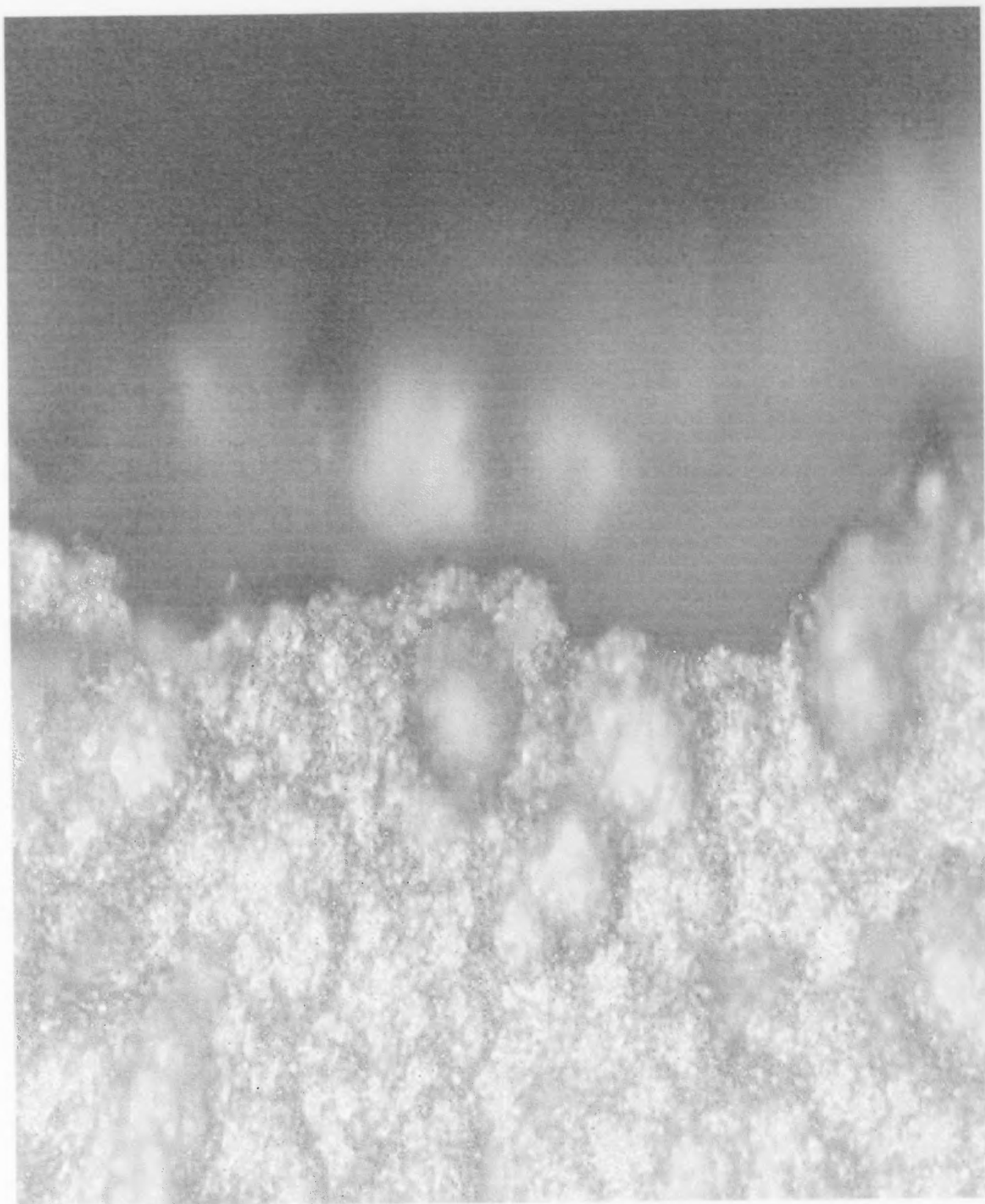
Fig. 4.18 Optical image of the edge of the cut surface (appears to rough or jagged). The coating appears to have fractured around the edges of the dimples because of higher stresses around the dimples (200X)

The surface of the steel substrate was extremely rough (fig.4.19) and there appeared to be numerous areas of nonmetallic inclusions present at the interface, as well as numerous voids and discontinuities. These inclusions could be oxides, however additional testing was necessary to verify the nature of their chemical species.

nonmetallic inclusions   voids
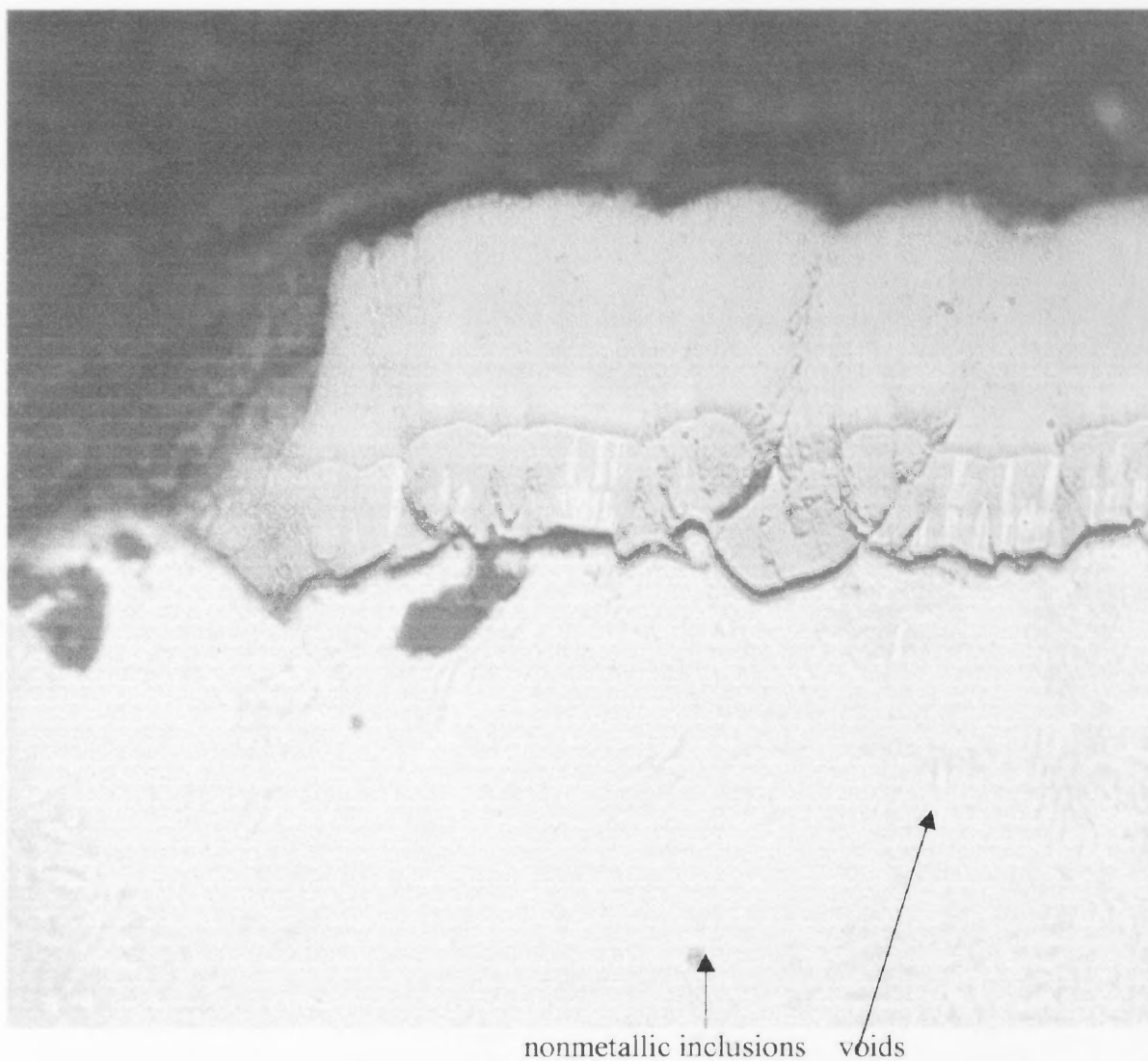
Fig. 4.19 Optical Image of the Surface of the Steel Substrate

The tantalum coating consisted of two individual layers of tantalum (fig. 4.20). The first, closest to the substrate, appears to consist of both α- Ta (alpha phase) and β-Ta (beta phase). It appears that the majority of the initial coating is alpha phase with fingers of the beta phase running perpendicular to the substrate. The second layered coating appears to be all alpha phase. The initial coating is between 0.64 to 0.88 mils thick (16 to 22 microns). The second layer was found to be 1.6 mils thick, (40 microns).

fingers of beta phase   alpha phase(40μ)   alpha phase($16-22\mu$)
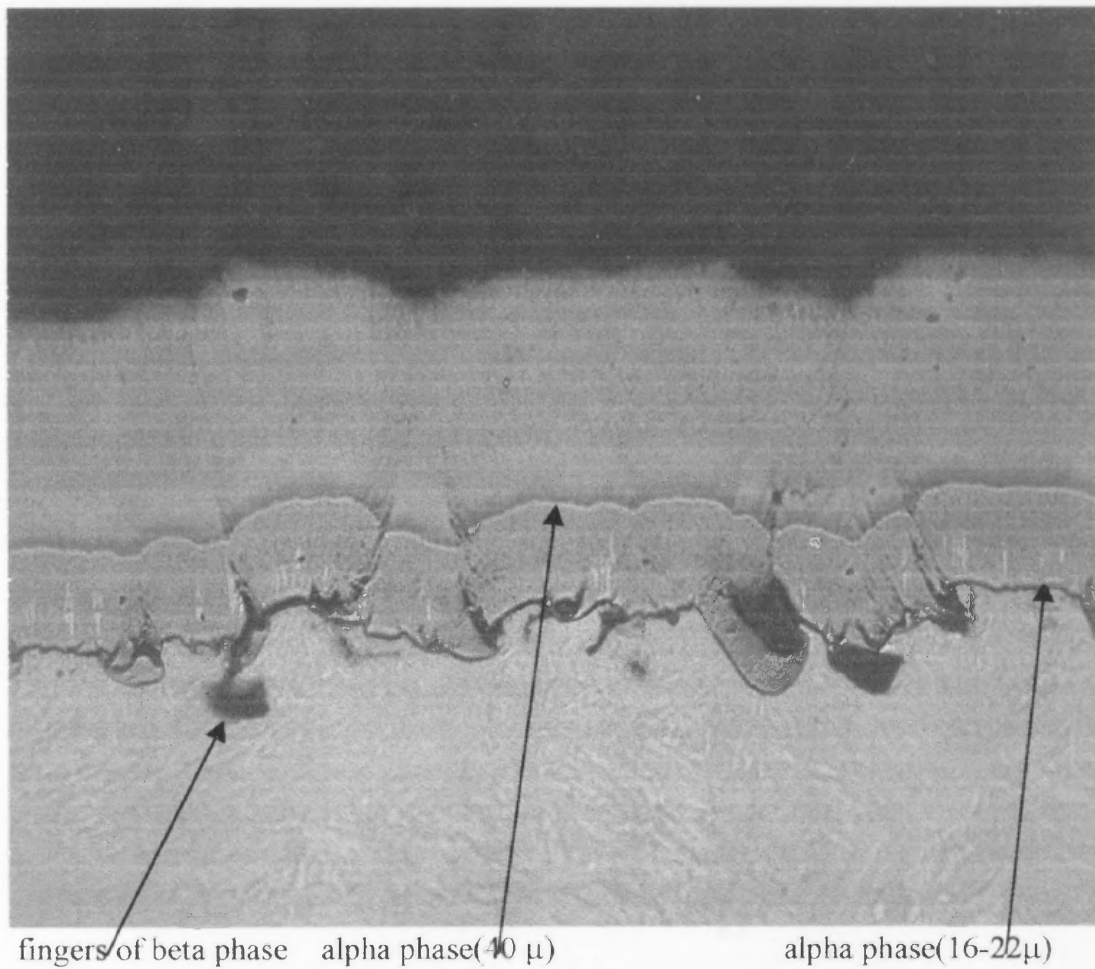
Fig. 4.20 Optical Image of the Tantalum Coating

Both the layers of tantalum coating appear to have numerous nodules, some of

which initiate at the interface, while others occur randomly within either layer

(fig.4.21)

nodules present randomly within either layer
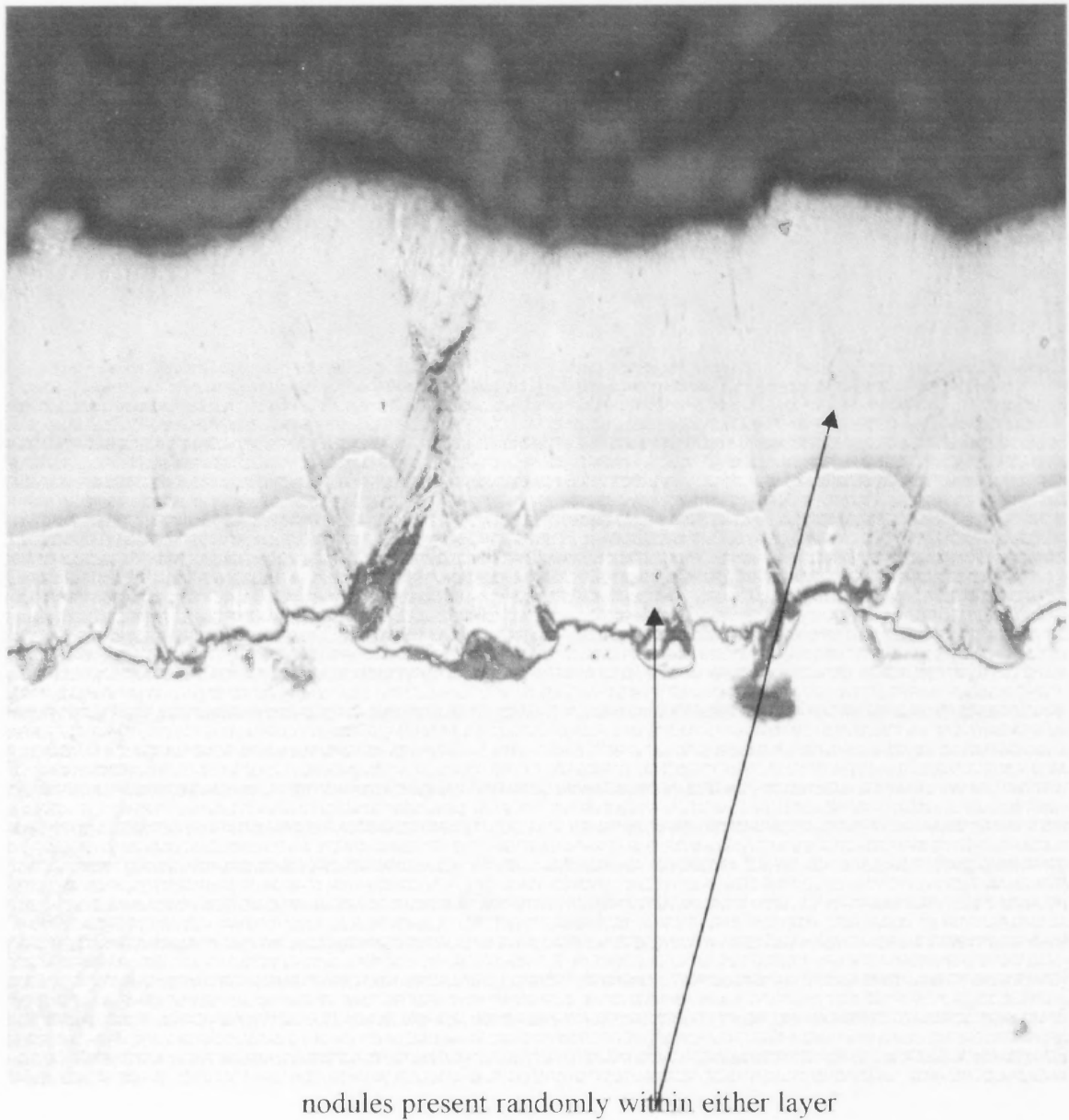
Fig. 4.21 Optical Image of Tantalum Coating

4.2.3 Energy Dispersive X Ray Spectroscopy

EDX is used for the determination of elemental composition and quantitative information of the local composition of the material. This analysis is used in conjunction with ESEM imaging, thereby allowing analysis to be directly performed on areas under electron beam observation.

EDX (energy dispersive spectroscopy) on tantalum coatings was performed using Kevex Sigma TM Quasar microanalyser attached to the ESEM unit. The tantalum coatings had high purity. Minor traces of argon, oxygen, sulfur and chlorine was also found. Iron peaks were seen for almost all samples, thus confirming that the coatings were not uniform. This result is consistent with the scanning electron micrographs. Since the steel substrate consist mostly of iron, the EDX spectrum showed iron peaks. The presence of chlorine peak can possibly be a result of inadequate rinsing of the steel substrate during specimen cleaning, prior to deposition. Argon was used as residual gas used during sputtering and thus its presence in some samples can be explained. The EDX spectrum for coatings has been attached for reference in the following pages.

EDX SPECTRUM FOR ALPHA, ARGON, Ta FOIL AND TS S1
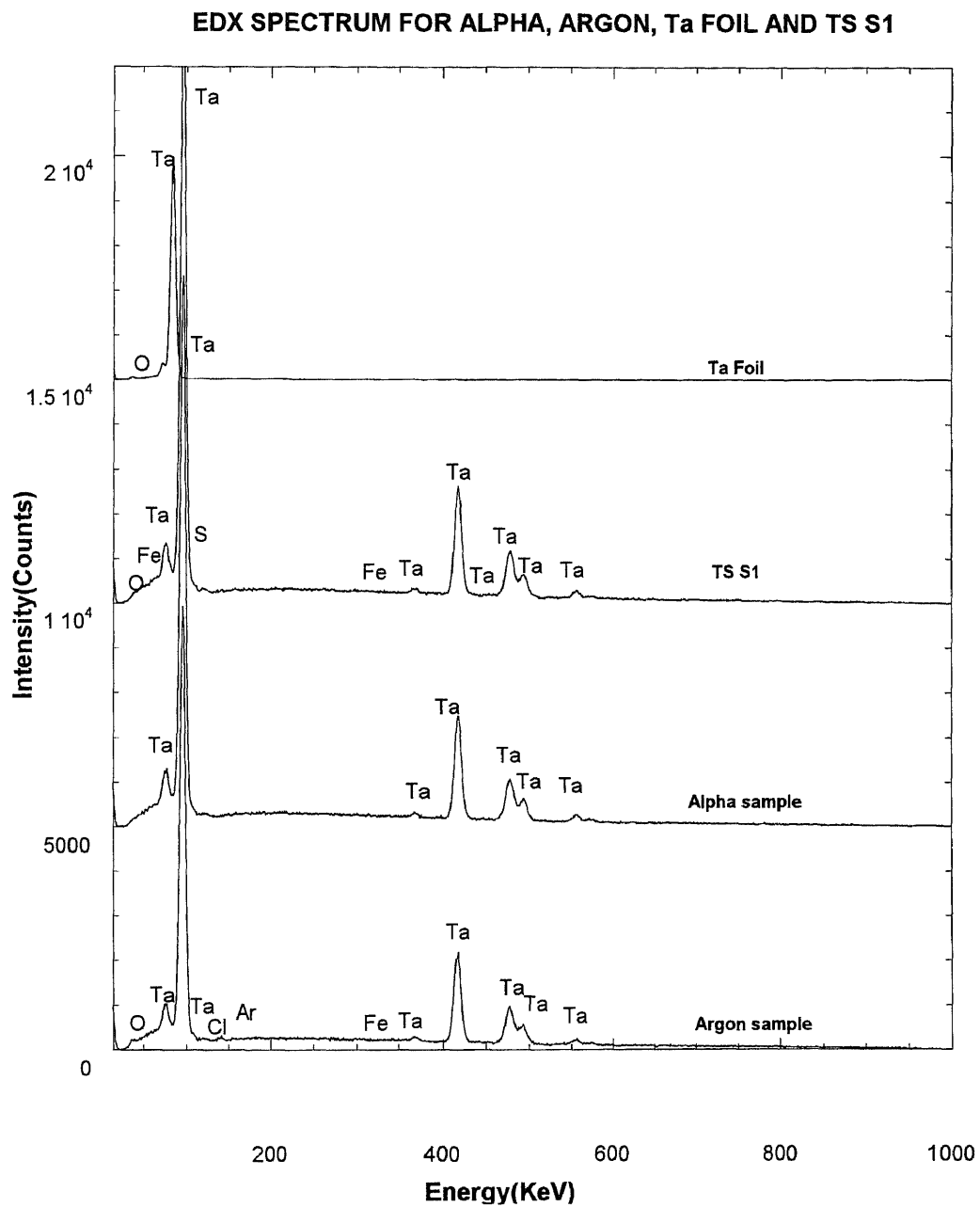
Fig. 4.22 EDX spectrum for different tantalum coatings on steel substrates

EDX SPECTRUM FOR BETA,NITROGEN,TS J4 AND TS J5

Ta

2 10⁴

1.5 10⁴

Intensity(Counts)

Ta

Ta   Ta

Ta   Ta   Ta   Ta

Ta   Ta   Ta   Ta   Ta   Beta sample

1 10⁴

Ta   S
O   TaCl   Ta   Fe Ta   Ta   Ta   Ta   TS J5

Ta

Ta

Ta   S
O   TaCl   Fe Ta   Ta   Ta Ta   Ta   TS J4

5000

Ta

Ta   S
O Zn   TaCl   Fe Ta   Ta   Ta   Ta   Nitorgen sample

0

200   400   600   800   1000

Energy(KeV)
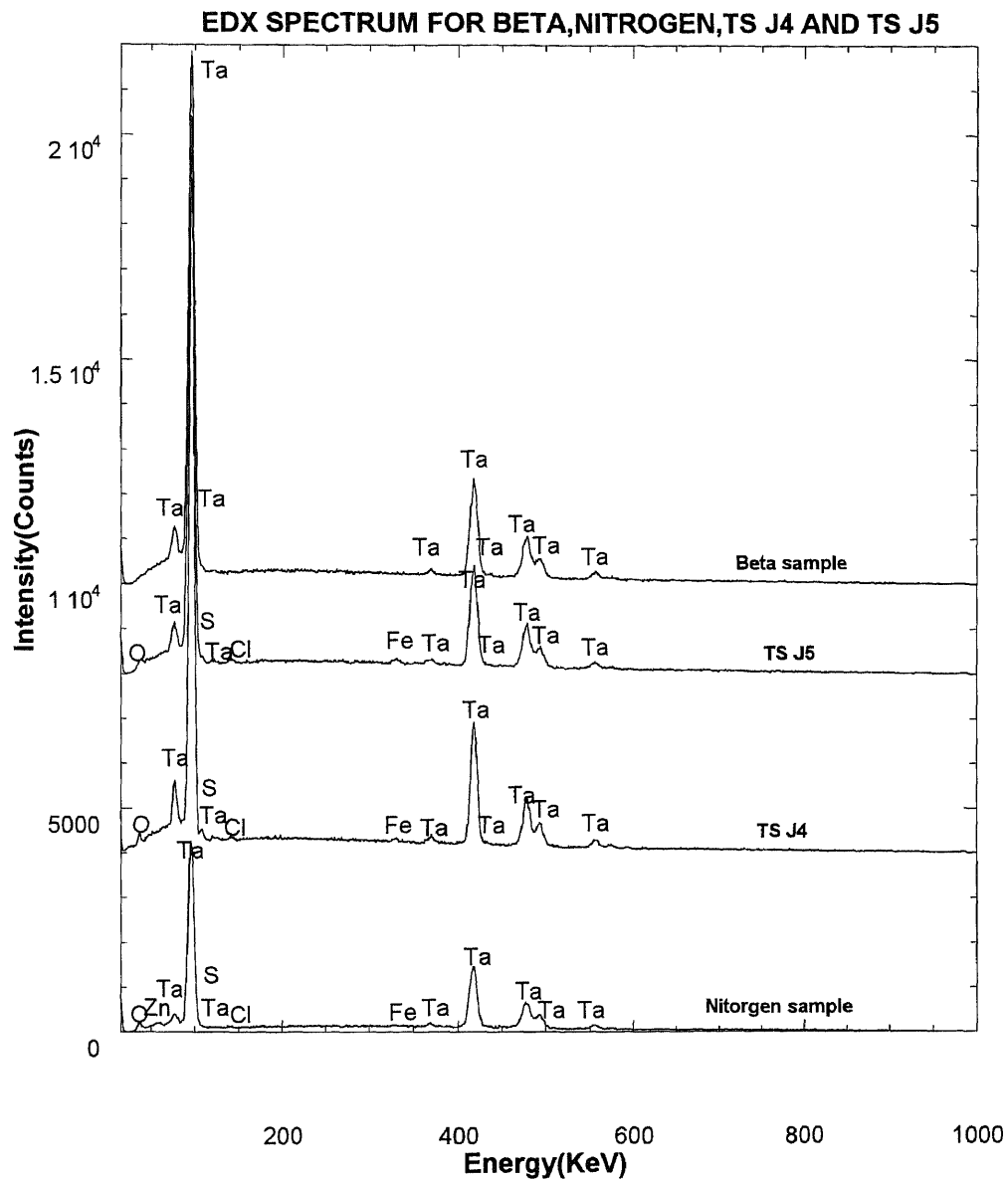
Fig. 4.23 EDX spectrum for tantalum coatings on steel substrates

4.3 X Ray Fluorescence

The X -ray fluorescence measurements for tantalum coatings were conducted using

Phillips X -ray spectrometer PW 2400R Sr. No. DY 825. X -ray fluorescence can be used

to identify and quantify the elements present in an unknown sample. Here the x-ray beam

is used to excite the specimen and the x-ray spectral lines of the elements in the specimen

are detected. For tantalum coatings, the qualitative analysis confirmed the presence of

tantalum, iron, sulfur, phosphorus and other elements present in steel. These results are in

concurrence with the results obtained by EDX measurements. The presence of elements

having an atomic number below 9 cannot be detected using XRF as it is beyond the

sensitivity of this equipment. Hence elements like Oxygen (Z=8), Nitrogen (Z=7), Boron

(Z=5 present in steel), could not be determined using XRF, even though their presence

was detected using EDX. In the present study the XRF was primarily used to quantify the

tantalum present in the coating and thereby establish a basis for the purity of the tantalum

coating. The XRF results were quantitatively obtained for tantalum by plotting a

calibration standard for tantalum powder in varying concentrations ranging from 95% to

100% pure tantalum powder. Tantalum pentoxide in known quantities was added as an

impurity in preparing the standard. By controlling energy of the penetrating x ray beam, x

-rays were allowed to penetrate only up to the tantalum film thickness. By using this

method we have been only able to quantify tantalum and have assumed that the balance

present are impurities, depending on different samples. In some samples, even though

there were no impurities, tantalum could not be quantified up to a 100%. This could be

due to errors in calibration that may have arisen from the instrument or from the

specimen [15]. The results of the XRF for tantalum coatings are reported in Table 4.2.

Table 4.2 XRF Quantitative Results for Tantalum Coatings

SAMPLE NAME	XRF QUANTITATIVE ANALYSIS RESULTS CONCENTRATION IN %
TA1	Ta=99.112% balance impurities
TAF2	Ta=99.139% balance impurities
TAF3	Ta=97.421% balance impurities
SAMPLE A	Ta=99.034% balance impurities
SAMPLE C	Ta=98.846% balance impurities
SAMPLE E	Ta=99.107% balance impurities
SAMPLE I	Ta=99.248% balance impurities
SAMPLE II	Ta=99.070% balance impurities
TS C1	Ta=99.561% balance impurities
TS J4	Ta=97.231% balance impurities
TS J5	Ta=98.001% balance impurities
TS K	Ta=99.902% balance impurities
TS S1	Ta=97.821% balance impurities
TS 11	Ta=99.316% balance impurities
ARGON SAMPLE	Ta=98.770% balance impurities
NITROGEN SAMPLE	Ta=98.945% balance impurities
TANTALUM FOIL 0.5 MM	Ta=99.773% balance impurities
TANTALUM FOIL 1MM	Ta=99.610% balance impurities
PURE BCC TANTALUM	Ta=99.966% balance impurities
PURE BETA TANTALUM	Ta=99.91% balance impurities

4.4 X- Ray Absorption Spectroscopy

The XAFS measurements were carried out at the National Synchrotron Light Source

(Brookhaven National laboratory, Upton, NY) on beam line X-11A using Si (111) double

crystal monochromator. The harmonic contamination was minimized by detuning the

incident intensity by 20%. The slit size of the beam was 1 mm (vertical) by 10 mm

(horizontal). Data, at the tantalum L_3 edge, was taken using the standard transmission

mode for tantalum powder and standards [Appendix C, fig. C2]. The films were

measured in fluorescence mode using a Lytle detector and argon gas [Appendix C, fig.

C3] equipped with nickel filter ($\mu t= 3$). Samples were positioned 45° to the incident

radiation beam (I_o). Soller slits was equipped between filter and detector to reject elastic

scatter. The XAFS data was collected over a range of 6900 to 8200 eV. For the alpha

sample, beta sample and tantalum foil, the extended fine structure appearing above the

tantalum L_3 absorption edge (9881 eV) were also measured using normal (with respect to

the film plane) incident radiation. The EXAFS data were subjected to established analysis

procedures [31-32] which included removal of a background, normalization of the

extended fine structure to the absorption edge step energy and height, conversion to

photoelectron wave vector (k) space, and Fourier transformation to radial r- coordinates.

By looking at the Fourier transforms of different samples one can qualitatively compare

different samples by the size of the FT, the width of the FT. To obtain quantitative

measurement of the average near-neighbor environment around tantalum atoms, the

entire range of 2.0 to 16.989Å was Fourier filtered to k space and fitted using theoretical

spectra. The theoretical EXAFS spectra were generated using FEFF 7 codes developed

by Rehr and co-workers [33]. This analysis allows the calculation of the average

coordination number, radial distance and Debye-Waller factors and higher order

corrections (C_3 and C_4) for shells when distorted, of atomic shells around tantalum atoms

in all the samples.
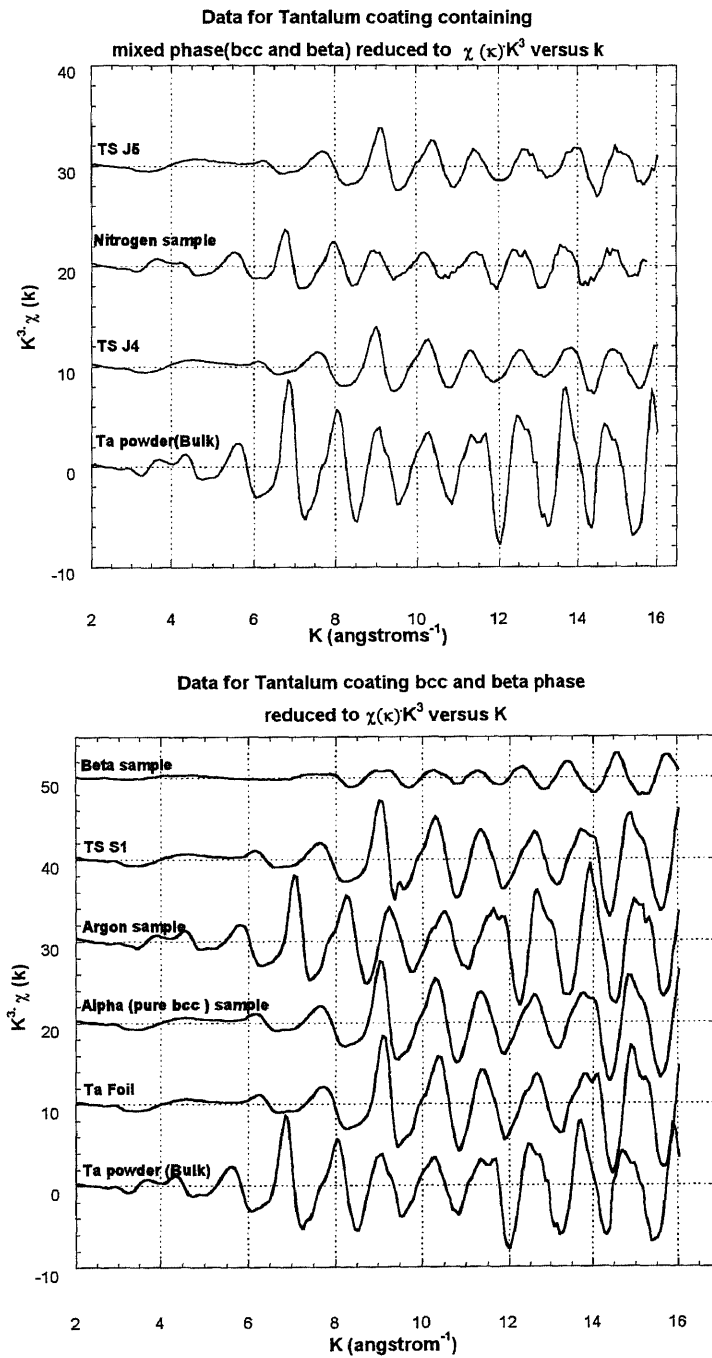
Fig. 4.24 χ (k) * k^3 for tantalum coatings, tantalum foil and tantalum powder

Fourrier Transorm [k³·χ (k)] versus Radial Coordinate

Filtered from 2.0 to 16.989 angstrom⁻¹
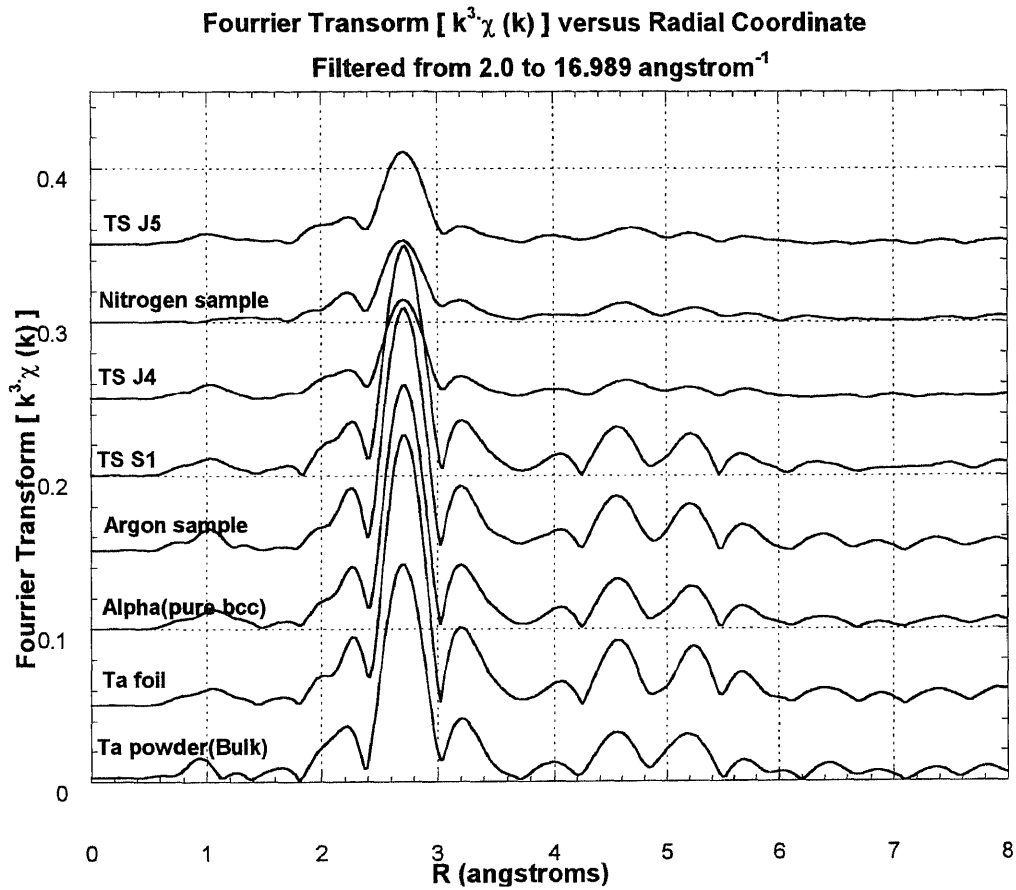
Fig. 4.25 Fourier transformed Tantalum EXAFS data for tantalum coatings, foil and bulk (k ranges of 2.0 to 16.989 Å⁻¹ with k^3 weighing, applied to the Fourier transformation)

The general characteristics of the above data suggests that all coatings have structures similar to the bulk tantalum powder and suggests that the tantalum is present as a bcc structure and not as disordered structure. However samples J4, J5and Nitrogen exhibit significant disorder.

Fourier Transform [k³·χ (k)] versus Radial Coordinate

Filtered from 2.0 to 14.0 angstrom⁻¹
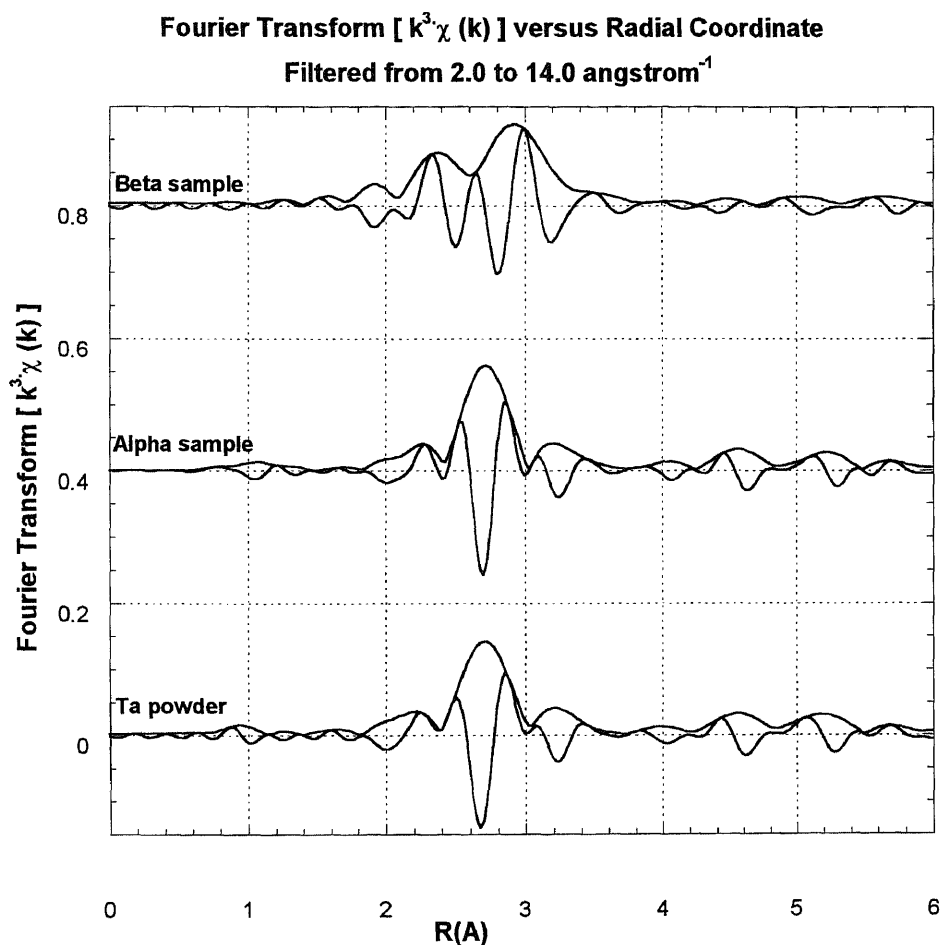
Fig. 4.26 Fourier transformed (magnitude and imaginary part) Tantalum EXAFS data for tantalum coatings, foil and bulk (*k* ranges of 2.0 to 16.989 Å^{-1} except beta sample for which k range is 2.0 to 14.0 Å^{-1} with k^3 weighing, applied to the Fourier transformation)

By comparing the general characteristics of the above data it is evident that the beta sample is disordered structure and has a multi component first shell while the alpha sample is comparable to bulk tantalum powder. This tells us that alpha sample has a bcc structure similar to the bulk and the beta sample has a highly disordered structure.

Fourier [k³·χ(k)] versus Radial Coordinate

Filtered from 2.0 to 16.989 angstrom⁻¹
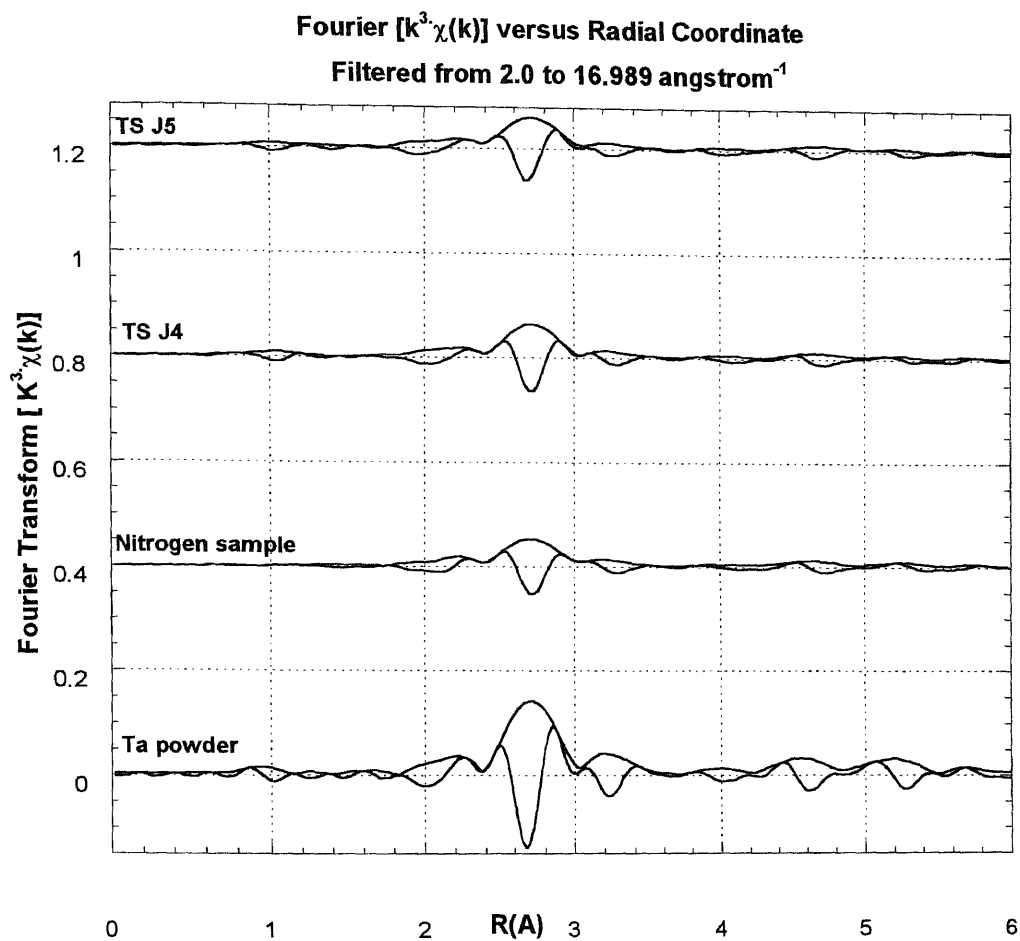
Fig. 4.27 Fourier transformed (magnitude and imaginary part) Tantalum EXAFS data for tantalum coatings, foil and bulk (k ranges of 2.0 to 16.989 Å⁻¹ with k^3 weighing, applied to the Fourier transformation)

The deviation from a pure bcc structure is observed in the above sample's which suggests

that these coatings may have some degree of distortion when compared to the bulk.

Fourrier transform [k³·χ (k)] versus Radial Coordinate

Filtered from 2.0 to 16.989 angstrom⁻¹
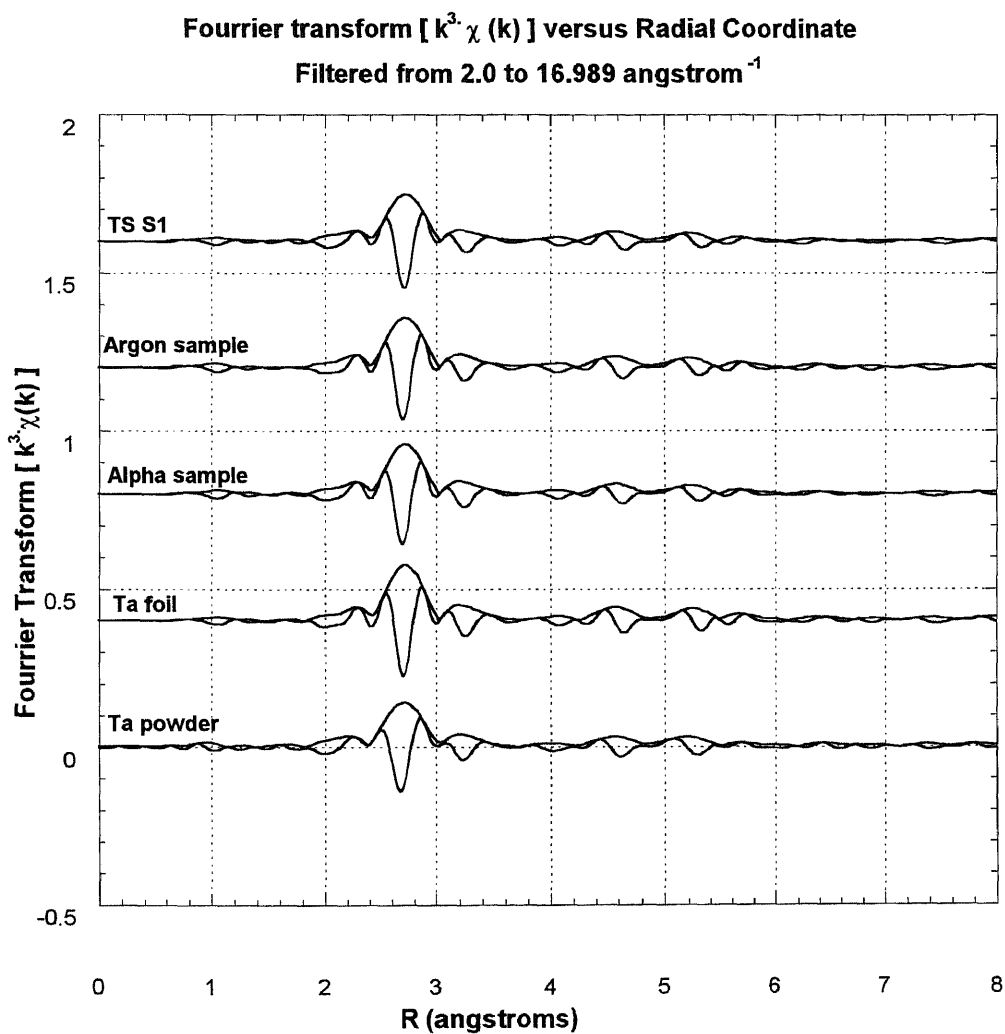
Fig. 4.28 Fourier transformed (magnitude and imaginary part) Tantalum EXAFS data for tantalum coatings, foil and bulk (k ranges of 2.0 to 16.989 Å^{-1} with k^3 weighing, applied to the Fourier transformation)

The general characteristics of the above data suggests that all coatings have structures similar to the bulk tantalum powder and suggests that the tantalum is present as a bcc structure and not as disordered structure.

Multishells Fits of Fourier Transform to Tantalum Data

_____ FT magnitude data   ...... FT model data
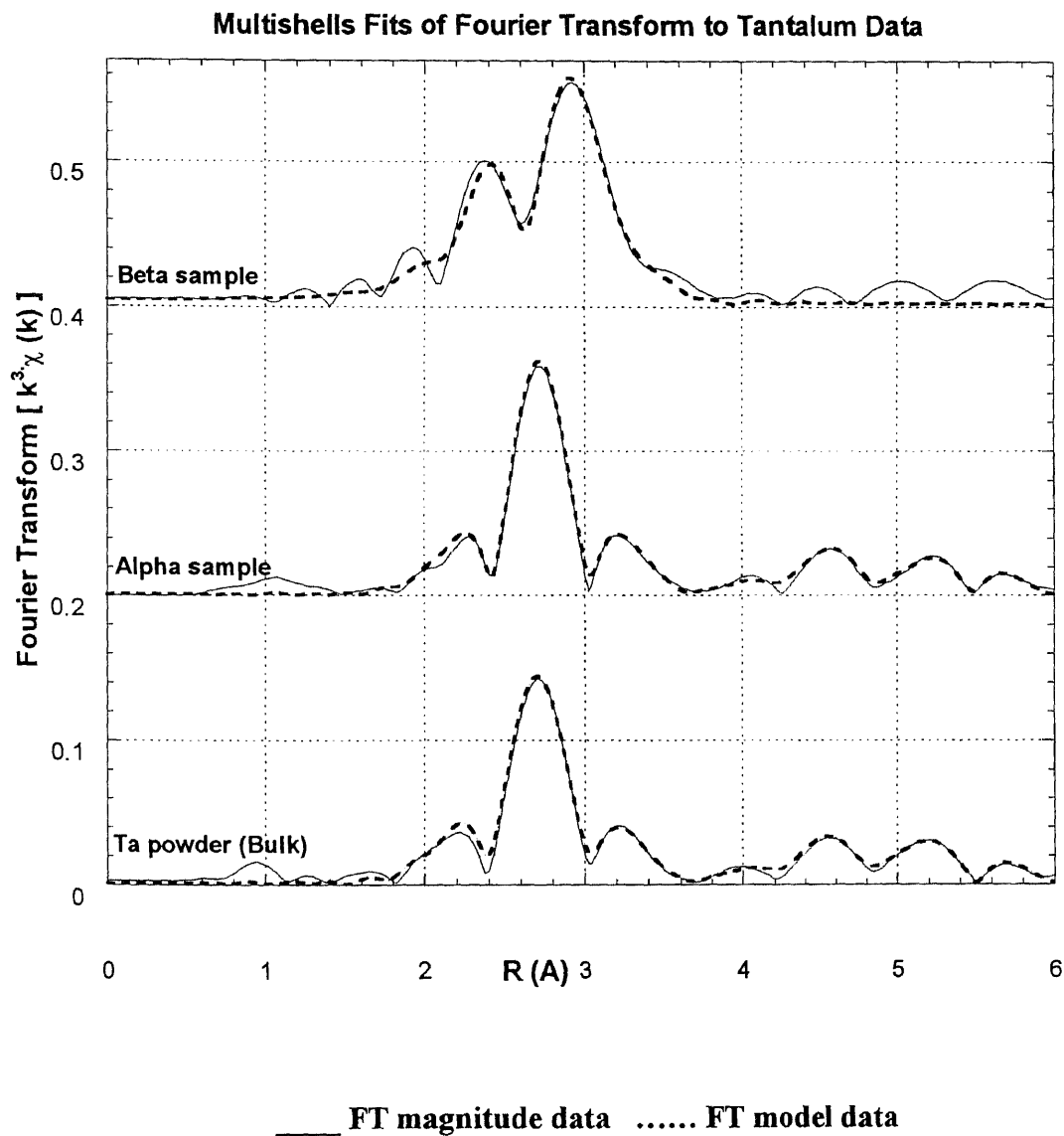
Fig. 4.29 Fourier transform along with curve fit where the solid lines represent the experimental data and the dotted lines represent fits to the data using the FEFF standards

Results of the fitting analysis indicate that the radial distance from Ta atom to its first nearest neighboring Ta atom is $2.86 \pm 0.001\text{Å}$. This results are very much in concurrence with the XRD analysis and comparison of the values of bond distances obtained from XRD and EXAFS analysis are presented in Table 4.3 & 4.4.
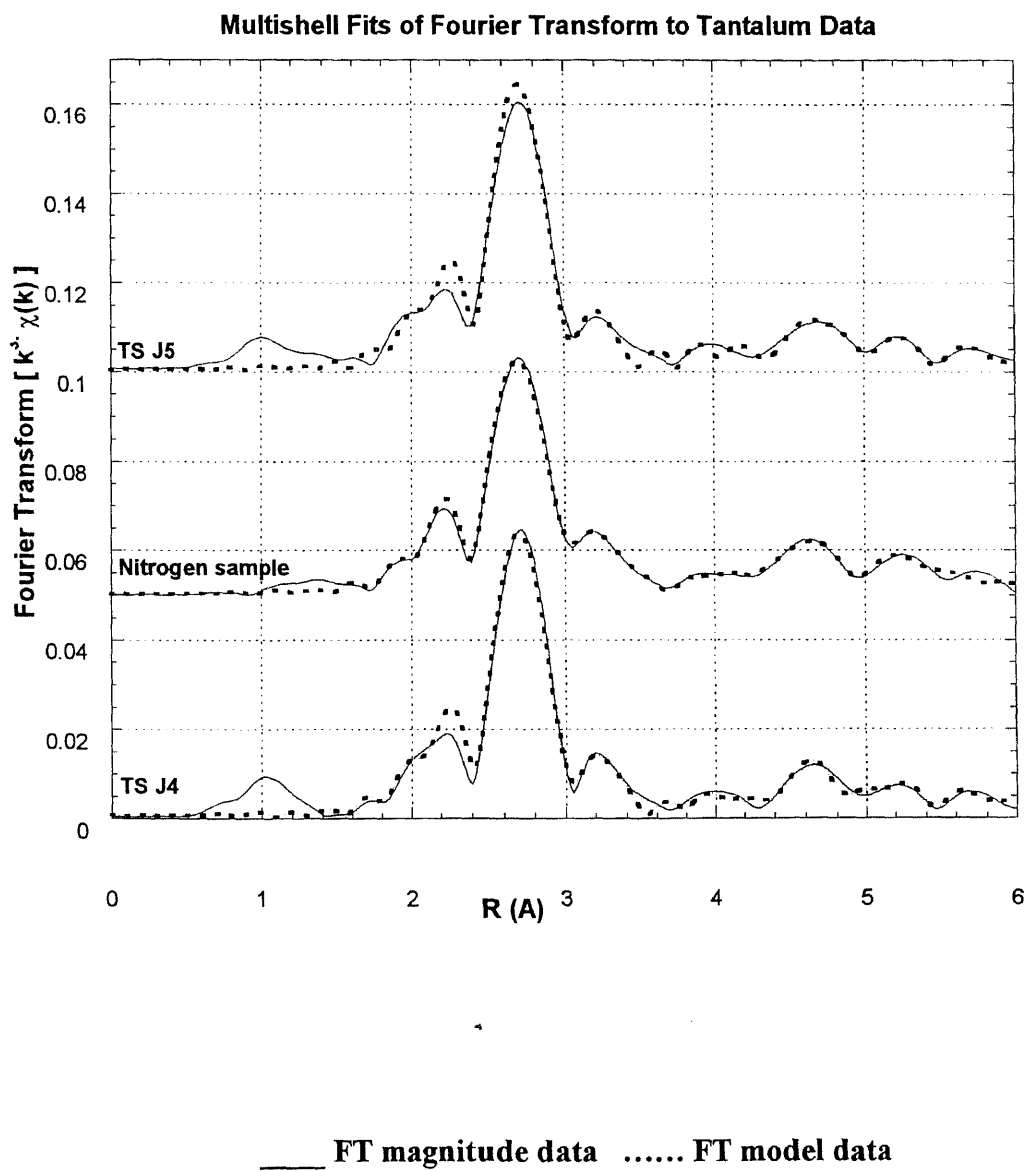
Fig. 4.30 Fourier transform along with curve fit where the solid lines represent the experimental data and the dotted lines represent fits to the data using the FEFF standards

Multishells Fits of Fourier Transform to Tantalum Data

_____ FT magnitude data ...... FT model data
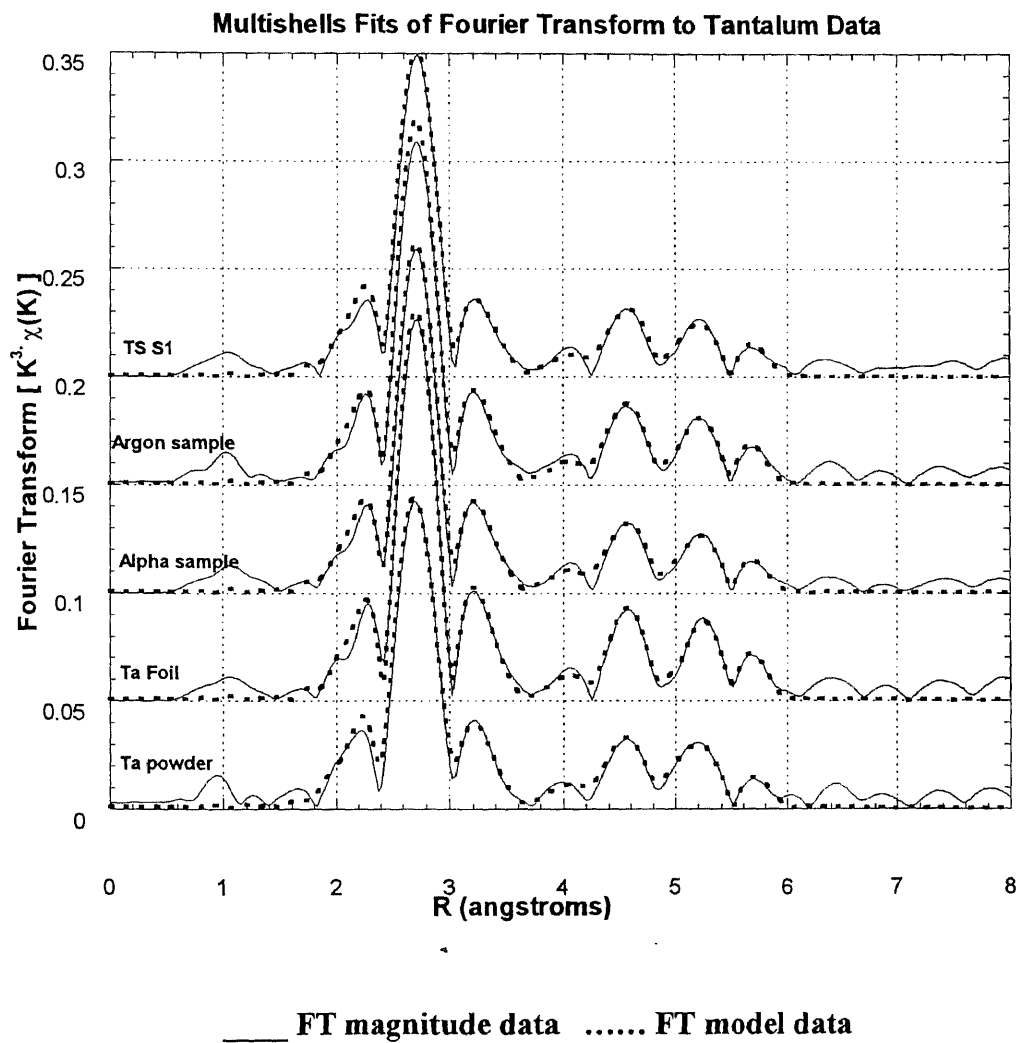
Fig. 4.31 Fourier transform along with curve fit where the solid lines represent the experimental data and the dotted lines represent fits to the data using the FEFF standards

4.4.1 Discussion of the EXAFS Analysis

For the analysis of samples which had nearly 100% bcc phase the coordination number

(N) and S_o^2 were fixed during fitting, while parameters like radial distance (R), E_o and σ

were allowed to vary. Samples alpha, argon, TS S1, tantalum foil exhibited structures

similar to the bulk tantalum powder. Slight variations in the bond distances can be

attributed to the presence of stresses in these films when compared to the bulk. This

factor is very much evident while comparing the tantalum foil with the bulk tantalum.

The width of the first shell for tantalum foil is more when compared to the bulk, thus

indicating some degree of deformation in the structure and this is reflected in the increase

of the radial distances in all the three shells. The radial distance for samples nitrogen, J4

and J5 is slightly larger than the bulk and this could be because of the presence of a

mixture of both phases; beta phase and bcc phase, although the beta phase is present in

very much smaller concentrations. The radial distances for samples alpha and TS S1 is

the same as that of bulk tantalum thus indicating that these two samples are nearly 100%

bcc tantalum.

In case of the beta sample, higher order corrections (C_3 and C_4 cumulants) were also

introduced because the structure showed significant disorder. In addition, the peak around

2 Å is split into an unresolved doublet indicating the presence of two close-by shells or

two or more phases containing either an impurity like Nitrogen or it could possibly be a

completely different arrangement of tantalum atoms themselves. In the present study the

choice of impurities have been eliminated. Fits for beta tantalum were done by assuming

different atomic ratios for the first two shell: SC (2:4), fcc (6:6), and distorted bcc.

The best fit was obtained while assuming that there are 4 atoms in the first shell and 6

atoms in the second shell. Hence the coordination number for the first two shells was co-

related in the ratio of 2:3. The S_o^2 was fixed during fitting, while parameters like radial

distance (R), E_o and σ were floated. In case of the beta sample no significant peaks are

observed beyond $\approx 4\text{Å}$ in the Fourier transform. In all the FT transforms the peak near 1

Å is probably spurious in nature and it may be attributed to errors in background removal

or multiple electron edges in the background.

The XANES region has been plotted for tantalum powder, alpha sample and beta sample

[Appendix C, Fig. C4] and for all the three samples the region is similar. This can be

explained because the average radial distances for beta sample is 2.83 Å while for

tantalum powder and alpha sample the values are 2.85 Å and 2.86 Å respectively. Thus

for beta sample the volume is maintained (16.9g/cc) in spite of the distortions in the

structure.

The value for the radial distances (bond distances), E_o and σ^2 are listed in Table 4.3

For all sample the bond distances values from XRD and EXAFS techniques are

comparable and these results are listed in Table 4.4.

Table 4.3 R, σ^2 And E_0 in the XAFS Fits for Tantalum Coatings

SAMPLE NAME	SHELL 1(N=8)	SHELL 2 (N=6)	SHELL 3 (N=12)
TA POWDER			
Distance R	2.851 ± 0.001	3.30 ± 0.003	4.516 ± 0.004
Sigma^2	0.0072 ± 0.0001	0.001 ± 0.0003	0.009 ± 0.001
E$_0$ Shift	0.1024 ± 0.306	0.1024 ± 0.306	0.102 ± 0.306
TA FOIL (45°)			
Distance R	2.862 ± 0.001	3.308 ± 0.0009	4.69 ± 0.001
Sigma^2	$0.007 \pm 2.62\times10^{-5}$	0.009 ± 0.0001	0.009 ± 0.000147
E$_0$ Shift	0.645 ± 0.155	0.645 ± 0.155	0.645 ± 0.155
TA FOIL (45°)			
Distance R	2.85 ± 0.0144	3.325 ± 0.125	4.713 ± 0.0295
Sigma^2	0.009 ± 0.001	0.01235 ± 0.002	0.0195 ± 0.003
E$_0$ Shift	1.107 ± 3.983	1.107 ± 3.983	1.107 ± 3.983
ALPHA (45°)			
Distance R	2.86 ± 0.0008	3.308 ± 0.001	4.68 ± 0.003
Sigma^2	$0.0071 \pm 3.96\times 10^{-5}$	0.009 ± 0.0001	0.001 ± 0.0002
E$_0$ Shift	0.251 ± 0.243	0.251 ± 0.243	0.251 ± 0.243
ALPHA SAMPLE (parallel)			
Distance R	2.850 ± 0.0039	3.308 ± 0.0060	4.679 ± 0.03824
Sigma^2	0.0085 ± 0.0006	0.009974 ± 0.002698	0.011141 ± 0.003292
E$_0$ Shift	0.508 ± 1.104	0.508 ± 1.104	0.508 ± 1.104
BETA SAMPLE (45°)			
Distance R	2.94 ± 0.0050	3.187 ± 0.154	-
Sigma^2	0.0098 ± 0.0045	0.014 ± 0.005	
E$_0$ Shift	21.90 ± 6.96	21.90 ± 6.96	
3rd cumulant	-0.00013 ± 0.0007	0.0019 ± 0.0001	
4th cumulant	-0.0004 ± 0.0001	$-7.74\times10^{-6} \pm 4.98\times10^{-5}$	
BETA SAMPLE (normal)			
Distance R	2.910 ± 0.0042	3.187 ± 0.005	-
Sigma^2	0.0014 ± 0.0074	0.0045 ± 0.0076	
E$_0$ Shift	31.50 ± 5.953	31.50 ± 5.953	
3rd cumulant	-0.0003 ± 0.0005	0.00177 ± 0.0002	
4th cumulant	-0.00019 ± 0.0003	$2.656\times10^{-6} \pm 5.76\times10^{-5}$	

Table 4.3 (cont.)

SAMPLE NAME	SHELL 1 (N=8)	SHELL 2 (N=6)	SHELL 3 (N=12)
ARGON SAMPLE			
Distance R	2.85 ± 0.002	3.30 ± 0.004	4.67 ± 0.004
Sigma^2	$0.007 \pm 7.9 \times 10^{-5}$	0.001 ± 0.0002	0.001 ± 0.0003
E$_0$ Shift	2.421 ± 0.347	2.421 ± 0.347	2.421 ± 0.347
TS S1			
Distance R	2.86 ± 0.0007	3.31 ± 0.00096	4.69 ± 0.0071
Sigma^2	$0.007 \pm 5.269 \times 10^{-5}$	0.0099 ± 0.037	0.009 ± 0.0006
E$_0$ Shift	0.9296 ± 0.152	0.9296 ± 0.152	0.9296 ± 0.152
NITROGEN SAMPLE			
Distance R	2.87 ± 0.002	3.21 ± 0.014	4.8128 ± 0.0459
Sigma^2	0.010 ± 0.0004	0.018 ± 0.001	0.018 ± 0.0048
E$_0$ Shift	-1.13 ± 0.57	-1.13 ± 0.57	-1.13 ± 0.57
TS J4			
Distance R	2.86 ± 0.002	3.33 ± 0.0105	4.70 ± 0.0098
Sigma^2	0.008 ± 0.0001	0.011 ± 0.002	0.0115 ± 0.0006
E$_0$ Shift	-1.491 ± 0.524	-1.491 ± 0.524	-1.491 ± 0.524
TS J5			
Distance R	2.86 ± 0.0027	3.35 ± 0.0142	4.56 ± 0.280
Sigma^2	0.010 ± 0.0003	0.016 ± 0.001	0.018 ± 0.010
E$_0$ Shift	-1.38 ± 0.688	-1.38 ± 0.688	-1.38 ± 0.688

Table 4.4 Comparison of R (Bond Distance) Value Obtained from XRD Analysis and XAFS Analysis

SAMPLE NAME	SHELL 1 N=8	SHELL 2 N=6	SHELL 3 N=12
TA POWDER (BULK)			
XRD	2.878Å	3.323	4.699
XAFS	2.851 Å	3.299	4.516
TA FOIL			
XRD	2.884	3.337	4.720
XAFS	2.862	3.308	4.689
ALPHA (PURE BCC)			
XRD	2.851	3.313	4.652
XAFS	2.860	3.308	4.690
ARGON SAMPLE			
XRD	2.865	3.308	4.68
XAFS	2.852	3.299	4.67
TS S1			
XRD	2.866	3.313	4.69
XAFS	2.863	3.315	4.698
NITROGEN SAMPLE			
XRD	2.866	3.309	4.679
XAFS	2.874	3.215	4.813
TS J4			
XRD	2.882	3.333	4.71
XAFS	2.863	3.331	4.704
TS J5			
XRD	2.848	3.337	4.72
XAFS	2.869	3.353	4.565

Mechanical Properties

4.2 Adhesion

The adhesion measurements presented in this thesis have been obtained by means of the

Micro-Scratch Tester (MST up to 30N) and Revetest Automatic Scratch Tester (RVT

greater than 30N) [34-37] using a Rockwell C diamond (conical angle 120°;

hemispherical tip of 200 μm radius). This instrument is capable of inducing scratches

under either constant or linearly increasing load. For progressive loading, the critical load

L_c is defined as the smallest load at which a recognizable failure; for the constant loading

mode, the critical load corresponds to the load at which a regular occurrence of such

failure along the track is observed. The driving forces for coating damage in the scratch

test are combination of elastic-plastic indentation stresses, frictional stresses and residual

internal stresses. In the lower load regime, these generally result in conformal or tensile

cracking of the coating that still remains fully adherent. The onset of these phenomena

defines a first critical load. In the higher load regime, one defines another critical load

that corresponds to the onset of coating detachment from the substrate by spalling,

buckling or chipping. The instrument is also equipped with an integrated optical

microscope, an acoustic emission system and a device to measure the tangential frictional

force (in the scratching direction), giving friction coefficient value during scratching.

Here the critical load for a coating-substrate system can be determined by optical,

acoustical or mechanical methods. In the present study, in order to test all the samples

with the same conditions, the scratch test for all samples was performed using similar set

of conditions. For both MST and RVT they are:

- Loading range: 0 to 200 N

- Scratching speed: 10mm/min

- Loading rate: 100N/min

- Acoustic emission(AE) sensitivity: 1/3

- Rockwell diamond tip: 200μm

For argon, nitrogen and TS S1 samples adhesion testing was conducted using MST as these coatings showed delamination at low loads. For other samples Revetest was used as loads greater than 30N was required to delaminate the coatings. The beta sample was the only sample to have exhibited more than one mode of failure while others showed only surface delamination. In case of the alpha sample no visible or acoustic evidence of coating failure was observed even when maximum load of 200 N was applied. The results of the MST/RVT is listed in Table 4.5:

Table 4.5 Results of Adhesion Measurements on Tantalum Coatings

SAMPLE NAME	CRITICAL LOAD(N)
Argon sample	4.73
Nitrogen sample	15.39
TS S1	24.63
TS J5	37.44
TS J4	41.22
Beta sample	70.70
Alpha sample	No coating failure
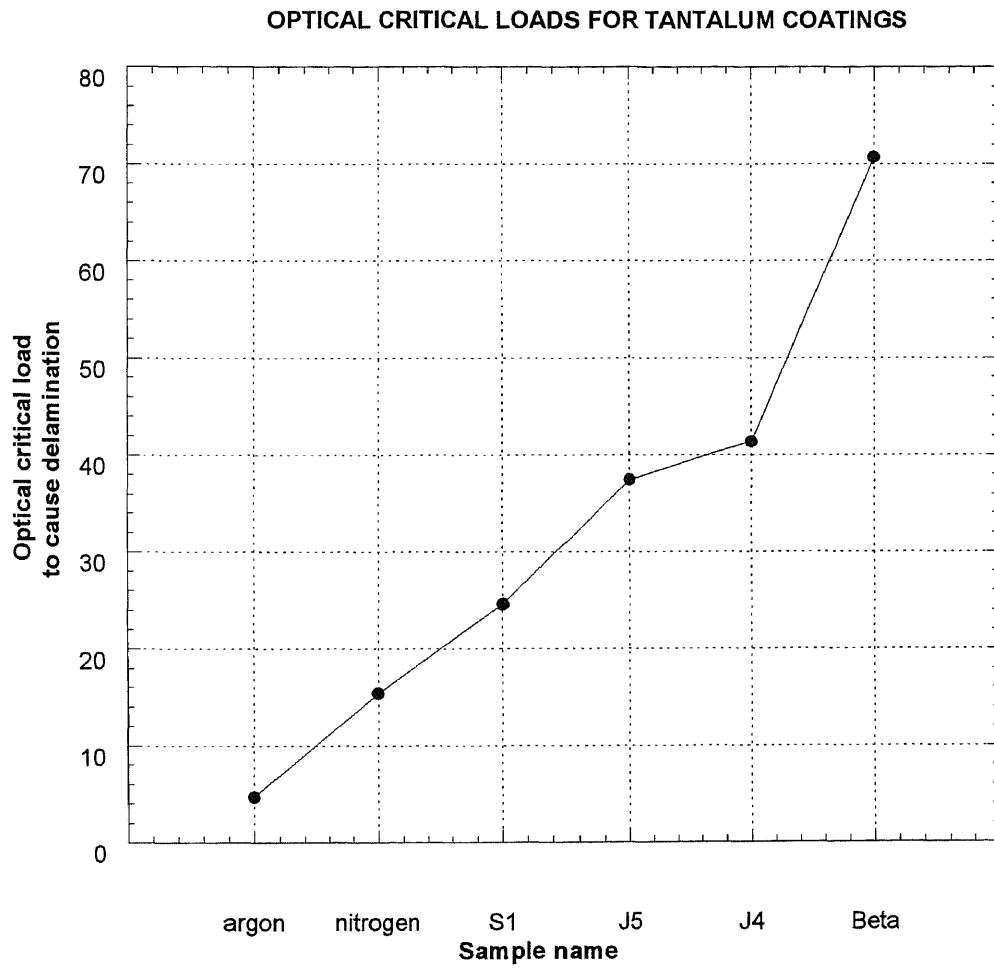
Fig. 4.32 Optical critical loads for Tantalum coatings on steel substrates

Electrical Properties

4.6 Resistivity

Interest in electrical properties of tantalum thin films over the past twenty years has been

stimulated by its potential applications in electronic devices and x-ray optics. Depending

on the deposition technique used, the as deposited crystal structure can vary between

alpha phase, beta phase or a mixture of alpha and beta phase tantalum. The changes in

resistivity have been explained by variations in microstructure (grain size, lattice damage)

or impurity content [4].

The beta phase has an as-deposited resistivity of 170-210 $\mu\Omega$ cm while the resistivity of

alpha tantalum is 15-60$\mu\Omega$ cm. L.A. Clevenger *et al.* [38] concluded that upon heating,

the resistance of the tantalum films decreases linearly with temperature from about 225

$\mu\Omega$cm at 25°C to about 200 $\mu\Omega$cm at 600°C and finally to 60 $\mu\Omega$cm at 800°C. He co-

related this decrease in resistance with the transformation of beta tantalum to alpha

tantalum.

The resistivity of tantalum coatings was measured using a four-point probe at the NJIT

clean room and Rapid Thermal Characterization Laboratory. In the present study both

resistivity and x-ray diffraction measurements were employed to differentiate between

beta and alpha (bcc) tantalum phases. Resistivities of the order of 60 or less were

indicative of alpha tantalum or cases where the coatings were predominantly bcc phase.

In case of beta tantalum resitivity values of around 165-180 $\mu\Omega$cm was characteristic of

very pure beta phase with no bcc phase in it. In cases where both the phases were

simultaneously present the resistivity values were around 60-150 depending on which

phase was predominant. The results of resistivity for tantalum coatings on steel substrates are reported in Table 4.6.

Table 4.6 Resistivity Measurements for Tantalum Coatings

SAMPLE NAME	RESISTIVITY ($\mu\Omega$ cm.)
TA1	25
TAF2	20
SAMPLE A	55
SAMPLE I	88
TS C1	30
TS J4	27
TS J5	35
TS K	20
TS S1	25
TS 11	35
ARGON SAMPLE	52
NITROGEN SAMPLE	45
ALPHA SAMPLE	23
BETA SAMPLE	175

CHAPTER 5

CONSLUSIONS

The purpose of this thesis was to evaluate and determine suitable coatings for replacement of chromium coatings on gun barrel steel and on steel substrates. Tantalum was found to be a suitable replacement material and chosen as a material for replacing chromium coatings on gun steel. The next step was to examine the characteristics of tantalum coatings on steel substrates and to evaluate structural, mechanical and electrical properties of tantalum coatings on steel substrates.

- The X-ray diffraction studies reveal the nature of tantalum coatings. In most cases, the tantalum coatings were obtained in pure bcc form, while in some cases a mixture of bcc and beta phase was found to occur simultaneously.

- The SEM/EDX results confirm that, depending on the deposition conditions, the microstructure can vary from irregular, dendritic structure to a well-defined step like structure. A "cauliflower type" structure has also been observed in this present study. All these structures have been well reported in literature.

- The XRF results were used to quantify the amount of tantalum in the coatings and thereby establish the purity of the coatings. The purity of tantalum coatings is between 97-99%.

- In EXAFS analysis, tantalum coatings have nearly 100% bcc phase could be easily fitted by curve fitting techniques. For beta phase 3rd and 4th cumulants was used as the structure showed significant disorder. The structure for beta tantalum is nither SC, bcc or fcc but is more complicated. More work needs to be done in order to determine

the exact structure of beta tantalum. The bond distances obtained from EXAFS results were similar to those obtained from XRD analysis and thus the consistency in the results was established using different characterization techniques.

- The pure bcc coatings have the best adhesion (>200N), while coatings with pure beta phase have low value of adhesion (< 100N), thus confirming that the beta phase is a brittle phase which fails at low loads as compared to alpha phase. For coatings which had a mixture of both phases the adhesion values were exceptionally low (< 40N).

- There were no specific trends observed in the resistivity values for tantalum coatings. However, the resistivity values were very much within limits of the values reported in literature.

LAYOUT FOR SPUTTER DEPOSITION
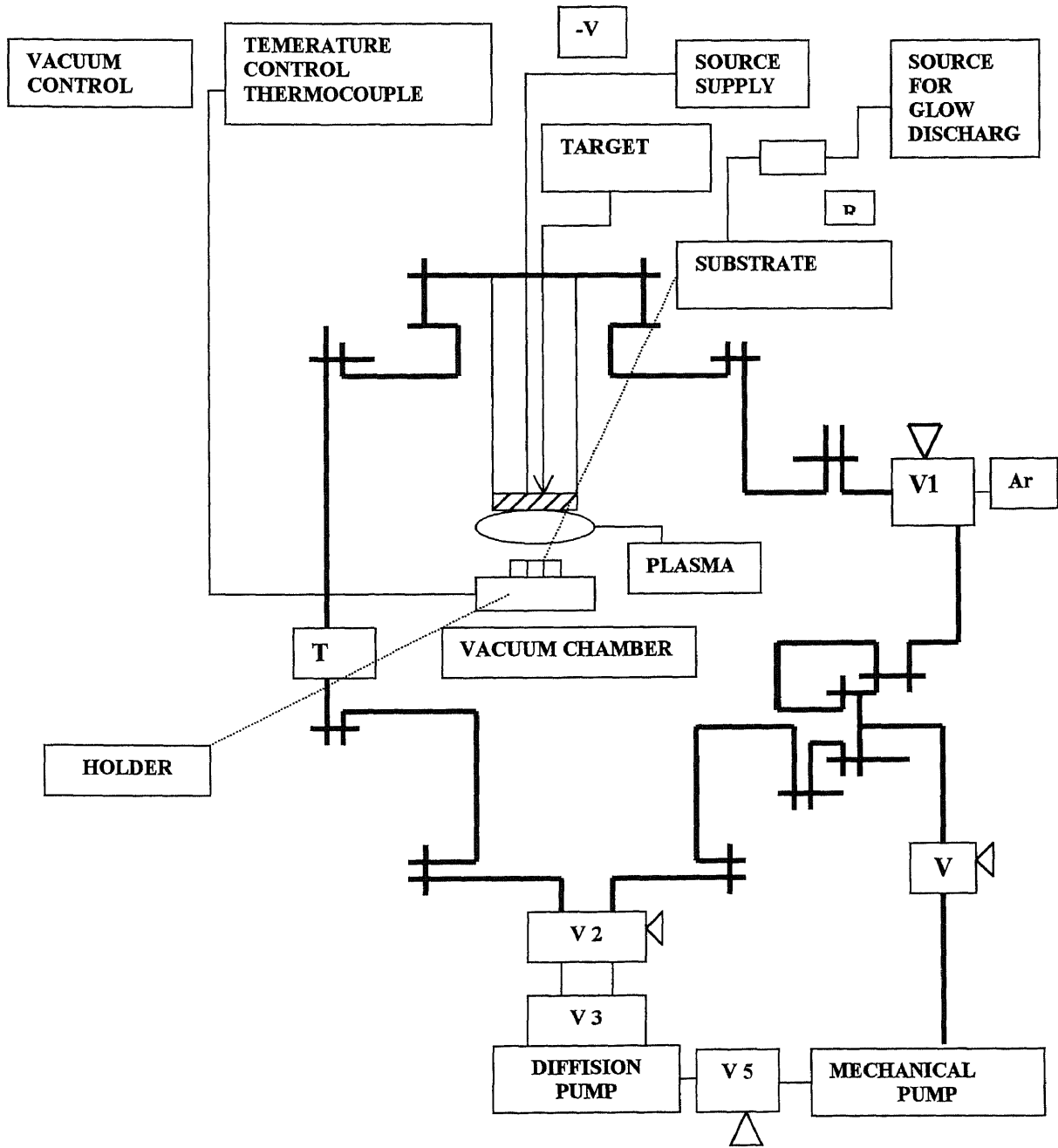
Fig. A1 Layout for Sputter Deposition

APPENDIX B

DEPOSITION DETAILS

Table B1 Details of Deposition for Tantalum Coatings

SAMPLE NAME	THICKNESS (MICRONS)	DEPOSITION DETAILS
TS 1299 Tantalum film deposited on a thin foil of steel	$0.5\mu m$	Temperature 30°C Pressure 4×10^{-2} Torr Time of deposition 30 min Voltage 347 V Current 1A
TS 5299 Tantalum film deposited on a thin foil of steel	1	Temperature 115°C Pressure 10^{-2} Torr Time 15 min Voltage 400V Current 1A
TS 1239 Tantalum film deposited on a thin foil of steel	1	Temperature 25°C Pressure 8×10^{-2} Torr Time 20 min Voltage 800 V Current 0.125A
TA 1 Tantalum film deposited on thin steel substrate	5	Temperature 25°C Pressure 10×10^{3} Torr Time 15 min Voltage 480V Current 0.75A Sample cleaned using alcohol and ultrasonic cleaning No water jet treatment
TA F2 Tantalum film deposited on a thick steel substrate	5	Temperature 25°C Pressure 10 μTorr Time 60 min Voltage 280V Current 1.4 A Sample cleaned using alcohol and ultrasonic cleaning No water jet cleaning

Table B1 (cont.)

SAMPLE NAME	THICKNESS (MICRONS)	DEPOSITION DETAILS
TA F3 Tantalum film deposited on a thick steel substrate	5	Temperature 25°C Pressure 10×10^3 Torr Time 120 min Voltage 420V Current 0.5 A Sample cleaned using alcohol and ultrasonic cleaning
SAMPLE A Tantalum film deposited on a thin steel substrate	10	Temperature 25°C Pressure 10×10^3 Torr Time 30 min Voltage 480V Current 0.75A Sample polished using polishing wheel and cleaned using alcohol and ultrasonic cleaning No water jet cleaning
SAMPLE C Tantalum film deposited on a thin steel substrate	10	Temperature 25°C Pressure 10μTorr Time 30 min Voltage 460V Current 1.4 A Sample polished cleaned using alcohol ultrasonic cleaning No water jet cleaning
SAMPLE E Tantalum film deposited on a thin steel substrate	15	Temperature 25°C Pressure 10×10^3 Torr Time 30 min Voltage 480V Current 0.75A Sample polished using polishing wheel and cleaned using alcohol and ultrasonic cleaning No water jet cleaning
TS 60199 Tantalum film deposited on a thin foil of steel	15	Temperature 144°C Pressure 4×10^{-2}Torr Time 60 min Voltage 307 V Current 1A

Table B1 (cont.)

SAMPLE NAME	THICKNESS (MICRONS)	DEPOSITION DETAILS
SAMPLE II Tantalum film deposited on a thin steel substrate	30	Temperature 25°C Pressure 10 μTorr Time 60 min Voltage 400V Current 0.75A Sample polished using polishing wheel and cleaned using alcohol and ultrasonic cleaning No water jet cleaning
ARMY SAMPLE	50	Not Known Sample received from the army
TS C1 Tantalum film deposited on a thick steel substrate	50	Temperature 25°C Pressure 10 μTorr Time 30 min Voltage 460V Current 1.4 A Sample cleaned using alcohol and ultrasonic cleaning and prepared using water jet treatment
TS J4 Tantalum film deposited on a thick steel substrate	60	Temperature 25°C Pressure 10 μTorr Time 60 min Voltage 460V Current 1.4 A ultrasonic cleaning water jet treatment
TS J5 Tantalum film deposited on a thick steel substrate	60	Temperature 25°C Pressure 10 μTorr Time 60 min Voltage 460V Current 1.4 A Sample cleaned using alcohol and ultrasonic cleaning water jet treatment
TS K Tantalum film deposited on a thick steel substrate	70	Temperature 25°C Pressure 10×10^{3} Torr Time 210 min Voltage 460V Current 1.4 A Sample cleaned using alcohol and ultrasonic cleaning and prepared using water jet treatment

TableB1 (cont.)

SAMPLE NAME	THICKNESS (MICRONS)	DEPOSITION DETAILS
TS S1 Tantalum film deposited on a thick steel substrate	70	Temperature 25°C Pressure 10×10^3 Torr Time 120 min Voltage 460V Current 1.4 A Sample cleaned using alcohol and ultrasonic cleaning and prepared using water jet treatment
TS 11 Tantalum film deposited on a thick steel substrate	100	Temperature 25°C Pressure 10×10^3 Torr Time 300 min Voltage 385V Current 1 A Sample cleaned using alcohol and ultrasonic cleaning and prepared using water jet treatment
ARGON SAMPLE Tantalum film deposited on a thick steel substrate	150	Temperature 25°C Pressure 10×10^3 Torr Time 360 min Voltage 385 V Current 1 A ultrasonic cleaning and prepared using water jet treatment
NITROGEN SAMPLE Tantalum film deposited on a thick steel substrate	150	Temperature 25°C Pressure 10×10^3 Torr Time 360 min Voltage 385V Current 1A Sample cleaned using alcohol and ultrasonic cleaning and prepared using water jet treatment
TANTALUM FOIL 1.0 MM	1 mm thick foil	Tantalum foil purchase from Alridge Chemical Co. 99.9 + % purity
PURE BCC(ALPHA) TANTALUM	25μ	Waterwilly sample, deposition details not known
TANTALUM POWDER	-325 mesh	Tantalum powder purchased from Alridge Chemical co. 99.9% purity
PURE BETA TANTALUM	25μ	Waterwilly sample, deposition details not known

APPENDIX C

XAFS SPECTRUM

XAFS SPECTRUM OF TANTALUM POWDER
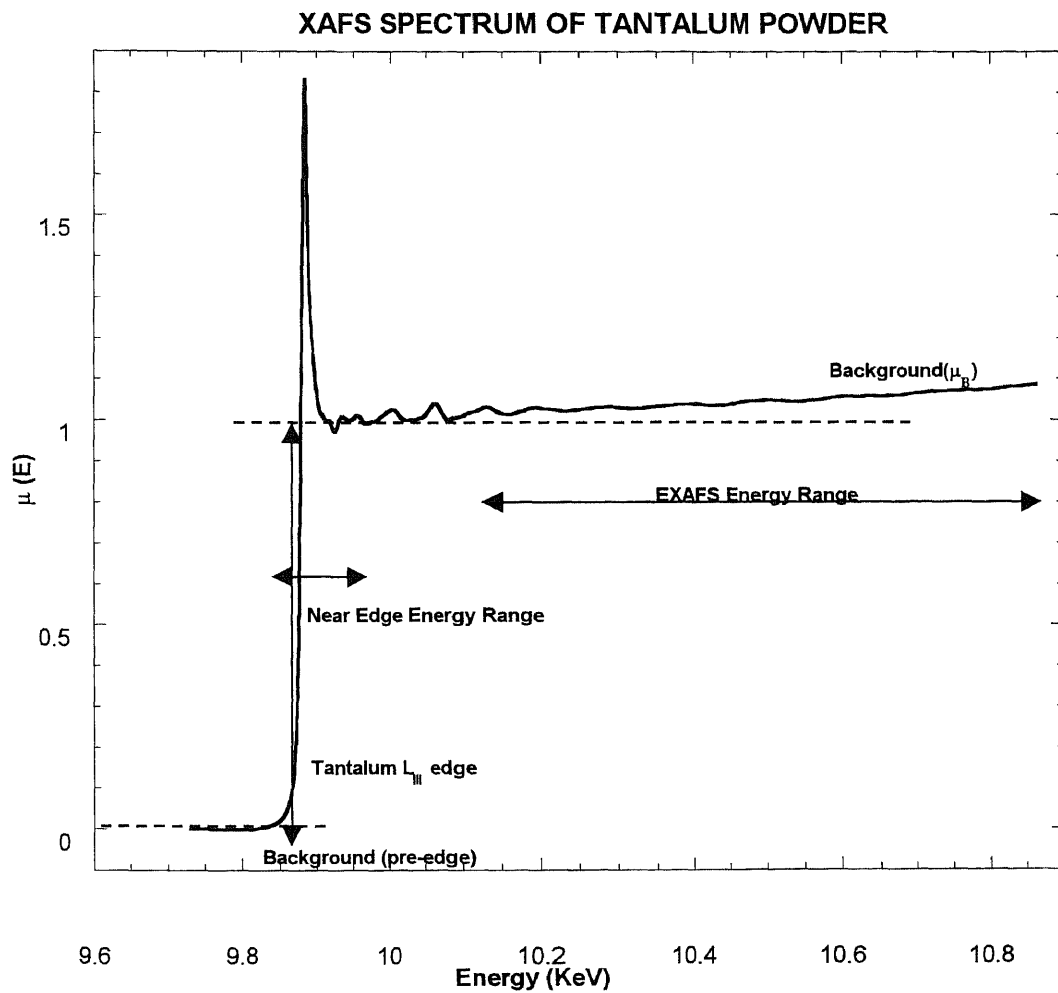
Fig. C1. XAFS Spectrum for Tantalum

APPENDIX C
(Continued)

X-Ray Beam → | Ionization Chamber I_o | → Sample → | Ionization Chamber I_i |
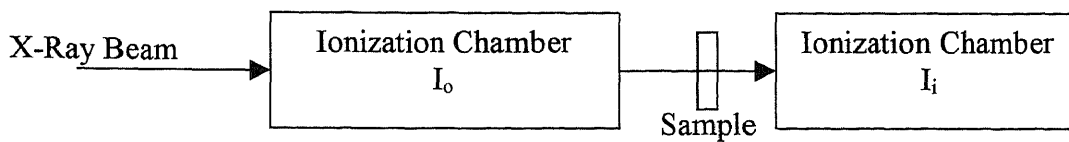
Fig. C2 (a) Schematic for XAFS experiment in Transmission mode

X-ray Beam → | Ionization Chamber I_o | → Sample

| Ionization Chamber F |
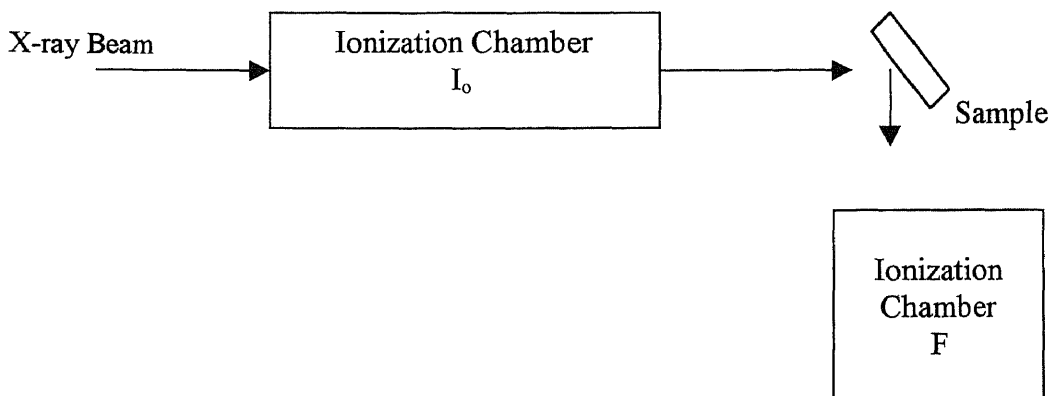
Fig. C2 (b) Schematic for XAFS experiment in Fluorescence mode

APPENDIX C
(Continued)

Fourier Transform [$k^{3.}\chi(k)$] versus Raidal Coordinate

Filtered from 2.0 to 16.989 angstrom^{-1}
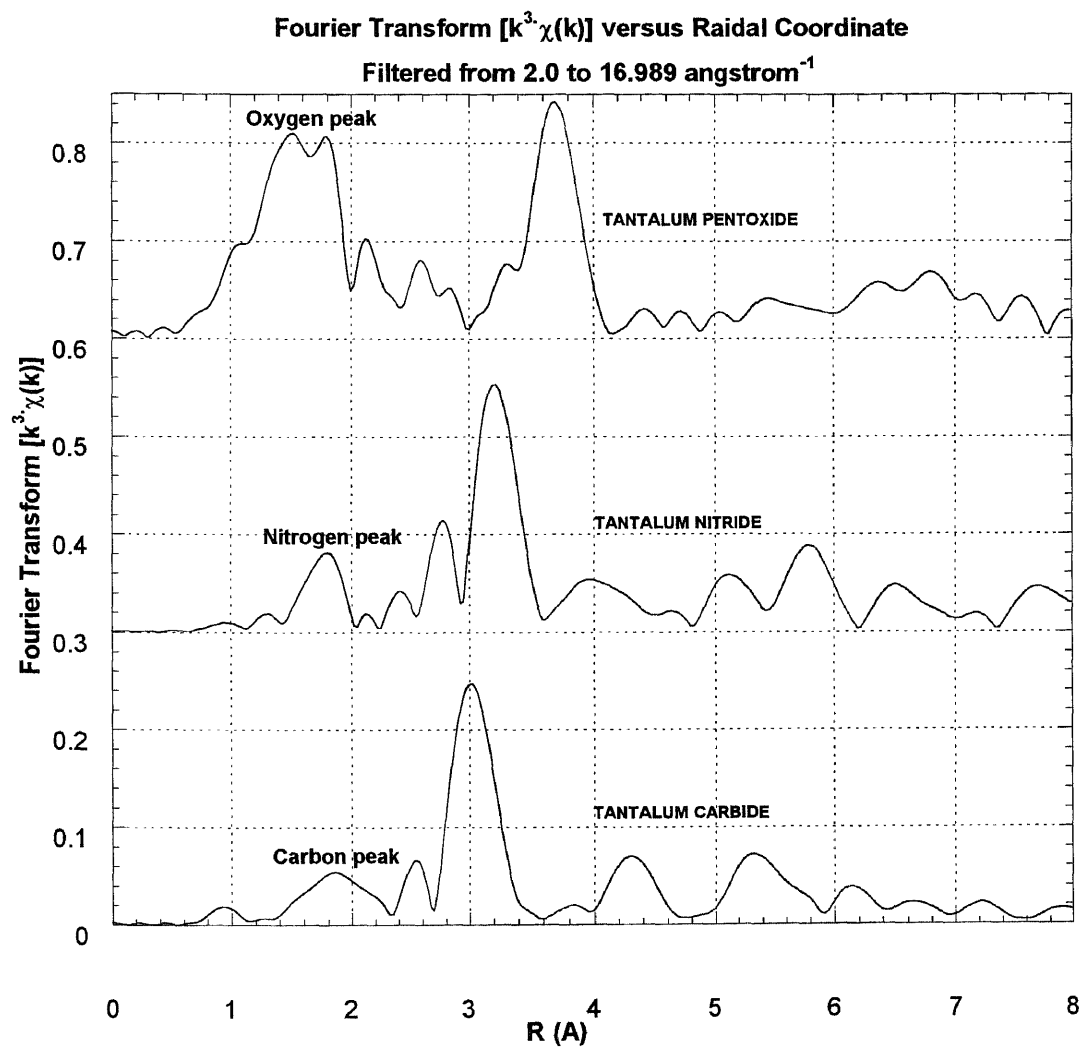
Fig. C3 Fourier Transform for Tantalum Carbide, Tantalum Nitride and Tantalum Pentoxide

APPENDIX C
(Continued)
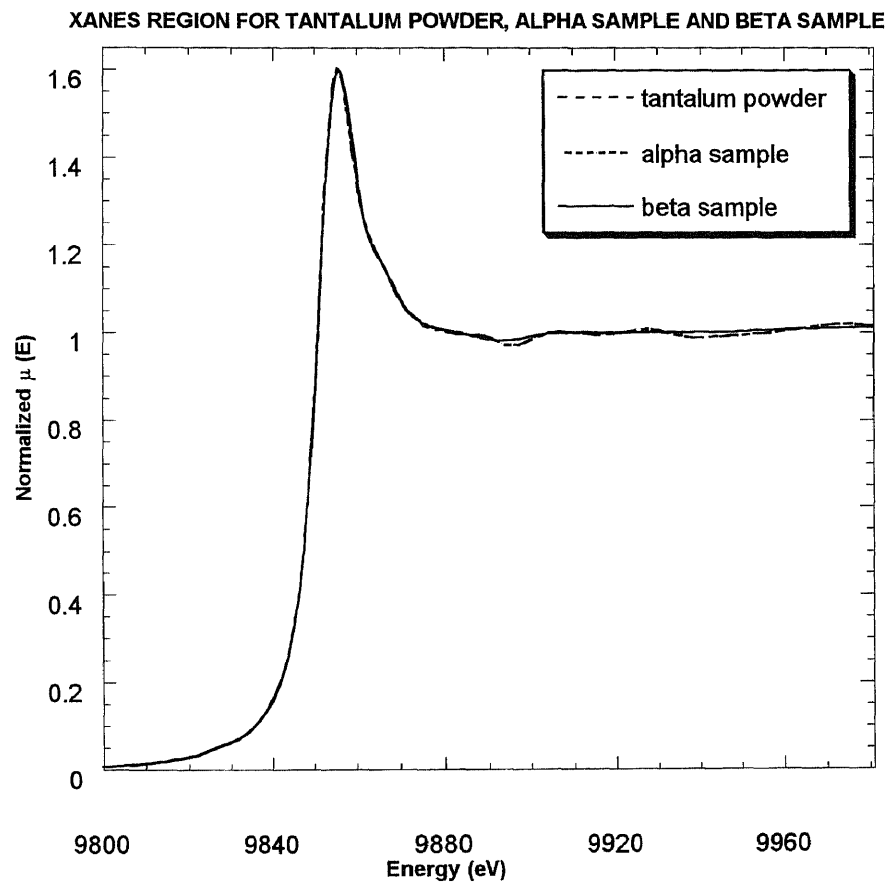
Fig. C4 XANES region for Tantalum powder, Alpha sample and Beta sample

APPENDIX C
(Continued)

XANES REGION FOR TANTALUM CARBIDE, TANTALUM NITRIDE AND TANTALUM PENTOXIDE
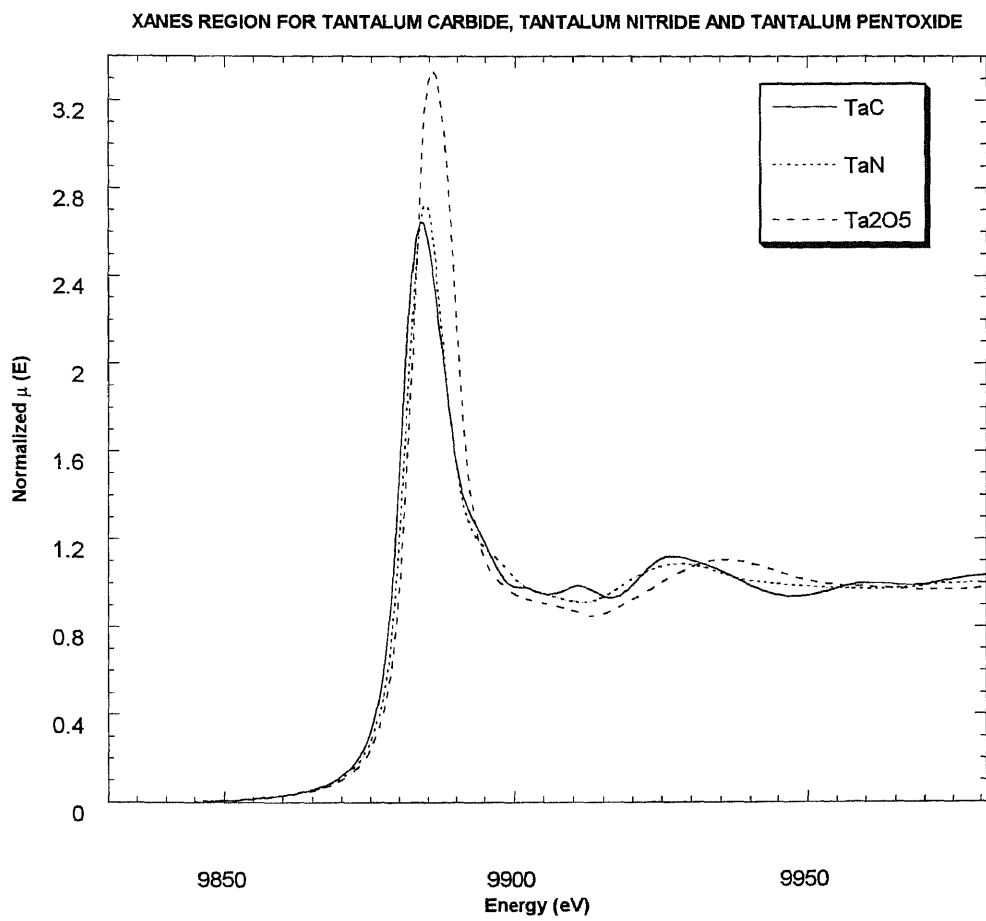
Fig. C5 XANES region for Tantalum Carbide, Tantalum Nitride and Tantalum Pentoxide

APPENDIX D

CELL CONSTANT, CRYSTALLITE SIZE AND LATTICE STRAIN

Table D1 X-Ray Diffraction

SAMPLE NAME	(hkl)	RI (%)	a(A)	% α:β	CRYSTALLITE SIZE	LATTICE STRAIN
TS 1299	(110) α	65	3.379	98:2	2097	0.115
	(200) α	5.7	3.3029		1498	0.111
	(211) α	65	3.337		692	0.136
	(220) α	7.2	3.327		479	0.153
	(310) α	3.2	3.3202		585	0.120
	(222) α	100	3.3039		-	-
	(510) β	2.5	10.216			
TS 5299	(110) α	100	3.307	100:0	150	0.811
	(200) α	11.5	3.3036		448	0.249
	(211) α	26	3.303		255	0.293
	(220) α	5.9	3.302		-	-
	(310) α	9.1	3.3033		970	0.085
	(222) α	-			-	-
TS 1239	(110) α	16.4	3.306	60:40	-	-
	(200) α	-	-		-	-
	(211) α	-	-		-	-
	(220) α	1.1	3.307		-	-
	(310) α	-	3.2016		-	-
	(222) α	-	-		-	-
	(510) β	100	10.329			
	(602) β	9.2	10.205			
TA 1	(110) α	100	3.34	80:20	2101	0.113
	(200) α	2	3.34		320	0.320
	(211) α	21.6	3.34		963	0.110
	(220) α	5.2	3.31		278	0.234
	(310) α	-	-		-	-
	(222) α	-	-		-	-
	(510) β	22.9	10.223			

Table D1 (cont.)

SAMPLE NAME	(hkl)	RI (%)	a(A)	% α:β	CRYSTALLITE SIZE	LATTICE STRAIN
TS F2	(110) α	100	3.306	100:0	150	0.788
	(200) α		-		-	-
	(211) α	30	3.304		-	-
	(220) α	12	3.3033		-	-
	(310) α	-	-		-	-
	(222) α	10	3.304		160	0.304
TS F3	(110) α	100	3.306	100:0	1052	0.172
	(200) α	-	-		-	-
	(211) α	28	3.304		254	0.295
	(220) α	3.5	3.304		-	-
	(310) α	-	-		-	-
	(222) α	5	3.307		-	-
SAMPLE A	(110) α	100	3.3036	70:30	2103	0.112
	(200) α	2	3.3048		321	0.317
	(211) α	14.9	3.3046		966	0.109
	(220) α	4.6	3.304		1053	0.087
	(310) α	-	-		1461	0.065
	(222) α	-	-		159	0.309
	(510) β	8.0	10.326			
	(631) β	87	9.992			
SAMPLE C	(110) α	99.1	3.315	60:40	-	-
	(200) α	1.8	3.303		204	0.453
	(211) α	8.9	3.29		210	0.347
	(220) α	5.1	3.313		229	0.275
	(310) α	1.1	-		226	0.252
	(222) α	1	-		476	0.123
	(002) β	48.2	C=5.305			
	(510) β	19.2	10.351			
	(602) β	100	10.220			

Table D1 (cont.)

SAMPLE NAME	(hkl)	RI (%)	a(A)	% α:β	CRYSTALLITE SIZE	LATTICE STRAIN
SAMPLE E	(110) α	2.2	3.311	60:40	841	0.202
	(200) α	3.5	-		-	-
	(211) α	80.69	3.3074		322	0.243
	(220) α	15	3.3049		352	0.193
	(310) α	-	-		-	-
	(222) α	-	-		-	-
	(002) β		C=5.29			
	(510) β		10.337			
	(602) β		10.198			
	(513) β		10.196			
TS 60199	(110) α	100	3.309	100:0	4196	0.077
	(200) α	6.5	3.309		2237	0.089
	(211) α	32	3.306		692	0.136
	(220) α	8	3.308		478	0.153
	(310) α	7.6	3.306		585	0.120
	(222) α	6.2	3.305		-	-
TS J4	(110) α	99.8	3.33	100:0	1401	0.145
	(200) α	-	-		-	-
	(211) α	5.4	3.33		-	-
	(220) α	-	-		-	-
	(310) α	-	-		-	-
	(222) α	0.7	3.34		827	0.083
SAMPLE I	(110) α	15.5	3.307	50:50	-	-
	(200) α	0.1	3.3125		321	0.316
	(211) α	1.3	3.3141		4831	0.042
	(220) α	1.3	3.303		311	0.213
	(310) α	0.4	3.303		420	0.152
	(222) α	0.1	3.309		258	0.201
	(002) β	100	C=5.31			
	(510) β	0.3	10.370			
	(602) β	1.3	10.198			
	(513) β	17.5	10.168			

Table D1 (cont.)

SAMPLE NAME	(hkl)	RI (%)	a(A)	% α:β	CRYSTALLITE SIZE	LATTICE STRAIN
SAMPLE II	(110) α	100	3.298	60:40	351	0.386
	(200) α	0.7	3.3035		449	0.247
	(211) α	10.9	3.3070		372	0.217
	(220) α	7.8	3.3044		406	0.172
	(310) α	2.4	3.3062		979	0.083
	(222) α	0.3	3.3051		159	0.306
	(002) β	86.5	C=5.30			
	(510) β	2.2	10.363			
	(602) β	7.6	10.197			
	(513) β	11.7	10.177			
ARMY SAMPLE	(110) α	65.0	3.379	100:0	1052	0.173
	(200) α	6.3	3.3498		249	0.386
	(211) α	65	3.3377		210	0.346
	(220) α	7.5	3.3272		754	0.109
	(310) α	3.2	3.3202		979	0.083
	(222) α	100	3.3082		160	0.304
TS C1	(110) α	100	3.304	95:5	-	-
	(200) α	5.1	3.306		204	0.455
	(211) α	20.6	3.304		694	0.135
	(220) α	13.2	3.304		196	0.312
	(310) α	6.2	3.30		-	-
	(222) α	0.6	3.304		-	-
	(002) β	21.2	C=5.17			
	(631) β	9.0	10.490			
TS J5	(110) α	100	3.244	90:10	843	0.197
	(200) α	3.8	3.26		250	0.379
	(211) α	14.3	3.29		156	0.445
	(220) α	11.6	3.30		196	0.314
	(310) α	2.6	3.31		140	0.382
	(222) α	1	3.32		196	0.256
	(631) β	15.3	10.164			
	(820) β	19.3	10.189			

TableD1(cont.)

SAMPLE NAME	(hkl)	RI (%)	a(A)	% α:β	CRYSTALLITE SIZE	LATTICE STRAIN
TS K	(110) α	100	3.31	100:0	421	00.336
	(200) α	5.2	3.308		2244	0.088
	(211) α	41.1	3.316		4830	0.042
	(220) α	6.4	3.318		752	0.109
	(310) α	5	3.316		139	0.384
	(222) α	3.6	3.314		159	0.306
TS S1	(110) α	100	3.309	100:0	300	0.439
	(200) α	1	3.317		561	0.210
	(211) α	11.4	3.312		1208	0.094
	(220) α	6	3.313		479	0.152
	(310) α	1.4	3.31		195	0.285
	(222) α	0.8	3.314		372	0.149
TS 11	(110) α	100	3.30	100:0	468	0.309
	(200) α	16.8	3.302		374	0.281
	(211) α	78	3.305		1613	0.078
	(220) α	8.9	3.302		755	0.108
	(310) α	8.3	3.305		1469	0.064
	(222) α	51.3	3.304		3367	0.034
TA POWDER	(110) α	100	3.344	100:0	-	-
	(200) α	15.1	3.33		-	-
	(211) α	29.7	3.316		-	-
	(220) α	7.8	3.319		-	-
	(310) α	10.8	3.316		-	-
	(222) α	1.6	3.314		-	-
ARGON SAMPLE	(110) α	100	3.26621	90:10	351	0.382
	(200) α	1.6	3.3183		-	-
	(211) α	0.8	3.3242		689	0.138
	(220) α	16.1	3.2844		2634	0.049
	(310) α	0.6	3.2918		-	-
	(222) α	2	3.2937		670	0.095
	(212) β	5	9.9490			
	(510) β	2.8	10.145			

Table D1 (cont.)

SAMPLE NAME	(hkl)	RI (%)	a(A)	% α:β	CRYSTALLITE SIZE	LATTICE STRAIN
NITROGEN SAMPLE	(110) α	100	3.3041	85:15	2111	0.108
	(200) α	30.7	3.2814		-	-
	(211) α	99	3.2985		970	0.108
	(220) α	12.6	3.2993		353	0.192
	(310) α	10.5	3.3095		976	0.084
	(222) α	18.3	3.3085		1118	0.067
	(322) β	33.7	10.494			
	(511) β	30.7	10.219			
	(601) β	30.7	10.240			
TA FOIL 0.5 mm	(110) α	9.6	3.359	100:0	4199	0.076
	(200) α	100	3.3378		2239	0.089
	(211) α	35.7	3.329		2410	0.062
	(220) α	0.4	3.3228		351	0.195
	(310) α	0.6	3.3253		194	0.288
	(222) α	5.9	3.3055		1117	0.067
TA FOIL 1 mm	(110) α	51.3	3.35	100:0	-	-
	(200) α	100	3.333		-	-
	(211) α	40.3	3.326		-	-
	(220) α	5.6	3.3206		-	-
	(310) α	26.3	3.317		-	-
	(222) α	4.533.	3.3058		-	-
ALPHA SAMPLE	(110) α	5.8	3.257	98:2	1054	0.170
	(200) α	-	-		-	-
	(211) α	100	3.307		4845	0.041
	(220) α	76.1	3.305		-	-
	(310) α	-	-		-	-
	(222) α	-	-		-	-
	(510) β	16.6	10.183			
BETA SAMPLE	(002) β	100	C=5.174	0:100	-	-
	(513) β	51	7.027		-	-
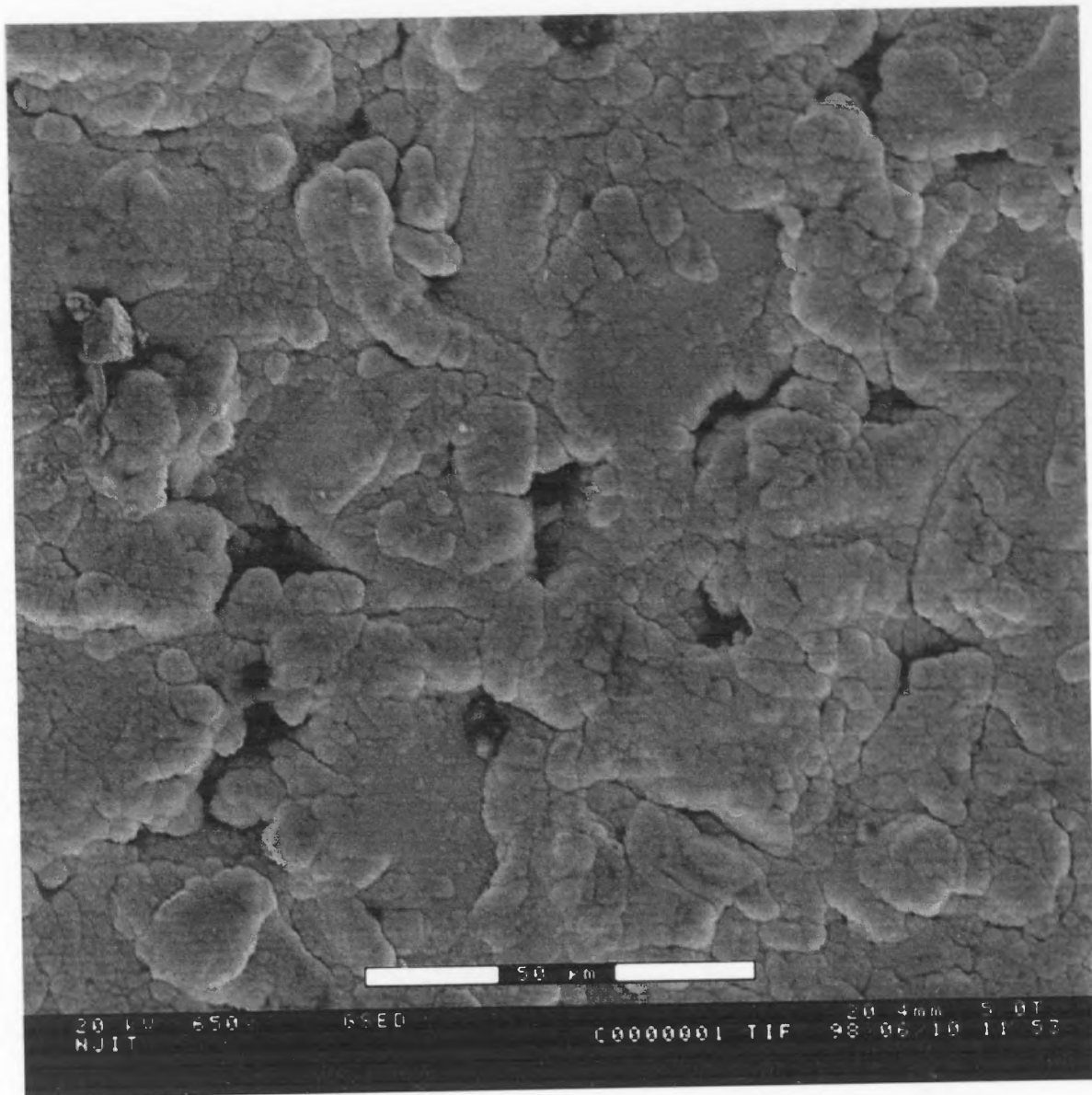
Fig. E1 TANTALUM SAMPLE C1
Scanning electron micrograph showing a globular morphology protruding from the
surface
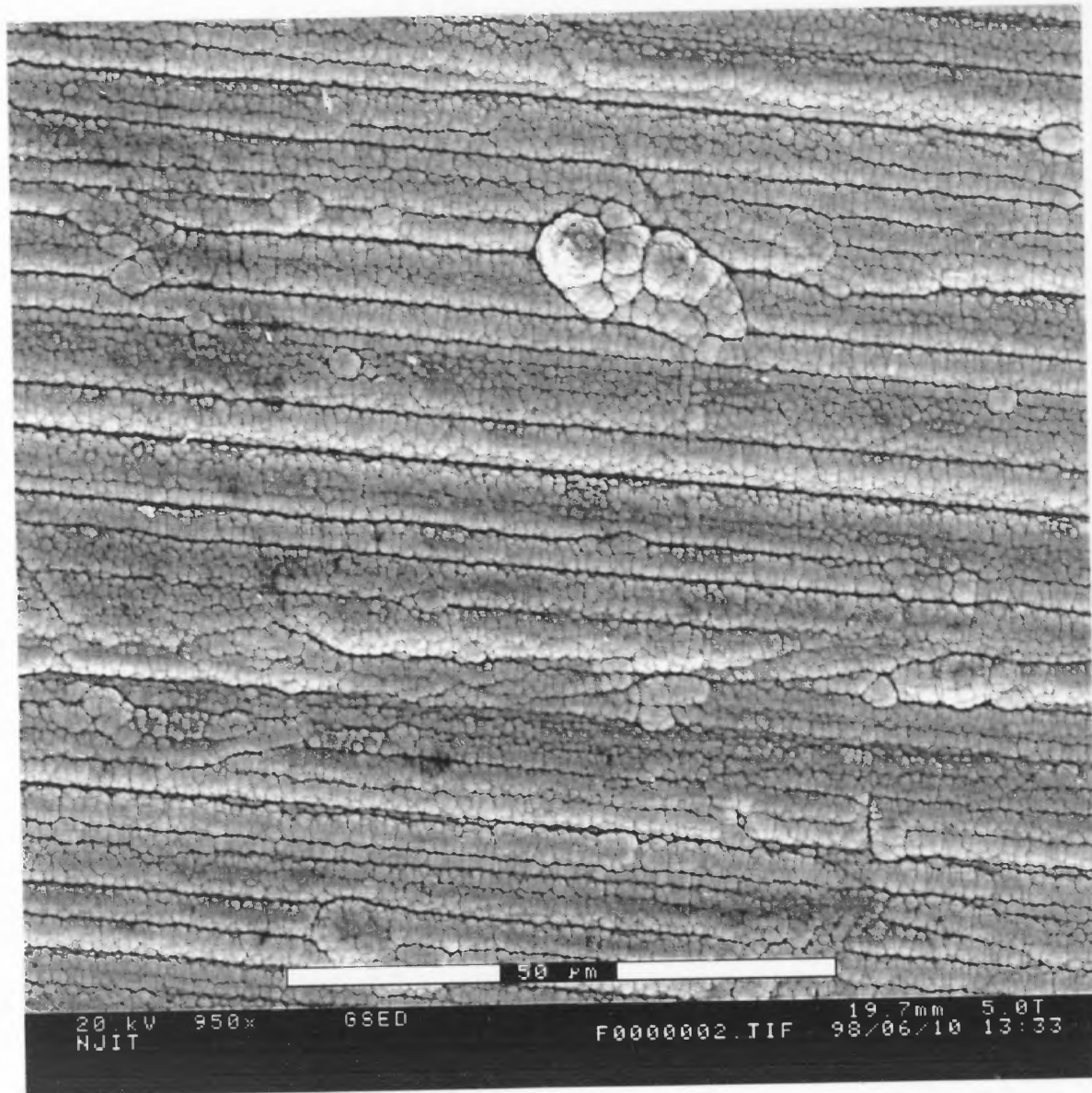
Fig. E2 TANTALUM SAMPLE F2
Scanning electron micrograph showing filamentary growth along the direction of
machining and polishing of the steel substrate
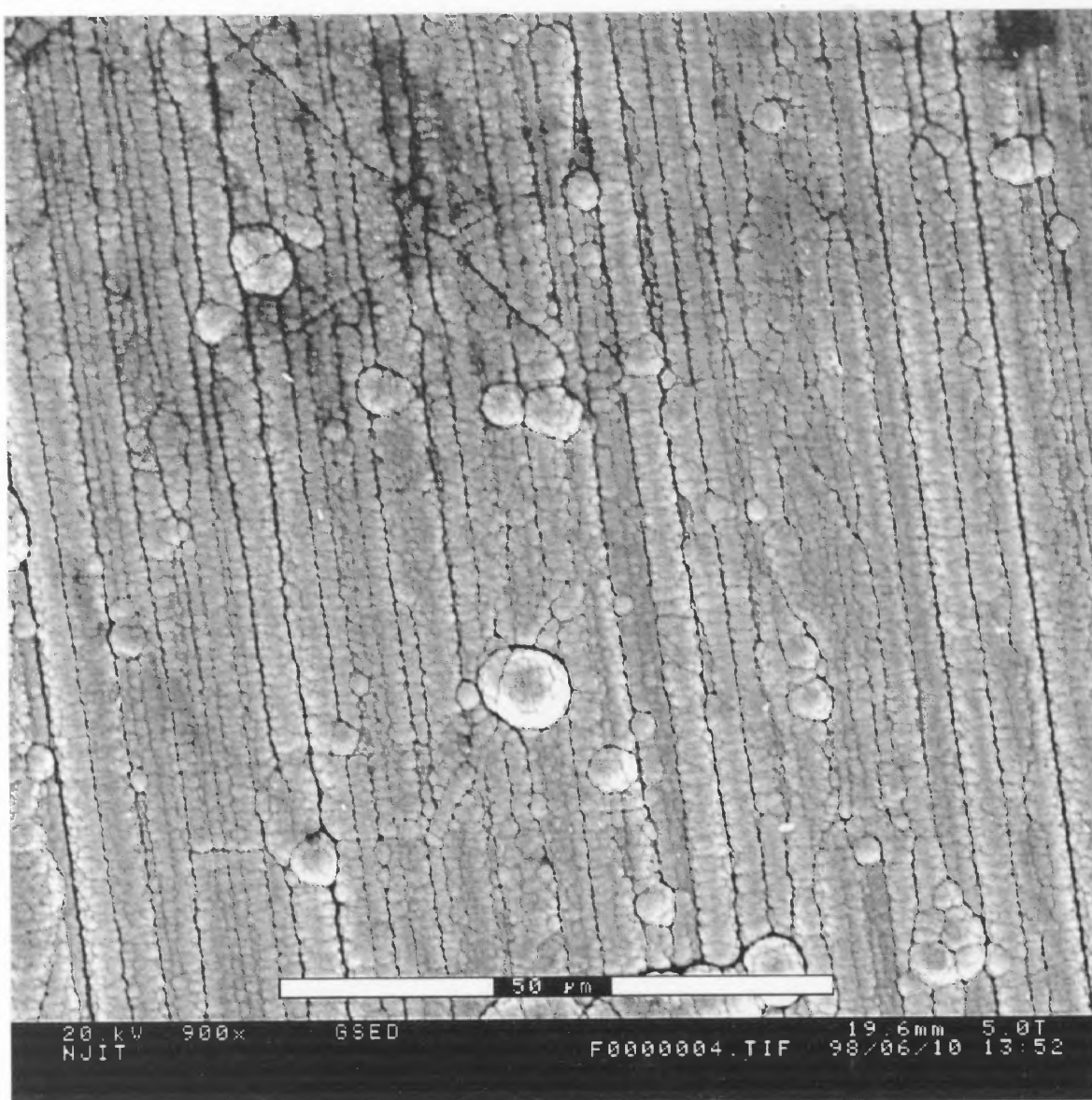
Fig. E3 TANTALUM SAMPLE F3
Scanning electron micrograph showing filamentary growth along the direction of machining and polishing of the steel substrate
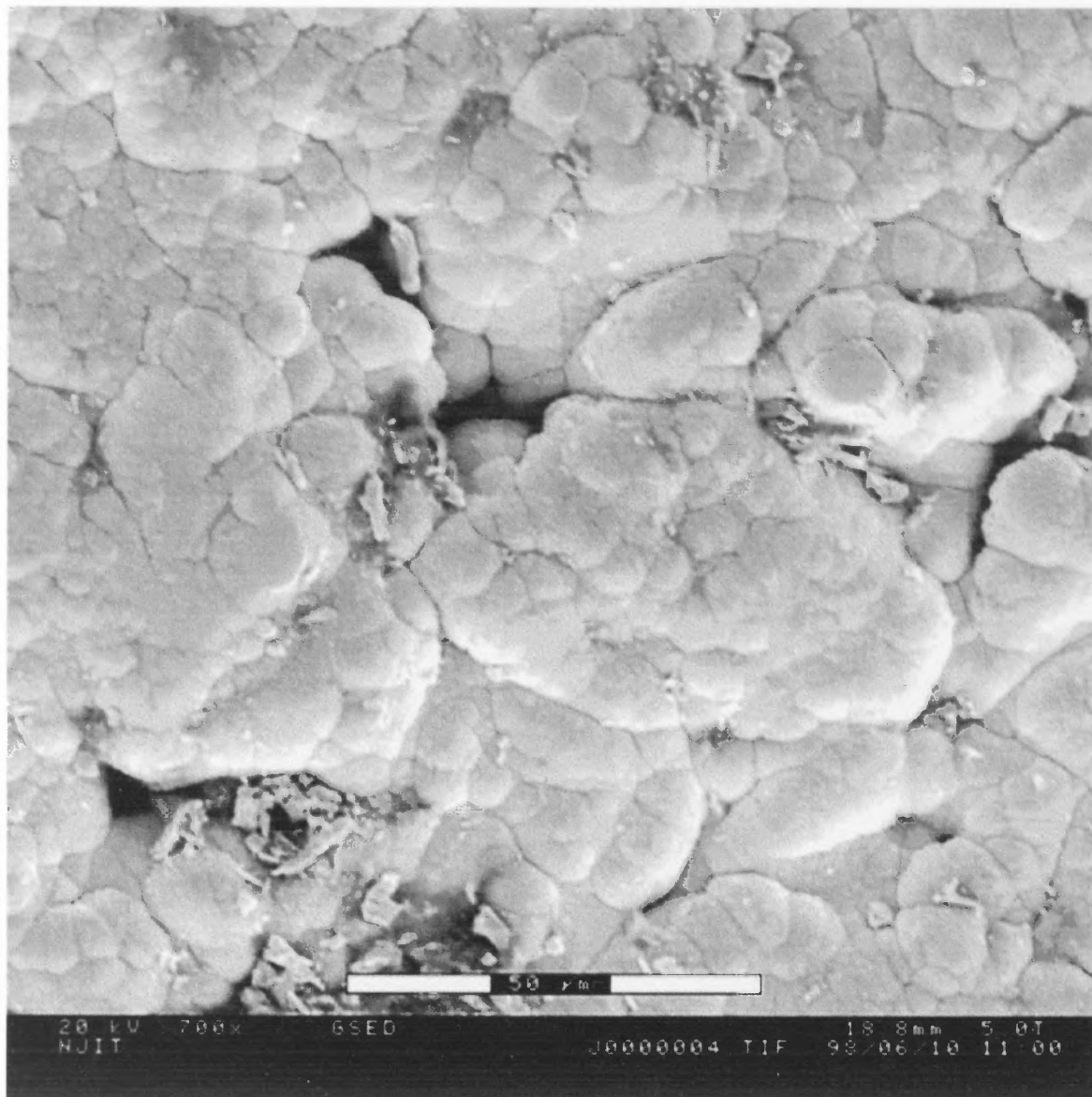
Fig. E4 TANTALUM SAMPLE J4
Scanning electron micrograph showing globular morphology in most of the areas while
some irregular growth can be observed in some areas along with the presence of voids
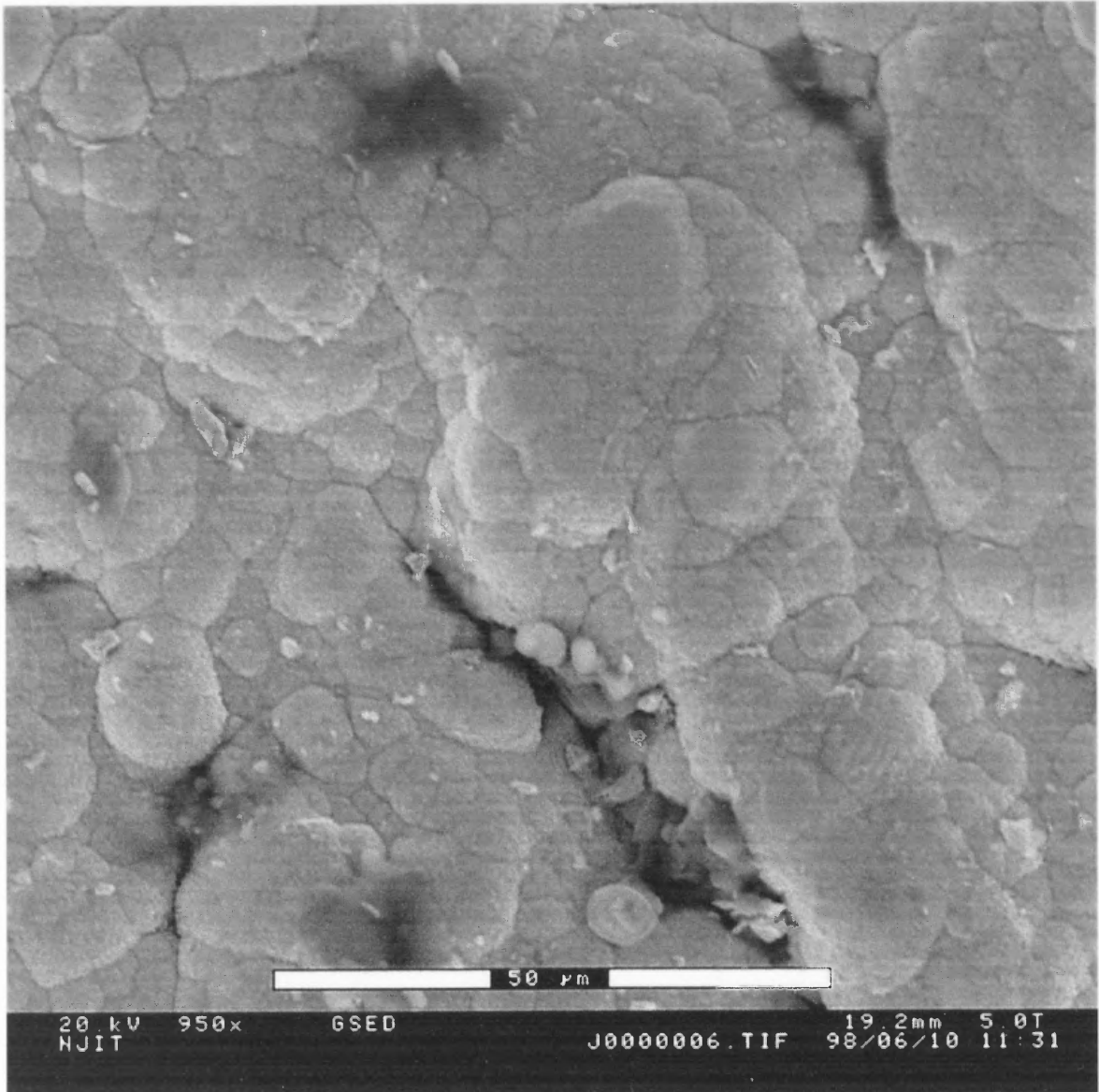
Fig. E5 TANTALUM SAMPLE J5
Scanning electron micrograph showing globular morphology
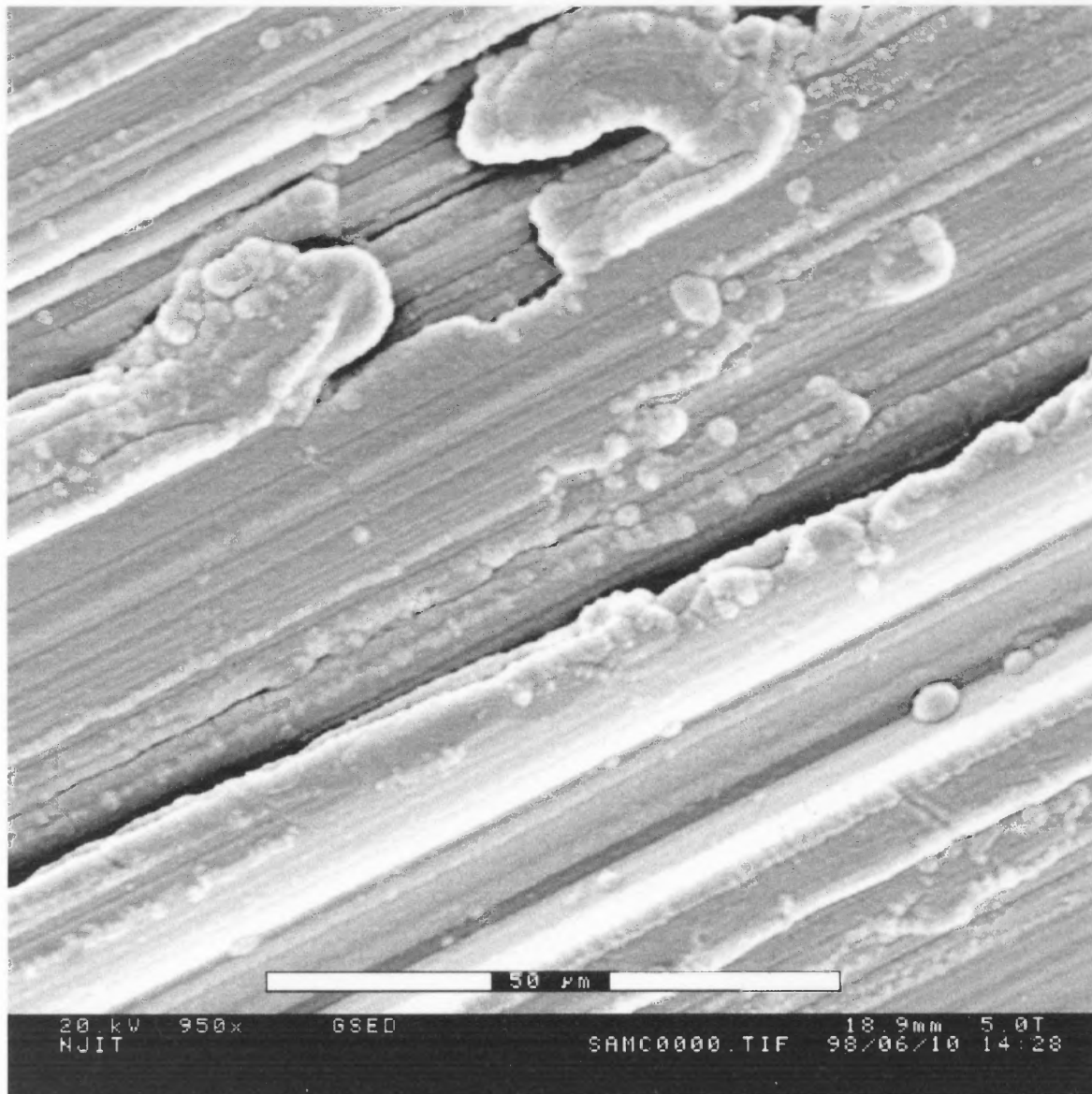
Fig. E6 SAMPLE C
Scanning electron micrograph showing filamentary growth along the direction of
machining and polishing of the steel substrate
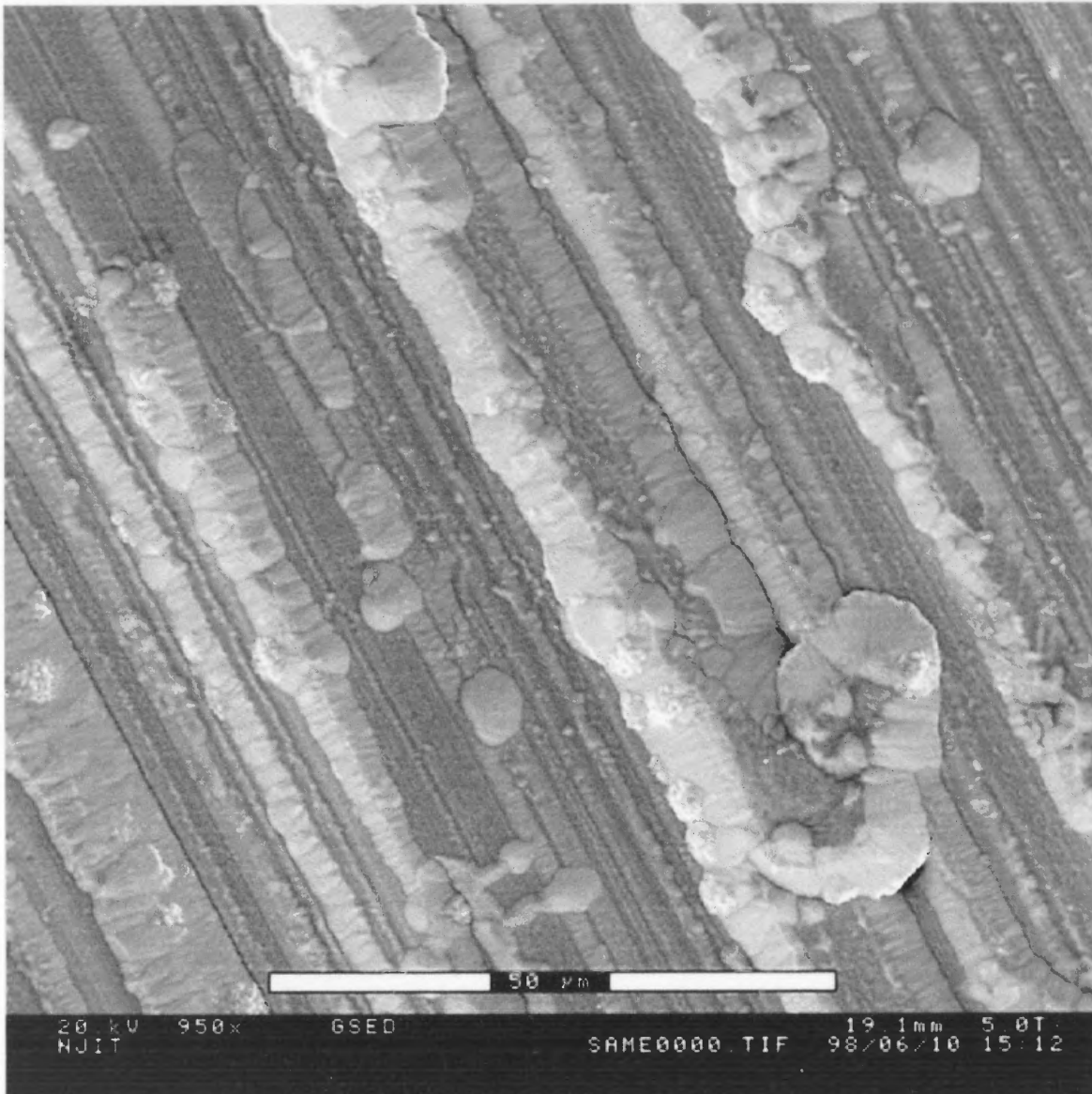
Fig. E7 SAMPLE E
Scanning electron micrograph showing filamentary growth in most of the areas, in some
areas globular morphology is also visible
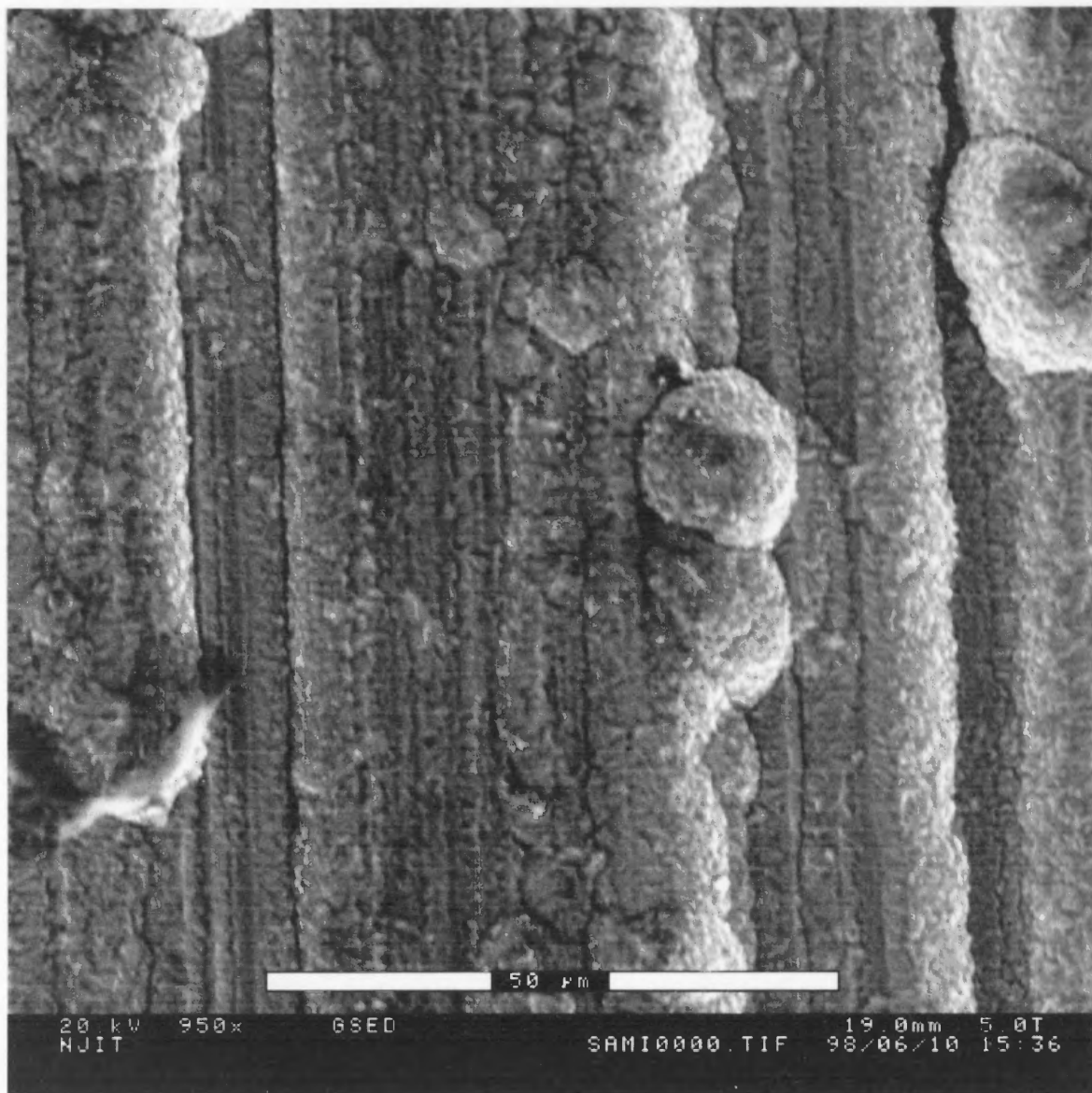
Fig. E8 SAMPLE I
Scanning electron micrograph showing filamentary growth, in some areas cauliflower
like structure is also observed
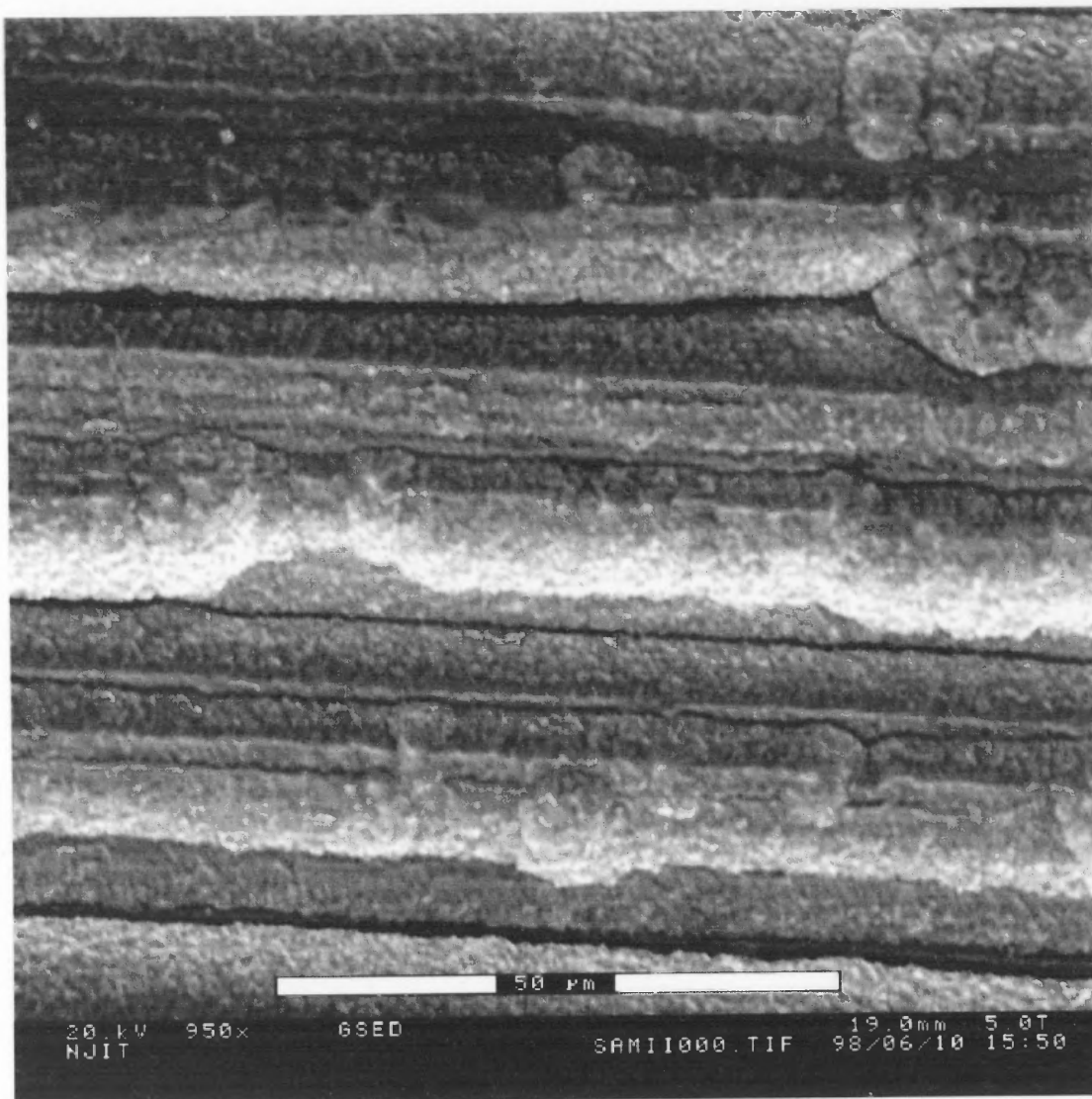
Fig. E9 SAMPLE II
Scanning electron micrograph showing filamentary growth
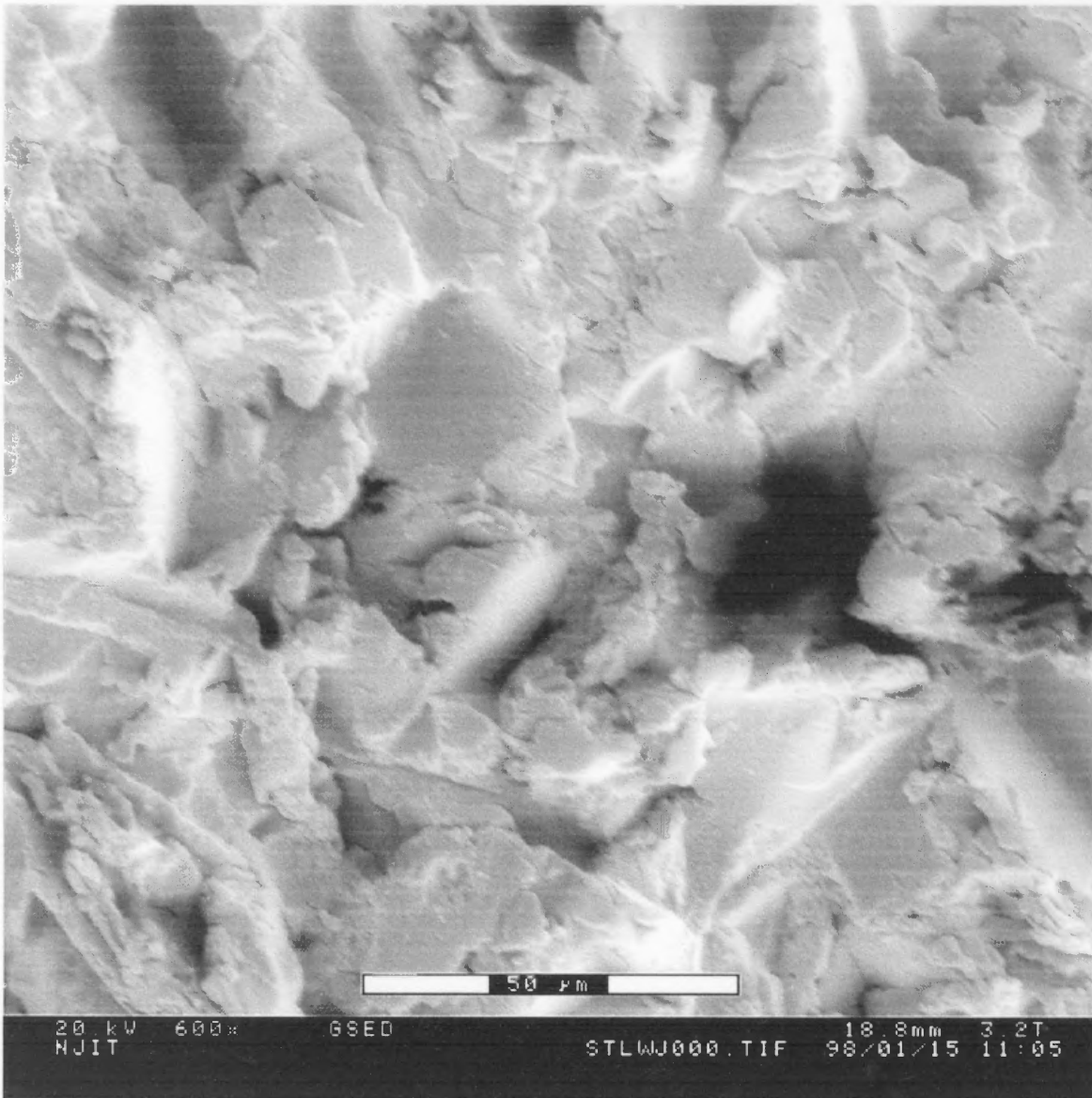
Fig. E10 STEEL WATER JET SAMPLE
Scanning electron micrograph taken for steel substrate after water jet cleaning clearly
showing a very rough surface

APPENDIX F

BOND DISTANCES FOR BCC STRUCTURE FOR FIRST, SECOND AND THIRD SHELLS

BODY CENTERED CUBIC SHELL STRUCTURE
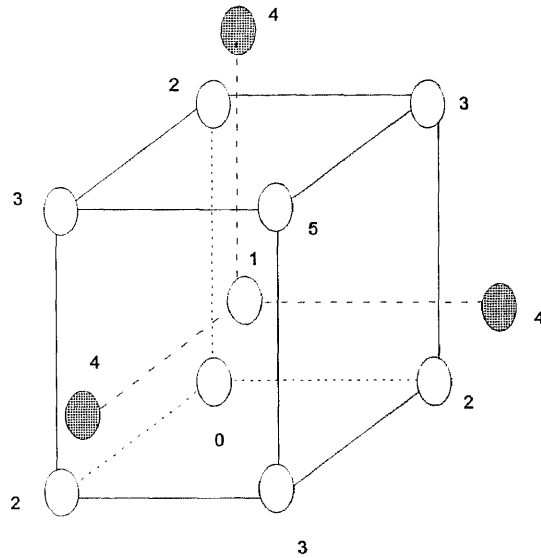
shell-1	body center	8	a.866	r
shell-2	adjacent corner	6	a	r 1.15
shell-3	opposite face corner	8	a 1.414	r 1.63
shell-4	next cell body center	24	a 1.658	r 1.91
shell-5	opposite corner	8	a 1.732	r 2.

APPENDIX G

SELECTED REFERENCE WORKS BY FIELD

Microscopy

[1] Phillip Catania, Ronnen A. Roy and Jerome J. Cuomo " Phase formation and microstructure changes in tantalum thin films induced by bias sputtering," *Journal of Applied Physics,* Vol. 74(2), pp. 1008-1013, 1993.

[2] L.J. Parfitt, O.P. Karpenko, Z.U. Rek, S.M. Yalisove and J.C. Bilello " Origins of residual stress in Mo and Ta films: The role of impurities, microstructural evolution and phase transformations," in *Proceedings of the 1997 Materials Research Society Symposium,* Vol. 236, pp. 505-510, 1997.

Resistivity

[1] Phillip Catania, James P. Doyle and Jerome J. Cuomo " Low resistivity body centered cubic tantalum thin films as diffusion barriers between copper and silicon," *Journal of Vacuum Science and Technology,* Vol. A 10(5), pp. 3318-3321, 1992.

Tantalum

[1] Francesco Brossa, Giovanni Piatti and Micheal Bardy " Tantalum protective coatings for fusion reactor applications," *Journal of Nuclear Materials,* Vol. 103 & 104, pp. 261-266, 1981.

[2] A.K. Malhotra, S.M. Yalisove and J.C. Bilello "Growth and characterization of Ta/W multiscalar multilayer composite films," *Thin Solid Films,* Vol. 286, pp. 196-202, 1996.

[3] K.Baba, R. Hatada, K. Udoh and K. Yasuda " Structure and properties of NbN and TaN films prepared by ion beam assisted deposition," *Nuclear Instruments and Methods in Physics Research,* Vol. B 127/128, pp. 841-845, 1997.

[4] Takuya Yoshihara and Katsumi Suzuki " Sputtering of fibrous-structured low-stress Ta films for x-ray masks," *Journal of Vacuum Science and Technology,* Vol. B12(6), pp. 4001-4004, 1994.

[5] B. Window, F. Sharples and N. Savvides " Plastic flow in ion-assisted deposition of refractory metals," *Journal of Vacuum Science and Technology,* Vol. A 6(4), pp. 2333-2339, 1988.

[6] Tayuka Yoshiyara and Katsumi Suzuki " Variation of internal stresses in sputtered Ta films," *Journal of Vacuum Science and Technology,* Vol. B 11(2), pp. 301-303, 1993.

[7] Peng-Heng Chang and Hung-Yu Liu " Structures of tantalum pentoxide thin films formed by reactive sputtering of Ta metal," *Thin Solid Films,* Vol. 258, pp. 56-63, 1995.

[8] D. Henstein and R.D. Huttemann " Factors controlling the structure of sputtered tantalum films," *Thin Solid Films,* Vol. 16, pp. 129-145, 1973.

[9] S. Kashu, T. Sano and C. Hayashi " Preparation and corrosion properties of a tantalum sputtered thick film," *Journal of Vacuum Science and Technology,* Vol. 9, No. 6, pp. 1399-1403, 1972.

[10] G. Das " A new structure of sputtered tantalum," *Thin Solid Films,* Vol. 12, pp. 305-311, 1972.

[11] John A. Thornton and David W. Hoffman " Internal stresses in titanium, nickel, molybedenum, and tantalum films deposited by cylindrical magnetron sputtering," *Journal of Vacuum Science and Technology,* Vol. 14, No. 1, pp. 164-168, 1977.

[12] John A. Shields Jr., " Tantalum: The refractory metal with low and high temperature applications," *Journal of Metals,* pp. 25, 1997.

X- Ray Diffraction

[1] L. Chekour, J. Krier, R. Halimi and A. Cornet " Analysis of tantalum PVD deposits by x-ray diffraction," *Journal De Physique,* Vol. 6, pp. C4-251-C4-258, 1996.

[2] Mildred H. read and B.H. Hensler " X-ray analysis of sputtered films of beta-tantalum and body centered cubic tantalum," *Thin Solid Films,* Vol. 10, pp. 123-135, 1971.

REFERENCES

[1] D.W. Matson, M.D. Merz and E.D. McClanahan "High rate sputter deposition of wear resistant tantalum coatings," *Journal of Vacuum Science Technology* Vol.A 10(4), pp.1791-1796 July/Aug 1992.

[2] Y.V. Dzyadykevich and L.I. Kytskay "Improving the oxidation protection of niobium and tantalum by the use of multilayer coatings," *Journal of Metals*, pp. 30-32,January 1997.

[3] C.E.D. Rowe "The use of tantalum in the process industry," *Journal of Metals*, pp. 26-28, January 1997.

[4] W.D. Westwood, N. Waterhouse, and P.S. Wilcox, *Tantalum Thin Films*, Academic Press, London, 1975.

[5] P.N.Baker "Preparation and properties of tantalum thin films," Invited Review, *Thin Solid Films*, Vol.14, pp.3-25, 1972.

[6] M.H.read and Carl Altman, "A new structure in tantalum thin films," *Applied Physics Letters*, Vol.7, No.3, pp.51-52, 1965.

[7] L.G. Feinstein and R. D. Huttemann, " Factors controlling the structure of sputtered tantalum films," *Thin Solid Films*, Vol. 16, pp.129-145 (1973).

[8] D.W. Face and DE Prober " Nucleation of bcc tantalum films with thin niobium under-layer," *Journal of Vacuum Science and Technology*, Vol. A5 (6), pp. 3408-3411 Nov/Dec 1987.

[9] Dr. Merek Sosnowski, EE Department NJIT, personal conversation March, 1998.

[10] F. Vratny, B.H. Vromen and A.J. Harendza-Harinxma, *Electrochemical Technology* Vol. 5, pp.283, 1967.

[11] B. Chapman, *Glow Discharge Processes: Sputtering and Plasma Etching*, John Wiley & Sons, NY, 1980.

[12] L.I. Maissal and R.Glang, *Handbook of Thin Film Technology* McGraw Hill, NY.

[13] Metals Handbook, V 10 on *Materials characterization*, McGraw Hill, NY, 1991.

[14] D.K. Skoog and J.J. Leary, *Principles of Instrumental Analysis*, Chapter 15, Harcourt Brace College Publishers, NY, 1991.

[15] J.F. Croke, Phillips Electronic Instruments, X-ray Applications Laboratory, Notes on X-ray Spectrometry.

[16] D.E. Sayers and B.A. Bunker, *X-ray Absorption: Basic Principles of EXAFS, SEXAFS and XANES*, Chapter 6, edited by D.C. Koningsberger and R.Prins, John Wiley & Sons, NY, 1988.

[17] G. Bunker, *Elements of X-ray Absorption Spectroscopy*, Physics Department of Illinois Institute of Technology, Chicago, IL

[18] Boon. K. Teo, *Extended X-ray Absorption Fine Structure Spectroscopy: Basic Principles and Data Analysis*, Chapters 2-6, Springer-Verlag, NY, 1985.

[19] G.G. Li, F. Bridges and C.H. Booth, "X-ray Absorption fine structure standards: A comparison of experiment and theory," *Physical Review B*, Vol.52, No. 9, pp. 6332-6341, 1995.

[20] A. A. Steinmann, Y. Tardy and H.E. Hintermann, "Adhesion Testing by the Scratch Test Method: The influence of intrinsic and extrinsic parameters on the critical load," *Thin Solid Films*, Vol. 154, pp. 333-349, 1987.

[21] Web site of Jandel Engineering Limited and web site of Bridge Technology at http:///www. getnet.com/bridge/jandel.html.

[22] Theory of four point probe Manual, web site address: **http://argon.eecs.berkeley.edu** and **http://www.ece.uiuc.edu**.

[23] E. Hesse, " A Four Point Probe Method with Increased Accuracy for the Local Determination of the Thickness of Thin, Electrically Conducting Layers," *IEEE Transactions on Instrumentation and Measurement*, Vol. IM-31, No. 3, pp. 166-175, 1982.

[24] M.A. Green and M.W. Gunn, " The Evaluation of Geometrical Effects in Four Point Probe Measurements," *Solid State Electronics*, Vol. 14, pp. 1167-1177, 1971.

[25] M.H. *Read* "X-Ray Analysis of Sputtered Films of Beta-Tantalum and Body Centered Cubic Tantalum," *Thin Solid Films*, Vol. 10, pp. 123-135, 1972.

[26] D.W. Face and D.E. Prober "Nucleation of Body Centered Cubic Tantalum Films with Thin Niobium Under-layer," *Journal of Vacuum Science and Technology*, Vol. A 5(6), pp. 3408-3411, 1987.

[27] P.T. Moseley and C.J. Seabrook "The Crystal Structure of Beta-Tantalum," *Acta Crystallography*, Vol. B 129, pp. 1170-1171, 1973.

[28] D.J. Jerreat and R.D. Rawlings, "Composition, Microstructure and Mechanical Properties of Chemically Vapor-Deposited Tantalum," *Kristall und Technik*, Vol. 11, no.8, pp. 825-833, 1976.

[29] A.J. Perry, C. Beguin and H.E. Hintermann " The Microstructure of Tantalum Coatings on Mild Steel," in *Proceedings of the 3rd European Conference on Chemical Vapor Deposition*, Neuchatel, Switzerland, pp. 131-139, April 1980.

[30] J.A. Thorton, *Annual Review of Material Science*, Vol. 7, pp. 239, 1977.

[31] K.M. Kemmer, V.G.Harris, W.T. Elam Y.C. Yeng, D.E.laughlin and J.C. Woicik " Polarization-dependent XAFS Studies on the Role of Ta in the Compositional Segregation of Co-Cr-Ta magnetic Recording Media," *IEEE Transactions on Magnetics*, Vol.31, No.6, pp. 2806-2808, 1995.

[32] K.M. Kemmer, V.G.Harris , W.T. Elam Y.C. Yeng, D.E.laughlin, J.C. Woicik and J.C. Lodder " Preferential site distribution of dilute Pt and Ta in CoCr-based films: An extended x-ray absorption fine structure study," *Journal of Applied Physics*, Vol.82, No.6, pp. 2912-2917, 1997.

[33] J.J. Rehr, J.Mustre de Leon, s.I. Zabinski and R. C. Albers " Theoretical X-ray Absorptions Fine Structure Standards," *Journal of American Chemical Society*, Vol. 113, pp. 3676-3678, 1991.

[34] Emmanuel C. Onyiriuka, Lyle D. Kinney and Norbert J. Binkowski, " Adhesion and delamination of tantalum and chromium films on glass," *Journal of Adhesion Science and Technology*, Vol. 11, No. 7, pp. 929-940, 1997.

[35] Results and details of the Adhesion test of tantalum coatings performed on Micro-scratch Tester and Revetest by A. Harris from Micro Photonics Inc. Irvine, CA.

[36] Ranjana Saha, Rama B. Inturi and John A. Bernard "Effect of thickness and shubstrates on the mechanical properties of tantalum and tantalum nitride thin films," *Materials Research Society*, Vol. 403, pp. 02-07, 1996.

[37] D.Muller and E. Fromm " Mechanical properties and adhesion strength of TiN and Al coatings on HSS, steel, aluminum and copper characterized by four testing methods," *Thin Solid Films*, Vol. 270, pp. 411-416, 1995.

[38] L.A. Clevenger, A. Mutscheller, J.M.E. Harper, C.Cabral Jr., and K. Barmak " The relationship between deposition conditions, the beta to alpha phase transformation, and stress relaxation in tantalum thin films," *Journal of Applied Physics*, Vol. 72(10), no. 15, pp. 4918-4925, 1992.